

Utah State University

DigitalCommons@USU

All Graduate Theses and Dissertations

Graduate Studies

5-2017

Modeling and Projection of the North American Monsoon Using a High-Resolution Regional Climate Model

Jonathan D.D. Meyer
Utah State University

Follow this and additional works at: <https://digitalcommons.usu.edu/etd>



Part of the [Climate Commons](#)

Recommended Citation

Meyer, Jonathan D.D., "Modeling and Projection of the North American Monsoon Using a High-Resolution Regional Climate Model" (2017). *All Graduate Theses and Dissertations*. 5802.
<https://digitalcommons.usu.edu/etd/5802>

This Dissertation is brought to you for free and open access by the Graduate Studies at DigitalCommons@USU. It has been accepted for inclusion in All Graduate Theses and Dissertations by an authorized administrator of DigitalCommons@USU. For more information, please contact digitalcommons@usu.edu.



MODELING AND PROJECTION OF THE NORTH AMERICAN MONSOON USING
A HIGH-RESOLUTION REGIONAL CLIMATE MODEL

by

Jonathan David Douglas Meyer

A dissertation submitted in partial fulfillment
of the requirements for the degree

of

DOCTOR OF PHILOSOPHY

in

Climate Science

Approved:

Jiming Jin, Ph.D.
Climate Science
Major Professor

Lawrence Hipps, Ph.D.
Environmental Physics & Biometeorology
Committee Member

Patrick Belmont, Ph.D.
Hydrology
Committee Member

Scott Jones, Ph.D.
Soil Environmental Physics
Committee Member

Bruce Bugbee, Ph.D.
Plant Physiology
Committee Member

Mark McLellan, Ph.D.
Vice President for Research and
Dean of the School of Graduate Studies

UTAH STATE UNIVERSITY
Logan, Utah

2017

Copyright © Jonathan D.D. Meyer 2017
All Rights Reserved

ABSTRACT

Modeling and Projection of the North American Monsoon using a
High-Resolution Regional Climate Model

by

Jonathan D.D. Meyer, Doctor of Philosophy

Utah State University, 2017

Major Professor: Dr. Jiming Jin
Department: Plants, Soils and Climate

This dissertation aims to better understand how various climate modeling approaches affect the fidelity of the North American Monsoon (NAM), as well as the sensitivity of the future state of the NAM under a global warming scenario. Here, we improved over current fully-coupled general circulation models (GCM), which struggle to fully resolve the controlling dynamics responsible for the development and maintenance of the NAM. To accomplish this, we dynamically downscaled a GCM with a regional climate model (RCM). The advantage here being a higher model resolution that improves the representation of processes on scales beyond that which GCMs can resolve. However, as all RCM applications are subject to the transference of biases inherent to the parent GCM, this study developed and evaluated a process to reduce these biases. Pertaining to both precipitation and the various controlling dynamics of the NAM, we found simulations driven by these bias-corrected forcing conditions performed moderately better across a 32-year historical climatology than simulations driven by the original GCM data.

Current GCM consensus suggests future tropospheric warming associated with increased radiative forcing as greenhouse gas concentrations increase will suppress the NAM convective environment through greater atmospheric stability. This mechanism yields later onset dates and a generally drier season, but a slight increase to the intensity during July-August. After comparing downscaled simulations forced with original and

corrected forcing conditions, we argue that the role of unresolved GCM surface features such as changes to the Gulf of California evaporation lead to a more convective environment. Even when downscaling the original GCM data with known biases, the inclusion of these surface features altered and in some cases reversed GCM trends throughout the southwest United States. This reversal towards a wetter NAM is further magnified in future bias-corrected simulations, which suggest (1) fewer average number of dry days by the end of the 21st century (2) onset occurring up to two to three weeks earlier than the historical average, and (3) more extreme daily precipitation values. However, consistent across each GCM and RCM model is the increase in inter-annual variability, suggesting greater susceptibility to drought conditions in the future.

(143 pages)

PUBLIC ABSTRACT

Modeling and Projection of the North American Monsoon using a
High-Resolution Regional Climate Model

Jonathan D.D. Meyer

The North American Monsoon (NAM) is a dominant climate feature across the southwestern United States and Mexico during the summertime. Rainfall from the NAM elicits a significant response from the regional ecology as well as supports the socioeconomic well-being of both rural and urban populations. Due to the large variability in the yearly intensity and location of where the NAM rainfall occurs, the region is highly susceptible to prolonged and exceptional periods of drought; compounded by significant population growth projections through the 21st century. Reliable prediction for the NAM is highly beneficial on timescales ranging from short-term weather forecasting to longer climate timescales spanning seasonal, decadal, or even century intervals. This project aims to better understand the NAM processes and mechanisms in order to improve the reliability of NAM predictability. To improve seasonal predictability, we examined biases across a network of western United States snowpack observations used to infer the NAM onset timing as well as the seasonal intensity. Furthermore, by using a high-resolution regional climate model (RCM), we improved upon current future projections of the NAM, which are based on global climate models (GCM). Whereas these coarse-resolution GCMs have proven to be inappropriate at resolving many of the processes controlling the NAM, the increased model resolution of the RCM (leading to a better representation of surface features and the land-atmosphere interactions represented in the model) yielded an improved historical evaluation period. Our RCM simulations suggest the overall future drying trend predicted by GCMs likely doesn't factor in important processes responsible for thunderstorm activity. By including these effects, our RCM future projections indicate the average state of the future NAM will (1) onset earlier in the year, (2) bring greater total seasonal

rainfall and, (3) contain more extreme daily rainfall amounts. However, despite the suggestion that average rainfall from the NAM will increase, analysis of year-to-year variability indicates a greater propensity for severe and frequent drought conditions during below-average years, suggesting the continued need to develop a more sustainable approach to long-term water resources across the region.

DEDICATION

This work is dedicated to my loving wife Nicole, your support through the long hours and stressful periods has meant the world to me. Although not nearly just-compensation, may my first true paycheck be devoted to repaying your devotion and support with a romantic dinner at Tandoori Oven. To my parents: this accomplishment is a direct result of the path you laid for me along with your constant support and motivation. This accomplishment is especially dedicated to my late Father, who I wish could attend my hooding ceremony. Additionally, for the many friends and colleagues I have made during my tenure, I extend heartfelt appreciation for the support both in and out of the office. Most of all, thank you to everyone who made it clear they loved me no matter how many years this process takes.

ACKNOWLEDGMENTS

This project was funded by the National Science Foundation Microsystem Program project NSFEP-1065730. I would like to thank Dr. Jiming Jin and extend my gratitude for the opportunity he has given me to improve myself as a scientist, teacher, and person. I would especially like to thank my committee members, Drs. Lawrence Hipps, Patrick Belmont, Scott Jones, and Bruce Bugbee for their support and assistance throughout the entire process. Special recognition is also extended to Drs. Lawrence Hipps, Shih-Yu (Simon) Wang, and Robert Gillies who have demonstrated a commitment toward my success as a scientist. Of special importance are the many department staff who have guided me through the rigorous process of surviving a Ph.D. program, for that you have my ultimate gratitude.

Jonathan David Douglas Meyer

CONTENTS

	Page
ABSTRACT.....	iii
PUBLIC ABSTRACT	v
DEDICATION.....	vii
ACKNOWLEDGMENTS	viii
LIST OF TABLES.....	xi
LIST OF FIGURES	xii
LIST OF ACRONYMS	xv
CHAPTER	
I. INTRODUCTION.....	1
The global monsoon system.....	1
The North American monsoon.....	2
Dynamics of the North American monsoon	5
The upper-level anticyclone.....	5
Moisture source.....	6
The low-level jet.....	8
The gulf surge phenomena.....	9
Global teleconnections and interannual variability of the North American monsoon	11
Climate modeling and projecting the future of the NAM	14
Global climate models	15
Regional climate models.....	16
References.....	18
II. OBSERVATIONS OF WESTERN UNITED STATES SNOWPACK USING THE SNOWPACK TELEMETRY (SNOTEL) NETWORK.....	24
Seasonal prediction of the North American monsoon using snowpack	25
Methodology and datasets.....	26
Biases between snow water equivalent and accumulated precipitation.....	28
Summary and conclusion.....	36
References.....	37
III. BIAS CORRECTION FOR IMPROVED REGIONAL CLIMATE MODELING OF THE NORTH AMERICAN MONSOON	39
Introduction.....	40
Methodology and model configuration.....	43
Climate Forecast System Reanalysis data.....	44
Community Climate System Model output	44
Gridded observation data	46
Regional climate model configuration.....	47
Simple linear regression bias correction	48
Deriving the remaining bias corrected variables	52

	x
Mean sea-level pressure	52
Geopotential height	55
Zonal and meridional winds.....	55
Soil temperature and moisture	58
Evaluation of impacts from bias correction	58
Historical evaluation	59
Lateral boundary conditions	59
Regional climate model simulations	63
North American monsoon precipitation.....	63
North American monsoon evolution.....	67
Summary and conclusion	74
References.....	78
IV. FUTURE PROJECTION OF THE NORTH AMERICAN MONSOON	84
Introduction.....	85
Data and methodology	91
General circulation model output.....	91
Regional climate model configuration.....	91
Bias correction of general circulation model output.....	94
Evaluation of future projections.....	94
North American monsoon forcing	95
North American monsoon mechanisms	99
North American monsoon precipitation.....	105
Summary and conclusion	114
References.....	117
V. CONCLUSION AND DISCUSSION.....	122
Curriculum Vitae	128

LIST OF TABLES

Table		Page
2.1	Comparison of high-bias (boxes 1, 2, and 3) and low-bias SWE regions (boxes 4, 5, and 6) illustrated by the six green boxes in Fig. 2.3a	33
3.1	Monthly and JJAS average bias and RMSE statistics for the northern and southern evaluation regions (Fig. 3.1) for the three WRF climatologies when compared to the CRU gridded observations	66

LIST OF FIGURES

Figure		Page
1.1	Monthly distribution of climatological precipitation for specific locations across the North American Monsoon domain	4
1.2	1979-1989 500-hPa analysis of streamlines (solid lines), winds (barbs), and dewpoint ($^{\circ}\text{C}$ dashed lines) for May (a), June (b), and July (c).....	7
1.3	Mean pilot balloon winds (dashed) and streamlines (solid) analysis at 450m AGL at 1200, 1800, 0000, and 0600 UTC over the monsoon region.....	10
1.4	Conceptualization of the various components involved in the gulf surge phenomena.....	12
2.1	Assessment of SNOwpack TELEmetry network biases.....	30
2.2	Regions of correlation between monsoon rainfall and wintertime snowpack conditions.....	31
2.3	Comparison between climatological wind speed and snow-liquid ratio (SLR)	33
2.4	Comparison of SNOwpack TELEmetry drifting patterns and wind speed.....	35
3.1	WRF model domain with model-resolved topography (meters)	49
3.2	Climatological (1979-2010) May-October 850-hPa Mixing Ratio (g kg^{-1}) for (A) CFSR, (B) original CCSM, and (C) bias-corrected CCSM datasets.....	53
3.3	As in Figure 3.2, but for 700-hPa	54
3.4	Comparison of the vertical profile of average bias (left) and RMSE (right) along each lateral boundary relax zone for temperature ($^{\circ}\text{C}$; solid lines) and mixing ratio (g kg^{-1} ; dashed lines) forcing data provided by CCSMO (red) and CCSMBC (green).....	60

3.5	Timeseries showing the climatological (1979-2010) 700-hPa lateral boundary conditions of temperature ($^{\circ}\text{C}$) and mixing ratio (g kg^{-1}) through the 01-Apr to 01-Nov time period	62
3.6	Timeseries of the sea surface temperatures in the Gulf of California for the CFSR (blue line), original CCSM (red line), and the bias-corrected CCSM (green line) after interpolation to the 20-km model grid.....	63
3.7	Average 1979-2010 June-July-August-September precipitation (mm day^{-1}) for (A) the CRU gridded-observations, (B) downscaled CFSR, (C) downscaled original CCSM, and (D) the downscaled bias-corrected CCSM.....	64
3.8	1979-2010 average monsoon onset dates for the three WRF climatologies (top row) with differences between the two WRF CCSM climatologies and WRF-CFSR (Bottom row).....	68
3.9	Time-versus-latitude plot for climatological precipitable water (mm) spanning 01 April to 01 November for WRF-CFSR (A), WRF-CCSMO (B), and WRF-CCSMBC (C)	69
3.10	As in figure 3.9, but for convective available potential energy (CAPE; color fill contours) and convective inhibition (CIN; contour lines).....	71
3.11	As in figure 3.9, but for Lifted Condensation Level (meters; color fill contours) and Level of Free Convection (meters; contour lines).....	73
4.1	Model resolved terrain for Community Climate System Model version 4(CCSM4) (a) and the 20-km WRF domain (b).....	93
4.2	Future change (future minus historical) for lateral boundary conditions vertical profile of mixing ratio (g kg^{-1}), temperature ($^{\circ}\text{C}$), and moist static energy (MSE; MJ kg^{-1}) for the original Community Climate System Model (CCSMO; red lines) and bias-corrected Community Climate System Model (CCSMBC; green lines).....	96
4.3	Future changes to Gulf of California (GoC) sea surface temperature (SST) and saturation vapor pressure.....	98
4.4	Historical vs. future Gulf of California (GoC) moisture flux comparison	100

4.5	Same as Fig. 4.2, but for the northern periphery (a,b,c) and North American monsoon core (d,e,f) evaluation regions shown in Fig. 4.1b.....	102
4.6	Vertical cross section of historical climatological July-August meridional component V-wind (m s ⁻¹) for observation based Climate Forecast System Reanalysis (CFSR; a), and Community Climate System Model version 4 (CCSM4; b)	104
4.7	Future June-September (JJAS) precipitation change (mm month ⁻¹) comparison	107
4.8	Changes to future average North American Monsoon (NAM) onset with earlier onset (blue colors) or later onset (brown colors)	109
4.9	Histogram distribution of June-September (JJAS) daily precipitation over the NAM core (left column) and the northern periphery (right column)	111
4.10	Future change to average number of June-September (JJAS) days (a,b,c) and percent change of the future difference relative to the historical normal dry days (d,e,f).....	113

LIST OF ACRONYMS

SST	Sea Surface Temperature
NAM	North American Monsoon
SMO	Sierra Madre Occidental
GoM	Gulf of Mexico
GoC	Gulf of California
ETP	Eastern Tropical Pacific
LLJ	Low Level Jet
ENSO	El Nino Southern Oscillation
GCM	Global Climate Model/General Circulation Model
RCM	Regional Climate Model
CMIP	Climate Model Intercomparison Project
IC	Initial Condition
LBC	Lateral Boundary Condition
MBC	Mean Bias Correction
SWE	Snow Water Equivalent
AP	Accumulated Precipitation
SNOTEL	SNOwpack TELemeter
NARR	North American Regional Reanalysis
QC	Quality Control
MSWE	Maximum Snow Water Equivalent
SLR	Snow Liquid Ratio
CCSM	Community Climate System Model
WRF	Weather Research and Forecasting
CFSR	Climate Forecast System Reanalysis
SLR	Simple Linear Regression
NCEP	National Center for Environmental Prediction
OISST	Optimum-Interpolation Sea Surface Temperatures
RCP	Representative Concentration Pathway
RMSE	Root Mean Square Error
CRU	Climate Research Unit
NCAR	National Center for Atmospheric Research
LSM	Land Surface Model
NER	Northern Evaluation Region
SER	Southern Evaluation Region
CAPE	Convective Available Potential Energy
CIN	Convective INhibition
LFC	Level of Free Convection
LCL	Lifting Condensation Level
NARCCAP	North American Regional Climate Change Assessment Program
MSE	Moist Static Energy

CHAPTER I

INTRODUCTION

1.1 The global monsoon system

Bisecting periods of dry climate, global monsoon systems provide critical water resources to both ecological and socioeconomic systems such as agriculture and urban centers (Webster 1998). Roughly half of the world's population lives in or depends on monsoon-influenced climates. These populations are mostly found in developing countries without well-established infrastructure and are currently experiencing urbanization, which makes these them highly vulnerable to monsoon variability. Monsoon systems of varying strengths can be found over all tropical and sub-tropical continents. However, the most dominant monsoon systems are found over India and Southeast Asia, Indo-Australia, and West Africa, with lesser monsoon systems occurring in North and South America (Webster 1998). The timing of monsoon onset, seasonal intensity, and interannual variability all have profound impacts on the various cultures dependent on the life-giving monsoon rainfall.

The fundamental mechanism behind global monsoons develops as solar insolation increases during the transition between spring and summer months. This transition period experiences significant heating of the landmasses that outpaces the heating of surrounding ocean bodies (Trenberth et al. 2000). This asymmetric heating alters the large-scale pressure patterns, resulting in the seasonal reversal of atmospheric winds characterized by an onshore, sea-breeze type flow. Additionally, existing in close

proximity to warm tropical sea surface temperatures (SST) with strong surface evaporation, the monsoon circulation pumps moisture-laden air into the interior of the continent by entraining the warm and humid tropical air mass. The combination of the shift in atmospheric circulation in reaction to the asymmetric land-ocean heating with the associated moisture transport from humid tropical air masses is what traditionally defines a monsoon system.

The degree to which monsoon rainfall impacts the annual total precipitation varies from monsoon to monsoon but the wettest locations on Earth coincide with the Indian-Asian monsoon. In fact, in association with the Indian-Asian monsoon the World Meteorological Organization lists the world record for 48-hour rainfall at 2,493 mm (98.15 inches), which fell at Cherrapunji, India in June 1995. This site also holds the record for greatest 12-month period of rainfall, at 26,470 mm (86 feet 10 inches) of rain from August 1860 to July 1861. While an extreme example, this goes to show the substantial weather and climate events that can occur with the associated flooding during such events cause substantial impacts to infrastructure as well as loss of life. However, monsoon systems are also susceptible to periods of drought, which can pose equally negative socioeconomic threats (Webster 1998).

1.2 The North American monsoon

Although much less intense than the Asian and Indo-Australian monsoons, the North American monsoon (NAM) occurs over a drought susceptible region, and therefore still plays a critical role in the regional hydrologic cycle. Regional ecology, agriculture, and

socioeconomic systems throughout Mexico and the southwestern United States are all highly dependent on NAM rainfall while experiencing threats from severe weather, flash flooding, and lightning-triggered wildfires (Ray et al. 2007).

Similar to other global monsoons, the North American Monsoon (NAM) bisects a period of extremely dry climate both preceding and following the pronounced seasonal shift in atmospheric circulation and moisture transport. Although substantially less intense than other global monsoons and with considerably larger spatiotemporal variability, the NAM can contribute upwards of 40% and 70% of the annual total precipitation for the perennially dry southwest U.S. and northwest Mexico, respectively (Douglas et al. 1993; Higgins et al. 1997). Reproduced from Adams and Comrie (1997), Fig. 1.1 shows the monthly climatological rainfall for specific locations across the NAM domain and illustrates the various contributions the NAM has on annual precipitation. During the mature phase of the NAM, locations across northwest Mexico and the southwestern United States can receive mean daily precipitation values up to 5 mm day^{-1} with the most intense precipitation of up to 10 mm day^{-1} occurring over southern Mexico and along the Sierra Madre Occidental (SMO) mountain range (Douglas et al. 1993).

Upper-air atmospheric observations indicate that the NAM system typically begins to organize in early June, and the transition to the summertime regime is often quick and dramatic, with rainfall onset first occurring along the southernmost extent of the SMO mountain range. This elevated topographical feature gives way to lowlands which receive up to 80% or 90% of the maximum possible solar insolation leading to summer surface

air temperatures which often exceed 40 °C (Adams and Comrie 1997). As the warm season progresses, the NAM system intensifies and expands northward bringing convective rain throughout the southwest United States before it reaches maturity around mid-July. A clear definition of the terminal date for the NAM season is muddled by ambiguity between synoptic- and NAM-driven rainfall, but lingering remnants of the NAM often last into late September.

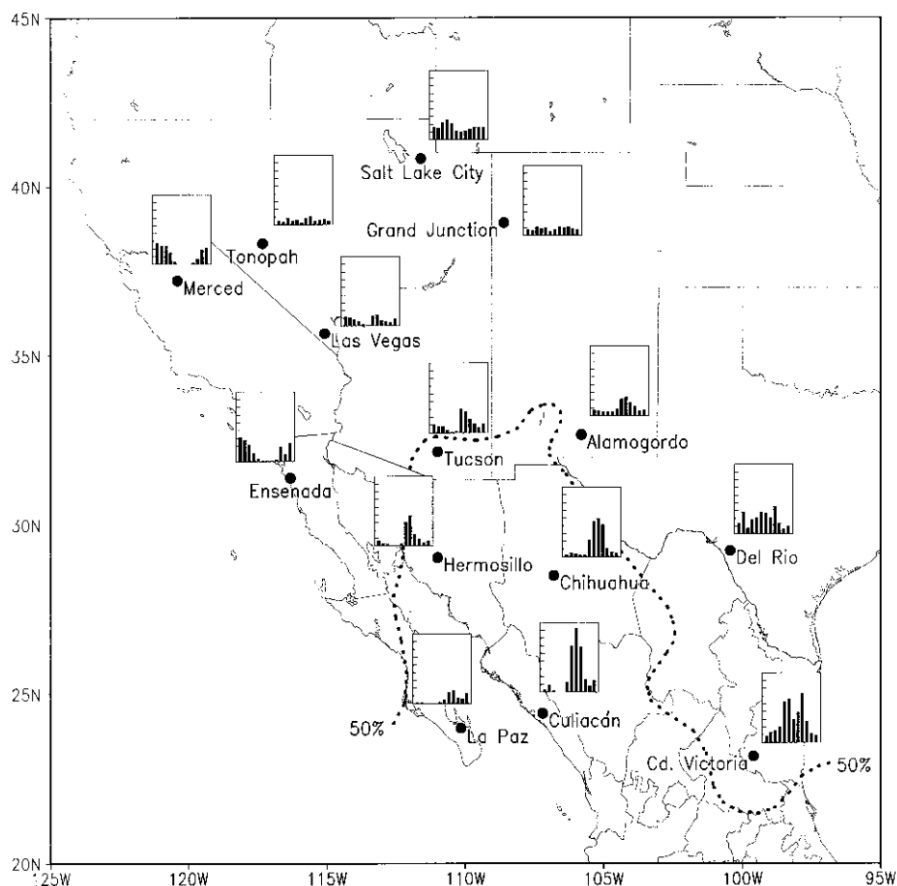


Fig. 1.1 Monthly distribution of climatological precipitation for specific locations across the North American Monsoon domain. Dashed black line delineates the region where greater than 50% of annual precipitation occurs between July and September. Taken from Adams and Comrie (1997).

1.3 Dynamics of the North American monsoon

What distinguishes the NAM is a reduced role of the dominant synoptic (large-scale) shift in atmospheric circulation and moisture transport typical of the other larger global monsoons. Instead, the controlling dynamics of the NAM span a broad range of scales from continental similar to other global monsoons down to the smallest mesoscales (Berbery 2001). The specific geographic orientation of the region's land and water bodies allows these smaller scales to play a larger role than other global monsoons, and what makes the NAM particularly well suited for higher resolution climate modeling. This section provides an overview of the various controlling dynamics of the NAM system across the synoptic and mesoscales. Although the traditional asymmetric land-sea heating and resulting shift in synoptic atmospheric circulation is still present in the NAM system, early work by Mosiño and Garcia (1974) noted that both orography and atmospheric disturbances are needed to explain the climatological rainfall patterns associated with the NAM. In part, the reliance on smaller-scale mechanisms associated with the regional topography is why such large spatiotemporal variability exists across the NAM region when compared to other global monsoons. It is these smaller scale interactions with the land surface, regional topography and coastal orientation that are now understood to be just as important as the large-scale synoptic conditions for the maintenance of the NAM system.

1.3.1 The upper-level anticyclone

Beginning at the largest scales, the synoptic evolution of the NAM anticyclone develops in reaction to several mechanisms. First, in response to the seasonal northward

shift of the Inter-Tropical Convergence Zone, the sub-tropical ridge/trough guide also shifts north (Trenberth et al. 2000). At the same time, warming SST's in the West Atlantic allows a westward expansion of the south Atlantic sub-tropical high-pressure (Barlow et al. 1998). Combining these two processes with the increased heating over the continental landmass allows the development and maintenance of the NAM anticyclone, which peaks over the southwestern United States and Northern Mexico. Furthermore, as the NAM season reaches maturity, diabatic heating in the upper troposphere from deep convection throughout the region further strengthens the NAM anticyclone (Barlow et al. 1998). Taken from Douglas (1993), Fig. 1.2 shows the May, 1979-1989 500-hPa analysis of winds, streamlines and dewpoint ($^{\circ}\text{C}$) for May, June, and July. The synoptic moisture transport is typically directed around the western edge of the NAM anticyclone, and therefore the seasonal position of this circulation often coincides with the location of most intense NAM rainfall, especially across the northern periphery of the NAM region across the southwest United States (Barlow et al. 1998). An eastward displacement of the anticyclone relative to normal typically produces a corresponding eastward shift in rainfall anomalies and vice versa.

1.3.2 Moisture source

Before reliable observations were made of the NAM environment, there was much debate in the literature regarding the true moisture source. Although it might appear trivial, the source of moisture has been implicated with seasonal predictability (Schmitz and Mullen 1996) and with the development of the convective environment (Stensrud et

al. 1995). The first attempts to describe the moisture source for the NAM was performed by Bryson and Lowry (1955) whose analysis of upper atmospheric geopotential height fields implied the Gulf of Mexico (GoM) was the sole source. Subsequent field studies performed by Reitan (1957) showed that the bulk of NAM precipitable water occurs below 800 hPa, which rules the GoM out as the primary moisture source when considering the continental divide rises above this level.

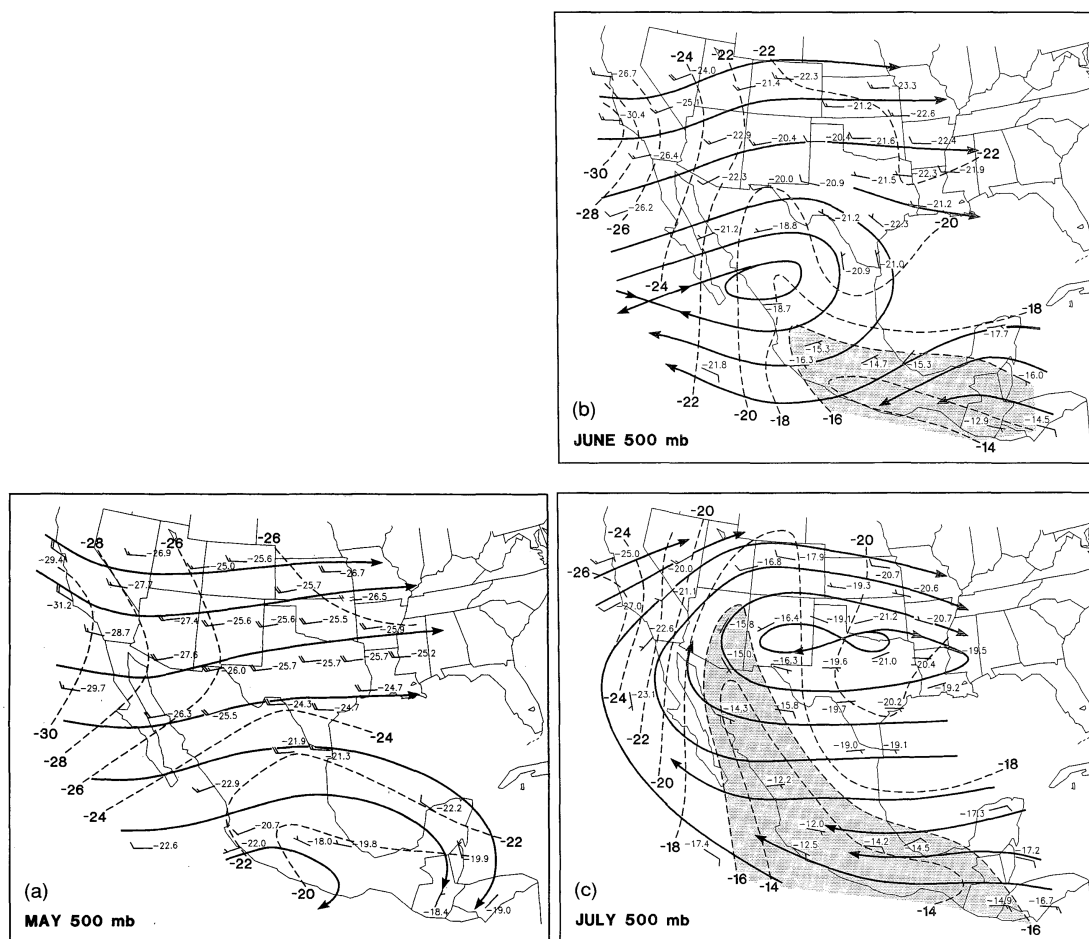


Fig. 1.2 1979-1989 500-hPa analysis of streamlines (solid lines), winds (barbs), and dewpoint ($^{\circ}\text{C}$ dashed lines) for May (a), June (b), and July (c). Taken from Douglas (1993).

Analyzing moisture flux across the region, Rasmusson (1967) showed the Gulf of California (GoC) and surrounding eastern tropical Pacific (ETP) was a more likely source for NAM moisture. This finding was further reinforced by studies by Hales (1972) and later by Brenner (1974) whose investigations coined the term “gulf surge” to describe impulsive events where atmospheric moisture from the GoC and ETP is funneled into the interior of the continent. These events are confined to the lower troposphere, typically below 700 hPa, and the moisture transported by these surge events is thought to augment convective activity over the interior of the landmass (Adams and Comrie 1997).

However, whereas the GoC and ETP are now understood to be the primary sources for the bulk of NAM moisture—especially at the lower levels—the GoM still contributes low-level moisture east of the continental divide, as well as upper-level moisture for the entire NAM region. A comprehensive description of the numerous studies describing the mechanics of gulf surge events is nicely summarized in Adams and Comrie (1997).

Cumulatively, these studies bring to light the fact that gulf surge events do not entirely account for the total moisture transport from the GoC and ETP over the desert southwest.

1.3.3 *The low-level jet*

Although the mechanisms at the time of early observations of gulf surge events were not fully understood, Hales (1974) speculated “a natural channel about 200 miles wide exists from the tropical Pacific to the deserts of the southwestern United States.” This early speculation on how the regional topography can funnel distant moisture over the desert southwest would ultimately turn out to be correct. Field studies using rawinsonde and aircraft observations across the region exposed the presence of a shallow southerly

low-level jet (LLJ) oriented parallel to the GoC (Douglas 1995; Reyes et al. 1994). This LLJ exhibits a highly diurnal cycle with peak wind speeds occurring during early morning hours that could reach $\sim 20 \text{ m s}^{-1}$, sometimes lasting into the late morning hours (Douglas 1995). The mechanism producing the LLJ occurs as a result of uneven heating between the GoC and SMO. The resulting temperature and pressure gradient drives an onshore and upslope flow perpendicular to the coastline. This sea breeze flow peaks in the late afternoon to early evening hours and the associated moisture convergence is responsible for the highly diurnal afternoon convection over the foothills and highlands of the SMO (Douglas, 1998). The onshore sea-breeze flow reverses to a downslope flow overnight as the land surface begins to radiatively cool. This offshore land-breeze flow peaks in the early morning hours. The strong diurnal nature of the LLJ occurs because daytime heating induces boundary layer convection that vertically redistributes the horizontal momentum of the southerly flow, the GoC LLJ is only allowed to strengthen during nocturnal cooling when the near-surface stable layer minimizes the vertical transfer of momentum. Taken from Douglas (1995), Fig. 1.3 represents pilot and balloon observations of the diurnal nature of the mesoscale circulation at 450m above ground level. The mesoscale circulations resulting from the interaction between the GoC and surrounding topography represents one of the controlling mesoscale mechanisms that distinguishes the NAM from other global monsoons.

1.3.4 The gulf surge phenomenon

Except for the core of the NAM region along the SMO (where the diurnal sea-breeze drives persistent afternoon convection) rainfall across northwest Mexico and the

southwest United States can be highly variable in space and time. Across the northern periphery, convective activity is closely tied with the frequency and intensity of gulf moisture surges, which despite occurring in nearly every monsoon season, have a large interannual (Brenner 1974) and interseasonal (Stensrud et al. 1997) variability.

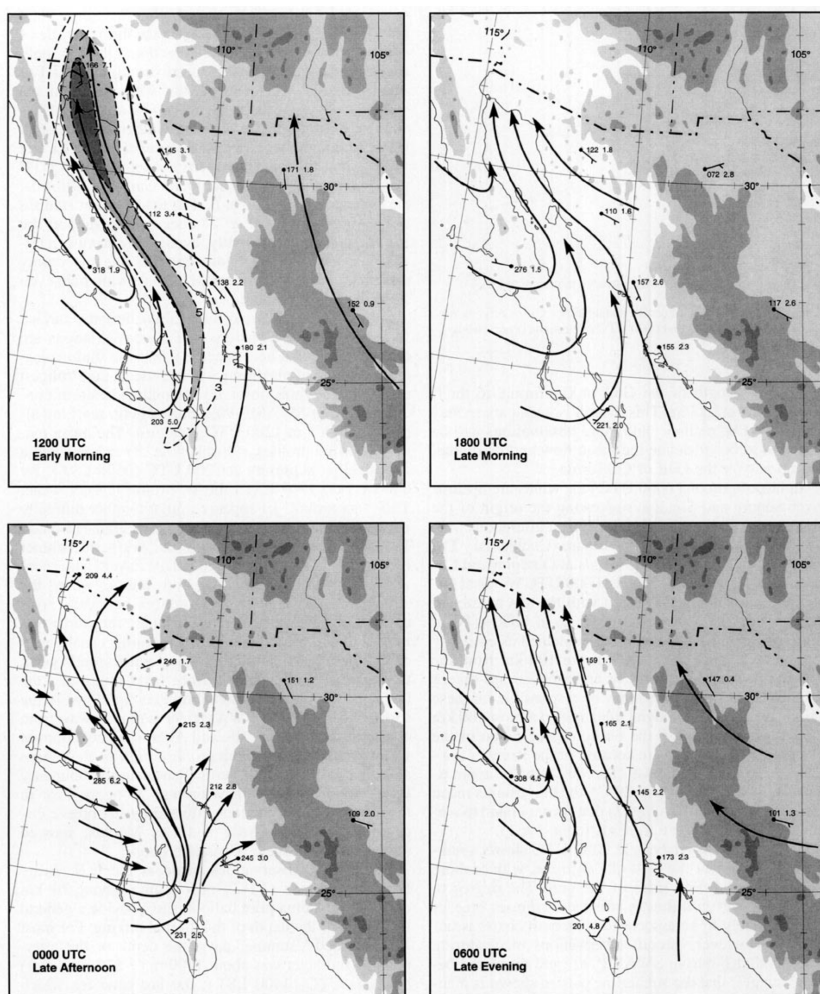


Fig. 1.3 Mean pilot balloon winds (dashed) and streamlines (solid) analysis at 450m AGL at 1200, 1800, 0000, and 0600 UTC over the monsoon region. Isotachs with contours at 3, 5, and 7 m s⁻¹ are also shown at 1200 UTC with the jet core shaded in the 1200 UTC panel. Terrain shading represents elevations above 915 m (3000 ft), 1830 m (6000 ft), and 2745 m (9000 ft). Taken from Douglas (1995).

Fig. 1.4 taken from Adams and Comrie (1997) illustrates the various components associated with the gulf surge phenomena. Mesoscale modeling studies by Stensrud et al. (1997) point to a few key components that when aligned, produce the strongest gulf surges. In the upper levels, the corresponding passage of a westward-moving mid-latitude trough with an easterly tropical wave helps enhance the synoptic northerly transport of tropical moisture. This enhanced synoptic moisture transport can be further augmented by the mesoscale moisture transport associated with the GoC LLJ. Lastly, the presence of a semi-permanent low-level thermal low that develops from the intense surface heating over the lowlands of the Colorado River valley helps further draw in moisture.

1.4 Global teleconnections and interannual variability of the North American monsoon

Whereas land and ocean systems help control the development and maintenance of the NAM, so do the anomalies within these systems help modulate the interannual variability. Due to the significantly dry mean annual conditions across the region, the interannual variability of the NAM can be quite large. In fact, the interannual variability in parts of the southwest United States can exceed the mean seasonal rainfall itself (Higgins et al. 1998). At the most fundamental level, the primary driving factor on NAM variability comes from the variability of global ocean SSTs, which can have both direct effects on the evolution and intensity of the NAM and indirect effects from antecedent climate conditions.

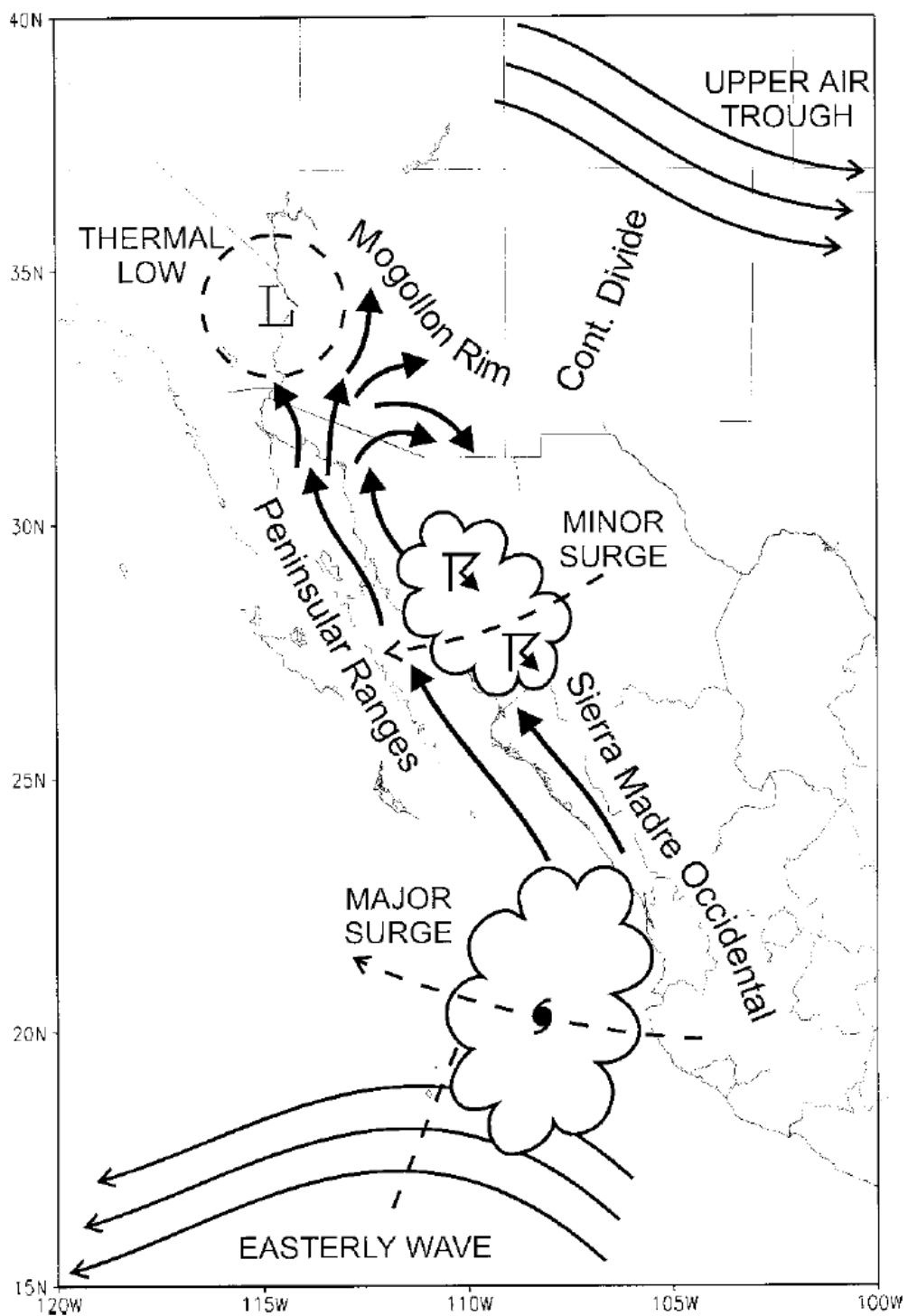


Fig. 1.4 Conceptualization of the various components involved in the gulf surge phenomena. Taken from Adams and Comrie (1997).

Technically, the impacts of western United States snow cover and soil moisture on the timing and evolution of the NAM system represents a direct effect. Zhu et al. (2005) described the connection between antecedent wintertime snowpack conditions such as springtime soil moisture and surface temperature with summertime rainfall across the southwest United States. This connection exists due to seasonal spatiotemporal variability of wintertime snowpack. As the spring equinox approaches and increasing solar insolation drives the spring meltoff shifts the landscape to a lower surface albedo, increasing net absorbed radiation. As the soil and surface become exposed, the increasing net radiation is preferentially partitioned towards latent heat of evaporation as opposed to sensible heat acting to warm the ground. An inverse relationship exists where wet winters tend to lead to later snowmelt and greater soil moisture, which can delay the timing of the necessary asymmetrical land-ocean heating driven by peak land-surface heating as the region's soil dries. Thus, variability in the wintertime conditions can directly affect the timing of the onset of the monsoon. Observational analysis by Higgins et al. (1998) showed that timing of onset plays a role in total seasonal NAM rainfall. By extending (shortening) the NAM season, years with early (late) NAM onset typically ended with above (below) average monsoon rainfall totals.

Although the direct impacts through the surface energy budget help modulate NAM variability, this mechanism actually represents an indirect effect when considering the variability of western United States wintertime precipitation is remotely modulated through teleconnections associated with ocean SSTs. Higgins et al. (1998) made the connection between equatorial Pacific SST variability and the aforementioned western

United States wintertime precipitation. This El Niño Southern Oscillation (ENSO) affects winter and springtime storm track over the West Coast on an approximately four- to seven-year frequency. In addition to the equatorial Pacific SST effects through the ENSO teleconnection, Mo and Paegle (2000) found a multi-decadal link between north Pacific SSTs and NAM variability that once again, influences western United States storm tracks. By directly influencing antecedent snow pack, these ocean teleconnections have an indirect effect on the NAM system and ultimately, the interannual variability of rainfall across the region.

In addition to indirect effects from antecedent climate conditions, past studies have found direct impacts from remote global teleconnections on the development and maintenance of the NAM system. Carleton et al. (1990) found a positive relationship between the evolution of the sub-tropical ridge and the surrounding Pacific Ocean, GoC, and GoM SSTs. Additionally, the spatiotemporal variability in SSTs can directly impact the magnitude and location of peak surface evaporation. Where above average SSTs are found, elevated surface evaporation can be entrained by the overlying NAM circulation resulting in periods of strong and frequent moisture surge events that can contribute to a strong overall NAM season.

1.5 Climate modeling and projecting the future of the NAM

Several unique types of modeling approaches are used to project future climate. Ranging from coarse-resolution global climate models (GCM) to higher-resolution regional climate models (RCM), each approach has a unique set of advantages and

disadvantages that ensures there is no perfect modeling approach for future climate projections. Due to the obvious societal implications, much effort has been given to investigating the impact of global warming on the future NAM system.

1.5.1 Global climate models

The Climate Model Intercomparison Project (CMIP) is an international assembly of GCM models independently developed by various nations including U.S. agencies. Investigation into global monsoon shifts in each of the phases 2, 3 and 5 of CMIP GCM simulations has shown an ensemble consensus for a shift in seasonality (delayed onset and retreat phases) with greater late season rainfall for the global monsoon system (Seager et al. 2007, CMIP2; Seth et al. 2011, CMIP3; Cook and Seager, 2013, Seth et al. 2013, CMIP5). During the pre-onset stage of the global monsoon season (May and June), increased tropospheric stability from a warmer climate and lesser low-level atmospheric moisture from decreased evapotranspiration reinforce each other to create what is commonly referred to as the springtime “convective barrier.” As the warm season progresses, increasing moisture convergence eventually overcomes this convective barrier resulting in a period of moderately enhanced precipitation activity relative to historical normals for the period (Seth et al. 2010). For the NAM, Bukovsky et al. (2013) reported that a combination of poorly resolved land-atmosphere interactions and biased atmospheric circulation led to CMIP simulations that contained sufficient uncertainty and spread between individual ensemble members.

The main deficiency of CMIP models stems from horizontal grid spacing, which is too coarse to appropriately describe finer-scale processes linked to complex terrain, coastlines or large surface heterogeneities (McGregor, 1997); all of which play a measureable role in the NAM system. In fact, mountain/no mountain GCM experiments performed by Broccoli and Manabe (1992) highlighted the importance of regional topography when developing a vigorous circulation across the global monsoon systems. Furthermore, studies by Lee et al. (2007) and Collier and Zhang (2007) describe the positive impact from increased horizontal resolution on the diurnal cycle of precipitation and the role of mesoscale processes such as those dependent on the Gulf of California (GoC).

1.5.2 Regional climate models

To circumvent the limitations of coarse-resolution GCM projections, either statistical or dynamical downscaling methods are used to describe small-scale processes that are not captured by GCM output. Statistical downscaling is the least computationally intensive method and uses an empirical relationship between GCM output and finer-scale station observations. Dynamical downscaling utilizes a higher resolution limited area model based on physical principles (Dickinson et al., 1989). Commonly referred to as a RCM, dynamic downscaling applications are often considered more capable as they have the potential to capture fine spatial-scale non-linear effects that statistical downscaling does not (Denis et al. 2002; Antic et al. 2004). With higher time and space resolutions, and more sophisticated physics, dynamic modeling results are greatly improved, thus resulting in stronger reliability in future climate projections over the coarser resolution

GCM output (Xu and Yang, 2012). Through higher horizontal resolution, RCMs have already proven to add value over GCM applications and produce a more realistic historical NAM (Higgins et al. 2006; Gutzler et al. 2009; Castro et al. 2012; Bukovsky et al. 2013; Bukovsky et al. 2015; Meyer and Jin, 2015). By including more of the interactions across spatial scales, future projections simulated using an RCM can be considered more reliable when compared to a GCM where certain climate mechanisms are diminished or even neglected.

As summarized in Warner et al. (1997), one limitation of RCMs is their dependence on GCM output for initial conditions (IC) and lateral boundary conditions (LBC). Systematic biases inherent to the GCM output are subsequently transmitted, and potentially magnified by internal non-linear model feedbacks within the RCM (Warner et al. 1997; Noguer et al. 1998; Misra et al. 2003; Christensen et al. 2008; Bruyère et al. 2013). These transmitted biases add uncertainty within the RCM and in extreme cases can render the RCM inferior to the GCM (Kanamaru and Kanamitsu, 2007). Recently, in an attempt to reduce uncertainties in RCMs, various GCM bias correction techniques have proven effective in improving their performance (Kanamaru and Kanamitsu, 2007; Misra, 2007; Jin et al. 2011; Colette et al. 2012; Bruyère et al. 2013; White and Toumi, 2013). Most commonly used is the specific bias correction process where individual LBC variables are subjected to long-term, mean (climatological) bias correction (MBC). MBC is a simple and straightforward procedure that has proven effective in improving the RCM's performance in climate modeling (Kirtman et al. 2002; Misra and Kanamitsu,

2004; Sato et al. 2007; Cook and Vizzy 2008; Wu et al. 2009; Patricola and Cook 2009; Xu and Yang, 2012; Jin et al. 2011; Bruyère et al. 2013).

The goals of this project are to simply offer with improved confidence a future projection of the state of the NAM with a thorough investigation into the sensitivity of specific NAM processes and mechanisms with regard to a warming climate system. Specifically, this project aims to answer the question of how impactful are ill-resolved climate processes within coarse-resolution GCMs on the future state of the NAM. To answer this question, a high-resolution RCM is paired with an augmented version of current-practice bias correction used to improve the RCM forcing. By comparing the parent GCM with RCM simulations driven by both untouched and bias-corrected GCM output, this project gains insight into the impact of climate modeling approach on the various impactful NAM processes while revealing the reliability that each approach is accurately resolving the NAM environment.

References

- Adams D, Comrie A (1997) The North American monsoon. *Bull Am Meteorol Soc* 78:2197–2213.
doi:[http://dx.doi.org/10.1175/1520-77\(1997\)078<2197:TNAM>2.0.CO;2](http://dx.doi.org/10.1175/1520-77(1997)078<2197:TNAM>2.0.CO;2)
- Antic S, Laprise R, Denis B, de Elia R (2004) Testing the downscaling ability of a one-way nested regional climate model in regions of complex topography. *Clim Dyn* 23:473–493. doi:<http://dx.doi.org/10.1007/s00382-004-0438-5>
- Barlow M, Nigam S, Berbery EH (1998) Evolution of the North American monsoon system. *J Clim* 11:2238-2257.
doi:[http://dx.doi.org/10.1175/1520-0442\(1998\)011<2238:EOTNAM>2.0.CO;2](http://dx.doi.org/10.1175/1520-0442(1998)011<2238:EOTNAM>2.0.CO;2)

- Berbery EH (2001) Mesoscale moisture analysis of the North American monsoon. *J Clim* 14(2):121-137. doi:[http://dx.doi.org/10.1175/1520-1442\(2001\)013%3C0121:mmaotn%3E2.0.co;2](http://dx.doi.org/10.1175/1520-1442(2001)013%3C0121:mmaotn%3E2.0.co;2)
- Brenner IS (1974) A surge of maritime tropical air-Gulf of California to the southwestern United States. *Mon Weather Rev* 102:375-389.
- Bryson RA Lowry WP (1955) Synoptic climatology of the Arizona summer precipitation singularity. *Bull Am Meteorol Soc* 36:329-339.
- Broccoli AJ, Manabe S (1992) The effects of orography on midlatitude Northern Hemisphere dry climates. *J Clim* 5(11):1181-1201. doi:[http://dx.doi.org/10.1175/1520-442\(1992\)005%3C1181:teoom%3E2.0.co;2](http://dx.doi.org/10.1175/1520-442(1992)005%3C1181:teoom%3E2.0.co;2)
- Bruyère CL, Done JM, Holland GJ, Fredrick S (2013) Bias corrections of global models for regional climate simulations of high-impact weather. *Clim Dyn* doi:<http://dx.doi.org/10.1007/s00382-013-2011-6>
- Bukovsky MS, Gochis DJ, Mearns LO (2013) Towards assessing NARCCAP regional climate model credibility for the North American monsoon: current climate simulations. *J Clim* 26:8802-8826. doi:<http://dx.doi.org/10.1175/jcli-d-12-00538.1>
- Bukovsky MS, Carrillo CM, Gochis DJ, Hammerling DM, McCrary RR, Mearns LO (2015) Toward assessing NARCCAP regional climate model credibility for the North American monsoon: Future climate simulations. *J Clim* 28(17):6707-6728. doi:<http://dx.doi.org/10.1175/jcli-d-14-00695.1>
- Carleton AM, Carpenter DA (1990) Mechanisms of interannual variability of the southwest United States summer rainfall maximum. *J Clim* 3:999-1015.
- Castro CL, Chang H-I, Dominguez F, Carrillo C, Schemm J-K, Juang H-M (2012) Can a Regional Climate Model Improve the Ability to Forecast the North American Monsoon? *J Clim* 25:8212-8237. doi:<http://dx.doi.org/10.1175/JCLI-D-11-00441.1>
- Christensen JH, Boberg F, Christensen OB, Lucas-Picher P (2008) On the need for bias correction of regional climate change projections of temperature and precipitation. *Geophys Res Lett* 35:L20709. doi:<http://dx.doi.org/10.1029/2008gl035694> .
- Colette A, Vautard R, Vrac M (2012) Regional climate downscaling with prior statistical correction of the global climate forcing. *Geophys Res Lett* 39:L13707. doi:<http://dx.doi.org/10.1029/2012gl052258>

- Collier JC, Zhang GJ (2007) Effects of increased horizontal resolution on simulation of the North American monsoon in the NCAR CAM3: An evaluation based on surface, satellite, and reanalysis data. *J Clim* 20(9):1843-1861.
doi:<http://dx.doi.org/10.1175/jcli4099.1>
- Cook BI, Seager R (2013) The response of the North American monsoon to increased greenhouse gas forcing. *J Geophys Res* 118(4):1690-1699.
doi:<http://dx.doi.org/10.1002/jgrd.50111>
- Cook KH, Vizy EK (2008) Effects of Twenty-First-Century Climate Change on the Amazon Rain Forest. *J Clim* 21:542–560.
doi:<http://dx.doi.org/10.1175/2007JCLI1838.1>
- Denis B, Laprise R, Caya D, Cote J (2002) Downscaling ability of one-way nested Regional climate models: the Big-Brother Experiment. *Clim Dyn* 18:627–646.
doi:<http://dx.doi.org/10.1007/s00382-001-0201-0>
- Dickinson RE, Errico RM, Giorgi F, Bates GT (1989) A regional climate model for the western United States. *Clim Change* 15(3):383-422.
doi:<http://dx.doi.org/10.1007/bf00240465>
- Douglas MW, Maddox R, Howard K, Reyes S (1993) The Mexican Monsoon. *J Clim* 6:1665–1677.
doi:[http://dx.doi.org/10.1175/1520-0442\(1993\)006%3C1665:tmm%3E2.0.co;2](http://dx.doi.org/10.1175/1520-0442(1993)006%3C1665:tmm%3E2.0.co;2)
- Douglas MW, (1995) The summertime low level jet over the Gulf of California. *Mon Wea Rev* 123:2334–2347.
doi:[http://dx.doi.org/10.1175/1520-0493\(1995\)123%3C2334:tslljo%3E2.0.co;2](http://dx.doi.org/10.1175/1520-0493(1995)123%3C2334:tslljo%3E2.0.co;2)
- Douglas MW, Valdez-Manzanilla A, Garcia Cueto R (1998) Diurnal variation and Horizontal extent of the low-level jet over the northern Gulf of California. *Mon Wea Rev* 126:2017–2025.
doi:[http://dx.doi.org/10.1175/1520-0493\(1998\)126<2017:dvaheo>2.0.co;2](http://dx.doi.org/10.1175/1520-0493(1998)126<2017:dvaheo>2.0.co;2)
- Gutzler DS, et al (2009) Simulations of the 2004 North American Monsoon: NAMAP2. *J Clim* 22:6716–6740. doi:<http://dx.doi.org/10.1175/2009jcli3138.1>
- Hales JE (1972) Surges of maritime tropical air northward over the Gulf of California. *Mon Wea Rev* 100(4):298-306.
- Higgins RW, Yao Y, Wang XL (1997) Influence of the North American monsoon system on the US summer precipitation regime. *J Clim* 10:2600–2622.
doi:[http://dx.doi.org/10.1175/1520-0442\(1997\)010%3C2600:iotnam%3E2.0.co;2](http://dx.doi.org/10.1175/1520-0442(1997)010%3C2600:iotnam%3E2.0.co;2)

- Higgins RW, and Coauthors (2006) The NAME 2004 Field Campaign and Modeling Strategy. *Bull Am Meteorol Soc* 87:79–94.
doi:<http://dx.doi.org/10.1175/bams-87-1-79>
- Higgins RW, Mo KC, Yao Y (1998) Interannual variability of the U.S. Summer Precipitation regime with emphasis on the Southwestern Monsoon. *J Clim* 11:2582-2606.
doi:[http://dx.doi.org/10.1175/1520-0442\(1998\)011%3C2582:ivotus%3E2.0.co;2](http://dx.doi.org/10.1175/1520-0442(1998)011%3C2582:ivotus%3E2.0.co;2)
- Jin J, Wang S-Y, Gillies R (2011) An improved dynamical downscaling for the western United States. *Clim Change: Research and Technology for Adaptation And Mitigation*, 23-38. doi:<http://dx.doi.org/10.5772/22991>
- Kanamaru H, Kanamitsu M (2007) Scale-Selective Bias Correction in a Downscaling Of Global Analysis Using a Regional Model. *Mon Wea Rev* 135:334–350.
doi:<http://dx.doi.org/10.1175/mwr3294.1>
- Kirtman BP, Fan Y, Schneider EK (2002) The COLA global coupled and anomaly coupled ocean-atmosphere GCM. *J Clim* 15:2301–2320.
doi:[http://dx.doi.org/10.1175/1520-0442\(2002\)015<2301:tcgcaa>2.0.co;2](http://dx.doi.org/10.1175/1520-0442(2002)015<2301:tcgcaa>2.0.co;2)
- Lee MI, Schubert SD, Suarez MJ, Held IM, Kumar A, Bell TL, et al (2007) Sensitivity to horizontal resolution in the AGCM simulations of warm season diurnal cycle of precipitation over the United States and northern Mexico. *J Clim* 20(9):1862-1881. doi:<http://dx.doi.org/10.1175/jcli4090.1>
- McGregor JL (1997) Regional climate modelling. *Meteorol Atmos Phys* 63(1):105-117.
doi:<http://dx.doi.org/10.1007/bf01025367>
- Meyer JDD, Jin J (2015) Bias correction of the CCSM4 for improved regional climate modeling of the North American monsoon. *Clim Dyn*
doi:<http://dx.doi.org/10.1007/s00382-015-2744-5>
- Misra V, Dirmeyer PA, Kirtman BP (2003) Dynamic downscaling of seasonal simulations over South America. *J Clim* 16:103–117.
doi:[http://dx.doi.org/10.1175/1520-0442\(2003\)016<0103:ddosso>2.0.co;2](http://dx.doi.org/10.1175/1520-0442(2003)016<0103:ddosso>2.0.co;2)
- Misra V, Kanamitsu, M (2004) Anomaly nesting: A methodology to downscale seasonal climate simulations from AGCMs. *J. Clim* 17:3249–3262.
doi:[http://dx.doi.org/10.1175/1520-0442\(2004\)017<3249:anamtd>2.0.co;2](http://dx.doi.org/10.1175/1520-0442(2004)017<3249:anamtd>2.0.co;2)
- Misra V (2007) Addressing the Issue of Systematic Errors in a Regional Climate Model. *J Clim* 20:801–818. doi:<http://dx.doi.org/10.1175/jcli4037.1>

- Mo KC, Paegle JN (2000) Influence of sea surface temperature anomalies on the precipitation regimes over the southwest United States. *J Clim* 13(20) 3588-3598.
- Mosiño, P. A., E. García, 1974: The climate of Mexico. *Climates of North America*, R. A. Bryson and F. K. Hare, Eds., Vol. 2, *World Survey of Climatology*, Elsevier, 373–404.
- Noguer M, Jones R, Murphy J (1998) Sources of systematic errors in the climatology of a regional climate model over Europe. *Clim Dyn* 14:691–712.
doi:<http://dx.doi.org/10.1007/s003820050249>
- Patricola CM, Cook KH (2009) Northern African climate at the end of the twenty-first century: an integrated application of regional and global climate models. *Clim Dyn* 35:193–212. doi:<http://dx.doi.org/10.1007/s00382-009-0623-7>
- Rasmusson EM (1967) Atmospheric water vapor transport and the water balance of North American: Part1. Characteristics of the water vapor flux field. *Mon Wea Rev* 96(10):720-734.
doi:[http://dx.doi.org/10.1175/1520-0493\(1967\)095<0403:AWVTAT>2.3.CO;2](http://dx.doi.org/10.1175/1520-0493(1967)095<0403:AWVTAT>2.3.CO;2)
- Ray AJ, Garfin GM, Wilder M, Vásquez-León M, Lenart M, Comrie AC (2007) Applications of monsoon research: Opportunities to inform decision making and reduce regional vulnerability. *J Clim* 20:1608–1627.
doi:<http://dx.doi.org/10.1175/JCLI4098.1>
- Reitan, C. H., 1957: The role of precipitable water vapor in Arizona's summer rains. Tech. Rep. No. 2 on the Meteorology and Climatology of Arid Regions, Institute of Atmospheric Physics, University of Arizona, 19 pp.
- Reyes, S, Douglas MW Maddox RA (1994) El monzon del suroeste de Norteamerica (TRAVASON/SWAMP). *Atmosfera* 7:117–137.
- Sato T, Kimura F, Kitoh A (2007) Projection of global warming onto regional precipitation over Mongolia using a regional climate model. *J Hydrol* 333:144–154. doi:<http://dx.doi.org/10.1016/j.jhydrol.2006.07.023>
- Schmitz JT and Mullen S (1996) Water vapor transport associated with the summertime North American Monsoon as depicted by ECMWF analysis. *J Clim* 9:1621-1634.
- Seager R, Ting M, Held I, Kushnir Y, Lu J, Vecchi G, et al (2007) Model projections of an imminent transition to a more arid climate in southwestern North America. *Science* 316(5828):1181-1184. doi:<http://dx.doi.org/10.1126/science.1139601>

- Seth A, Rauscher SA, Biasutti M, Giannini A, Camargo SJ, Rojas M (2013) CMIP5 projected changes in the annual cycle of precipitation in monsoon regions. *J Clim* 26(19):7328-7351. doi:<http://dx.doi.org/10.1175/jcli-d-12-00726.1>
- Seth A, Rauscher SA, Rojas M, Giannini A, Camargo SJ (2011) Enhanced spring convective barrier for monsoons in a warmer world? *Clim Change* 104(2):403-414. doi:<http://dx.doi.org/10.1007/s10584-010-9973-8>
- Stensrud DJ, Gall RL, Nordquist MK (1997) Surges over the Gulf of California during the Mexican monsoon. *Mon Wea Rev* 125(4):417-437. doi:[http://dx.doi.org/10.1175/1520-0493\(1997\)125%3C0417:sotgoc%3E2.0.co;2](http://dx.doi.org/10.1175/1520-0493(1997)125%3C0417:sotgoc%3E2.0.co;2)
- Trenberth KE, Stepaniak DP, Caron JM (2000) The global monsoon as seen through the divergent atmospheric circulation. *J Clim* 13:3969-3993.
- Warner TT, Peterson RA, Treadon RE (1997) A Tutorial On Lateral Boundary Conditions As A Basic And Potentially Serious Limitation To Regional Numerical Weather Prediction. *Bull Am Meteorol Soc* 78:2599–2617. doi:[http://dx.doi.org/10.1175/1520-0477\(1997\)078<2599:atolbc>2.0.co;2](http://dx.doi.org/10.1175/1520-0477(1997)078<2599:atolbc>2.0.co;2)
- Webster PJ, Magaña VO, Palmer TN, Shukla J, Tomas RA, Yanai M, Yasunari T (1998) Monsoons: Processes, predictability, and the prospects for prediction. *J Geo Res* 103(C7):14451-14510.
- White RH, Toumi R (2013) The limitations of bias correcting regional climate model inputs: BIAS CORRECTION LIMITATIONS. *Geophys Res Lett* 40:2907–2912. doi:<http://dx.doi.org/10.1002/grl.50612>
- Wu P-L, Lin P-L, Juang H-MH (2009) Local Mean Bias Correction in a Regional Model Downscaling: A Case Study of the South China Sea Summer Monsoon of 1998. *Mon Wea Rev* 137:2869–2892. doi:<http://dx.doi.org/10.1175/2009mwr2784.1>
- Xu Z, Yang Z-L (2012) An Improved Dynamical Downscaling Method with GCM Bias Corrections and Its Validation with 30 Years of Climate Simulations. *J Clim* 25:6271–6286. doi:<http://dx.doi.org/10.1175/jcli-d-12-00005.1>
- Zhu C, Lettenmaier DP, Cavazos T (2005) Role of antecedent land surface conditions on North American monsoon rainfall variability. *J Clim* 18(16):3104-3121.

CHAPTER II
OBSERVATIONS OF WESTERN UNITED STATES SNOWPACK USING THE
SNOWPACK TELEMETRY (SNOTEL) NETWORK

Abstract

Observations of the springtime maximum of snowpack across the western United States can provide a useful indicator for seasonal predictability of the North American Monsoon. Therefore, quantifying the accuracy of these observations is crucial in order to better understand the limitations when using such observations to predict NAM onset and seasonal intensity. Here, we investigated the accuracy of snow water equivalent (SWE) observations when compared to accumulated precipitation (AP) observations compiled by 748 SNOWpack TELemetry stations. Our analysis suggests a regionally dependent systematic bias between SWE measurements and AP. Often observed, SWE outpaces accumulated precipitation (AP) which can be statistically and physically explained through (1) precipitation under-catchment and/or (2) drifting snow. Forty-four percent of the 748 stations studied reported at least one year where the maximum SWE was greater than AP, while sixteen percent of the stations showed this inconsistency for at least 20% of the observed years. Regions with a higher likelihood of inconsistency contained drier snow and are exposed to higher winds speeds, both of which are positively correlated to drifting snow potential. Days when SWE increased but AP remained constant occurred on an average of 10.75 days per year for all stations, with 31% greater wind speeds at 10 meters for such days (using reanalysis winds). Findings suggest accurate SWE

observations throughout the Cascade Mountains and lower elevations of the Interior West while indicating a potential for overestimated SWE observations throughout the higher elevations of the Rocky Mountains, Utah mountain ranges, and the Sierra Nevada.

1. Seasonal prediction of the North American monsoon using snowpack

Antecedent wintertime conditions across the western United States can influence the timing of onset and seasonal intensity of the North American Monsoon (NAM; Gutzler and Preston 1997). Variability in the region's snow cover, soil moisture and temperature influences the timing of NAM onset by modulating the partitioning of net radiation through the surface energy budget (Zhu et al. 2005). As such, the observations of the region's snow cover are often used as a predictor for the impending NAM season.

Therefore, it is important to acknowledge the uncertainties and biases associated with these observations. This study investigates sources responsible for a frequently observed inconsistency between measurements of snow water equivalent (SWE) and accumulated precipitation (AP) reported by the SNOwpack TELemetry (SNOTEL) network (Schaefer et al. 1996). The inconsistency occurs in the sense that SWE exceeds AP (which is physically unlikely) at some point in time or throughout the snow season. Possible biases of the SNOTEL observations have been attributed to the two distinct measuring devices in observing SWE and AP (Johnson and Marks 2004): While SWE is measured using a snow pillow sensor equipped with a pressure transducer, AP is measured with a standard 30.5-cm orifice storage-type gauge (equipped with an alter shield to reduce turbulence around the gauge orifice and maximize catch efficiency). Bias in SWE measurement occurs when temperature differences exist between surrounding ground cover and the

pillow sensor, creating uneven distribution of snow between the sensor and the surrounding ground cover. However, these conditions can lead to *both* under- and over-measurement depending on the snowmelt conditions and the snow density rate of change (Johnson and Marks, 2004), so the bias should be random throughout the whole network. Regarding AP, it is known that the accuracy of precipitation catchment decreases with increasing wind speed (Neff, 1977). The types of gauge similar to those of the SNOTEL network have a margin of error between 10% and 50%, possibly more in mountainous regions (WMO, 2008). Losses in AP due to wetting or evaporation and trace underestimates may also contribute to the bias.

The SNOTEL network was designed to observe surface meteorological variables for hydrologic and climatic uses. Given the now 30-year data period, SNOTEL observations have been used extensively used for the depiction of decadal trends in surface hydrological conditions (Serreze et al., 1999, 2001; Fassnacht et al., 2003; Mote et al., 2004; Hamlet et al., 2005; Carson, 2007; Pederson et al., 2011) and to evaluate against climate model simulations (e.g., Jin and Miller 2011). Thus, a comprehensive understanding of possible biases influencing the SNOTEL data is paramount. This paper examines the full archive of SNOTEL data and addresses one potential cause for the frequently observed systematic inconsistency between SWE and AP.

2. Methodology and datasets

SNOTEL stations operate on a water year (October 1 – September 30) and report at least daily values of SWE and AP (near surface air temperature is also measured but is

not examined in this study). SWE and AP values are reset to zero on October 1 of each year. SWE and AP are reported in inches with a sensor resolution of 0.1 inch (2.54 mm). In addition to the ~800 SNOTEL stations currently in operation (NRCS <http://www.wcc.nrcs.usda.gov/nwcc/inventory>), we also utilize six-hourly 10-m winds from the North American Regional Reanalysis (NARR) for investigation of drifting snow. NARR assimilates meteorological and land-surface observations and outputs data on a 32-km horizontal resolution grid (Mesinger et al., 2006). Accurate representation of 10-m wind conditions over complex terrain on daily scales is not possible; however, comparison of ambient wind conditions of each SNOTEL site under various synoptic scenarios is still useful.

To avoid undue biases in the daily measurements of SWE and precipitation due to reporting errors, data used in this study was subjected to two quality control (QC) filters. QC filters address the following issues: (1) accurate reset and appropriate daily corrections of SWE and AP for new water years and (2) allowable number of missing data points in a usable year for either SWE or AP. These filters ensure the most reliable daily measurements as well as remove years with large gaps in the data where accurate observations are questionable. A final count of 748 stations remained after exclusion of stations throughout the state of Alaska and unfit stations removed through QC filtering. Here, ice-bridging conditions leading to uneven distribution of snow are assumed to have negligible effects on daily observations as they typically occur during the transition from late winter to spring and this study focuses on the snow accumulation period before melt conditions occur.

3. Biases between snow water equivalent and accumulated precipitation

Under ideal conditions, any measurements of SWE greater than AP suggest that more water is contained within the snowpack than has been observed as precipitation. Fig. 2.1 illustrates (a) such a situation between SWE and AP, and (b) the daily difference between the two variables measured at Tony Grove, for water year 2005 (areas of red/blue indicate where SWE is greater/less than AP). SWE remains below AP in the early water year, as expected, but then increases to exceed and outgrow AP around January. SWE then remains greater than AP until the maximum SWE (MSWE) value predates the spring melt off. By using the difference between the MSWE and the associated AP we examine the frequency and magnitude of the inconsistency between SWE and AP throughout the SNOTEL network. Instances when the MSWE was at least 5% greater than the associated AP were used to identify “inconsistent years” of a particular station, ignoring years with smaller differences. Fig. 2.1c illustrates the actual number of occurrences throughout the network, while Fig. 2.1d shows the percentage of occurrence (number of years divided by total number of years on record). Forty-four percent of the 748 stations studied reported at least one year where the maximum SWE was greater than AP, with inconsistencies found in at least 20% of the observed years for 16 percent of the stations. Computed differences between the average MSWE and AP for all years when MSWE was greater than AP are shown in Fig. 2.1e to illustrate regions with the largest inconsistency throughout the network. It is apparent that the inconsistency between MSWE and AP is geographically dependent. For instance, a much higher and concentrated likelihood of inconsistency occurs in the Rocky Mountains, the Utah mountain ranges and the Sierra Nevada. Conversely, stations throughout the Pacific

Northwest generally show little to no occurrences of yearly MSWE greater than AP. Geographical correlation of inconsistencies between MSWE and AP (Fig. 2.1 c-e) provides evidence for a systematic (regional) controlling factor for the frequency and magnitude of such inconsistencies. When attempting to predict impending NAM onset and seasonal intensity, this regional proclivity for where SNOTEL bias occurs throughout much of where Zhu et al., (2005) found the highest correlations between antecedent wintertime conditions and the NAM. Taken from Zhu et al., (2005), Fig. 2.2a shows the correlation between June-September NAM rainfall across Northern Mexico and parts of Arizona and New Mexico with antecedent January-March precipitation. Fig. 2.2b shows the correlation between April SWE and May/June surface air temperature between 1965-99 and suggests that southern Rocky Mountain snow cover could be a key factor influencing surface temperature, and thus the development of the NAM. Note that much of the statistically significant area (shaded grey) occurs over the Colorado and Utah ranges as well as the southern extent of the Sierra Nevada range where SNOTEL SWE observations contain the greatest bias.

We next examine whether or not the geographically systematic inconsistency between MSWE and AP, as shown in Fig. 2.1 is related to biases resulting from precipitation under-catchment and snow drifting. Since a region's proclivity for snow drifting is a function of snow condition and wind speed, where snow condition determines the necessary wind speed threshold to initiate transport of the snow particles, we first analyze the climatological 10-m wind fields.

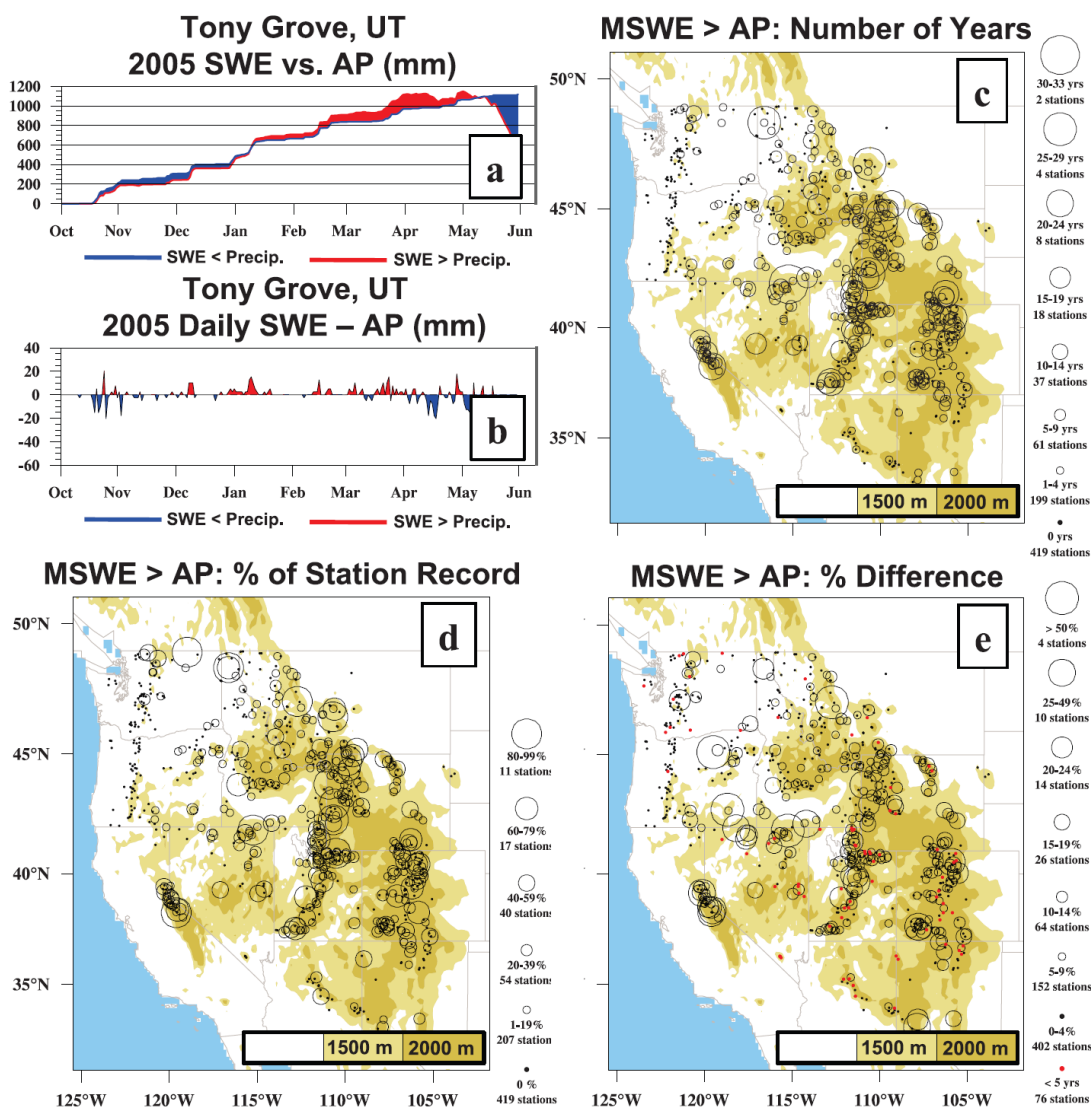


FIG. 2.1. Assessment of SNOwpack TELelemetry network biases. (a) 2005 measurements of SWE and AP for the Tony Grove, UT, site, (b) the 2005 difference between daily SWE and AP, (c) total number of years for each SNOTEL station where the MSWE was greater than AP, (d) percentage of each station's period of record where the MSWE was greater than AP (number of years divided by total number of years on record), and (e) percentage difference between each SNOTEL station's MSWE and AP values averaged over all inconsistent years $[(MSWE_{avg} - AP_{avg})/AP_{avg}]$. Light brown contours found in (c)–(e) represent elevations above 1500 m with dark brown representing above 2000 m. Increasing circle size represents increasing magnitude, while black dots in (c), (d) represent stations with no instances of MSWE greater than AP. Black dots in (e) represent stations where the average differences was below 5%, while red dots represent stations with less than 5 years of operation.

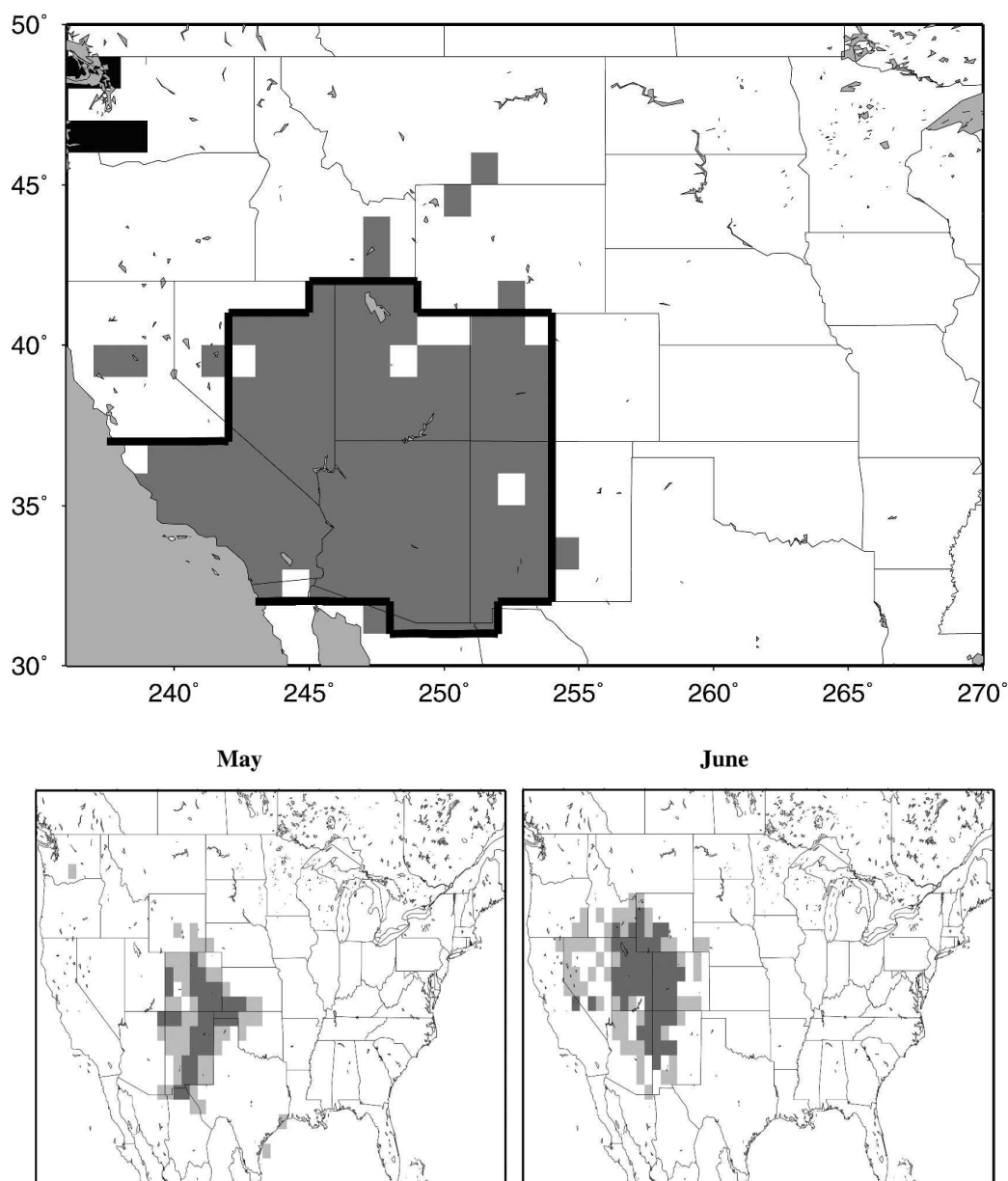


FIG. 2.2. Regions of correlation between monsoon rainfall and wintertime snowpack conditions. (a) Correlation between June-September precipitation and antecedent January-March precipitation during 1965-1999. Significant correlations at the 5% level or greater are shaded gray (< -0.33) or dark (> 0.33). (b) correlation of April snow water equivalent index vs May and June surface air temperature during 1969-1999. Shaded area is at the 10% (gray, < -0.28) and 5% (dark gray, < -0.33) significance level or greater. Taken from Zhu et al., (2005).

Fig. 2.3 (a) shows the climatological (1979-2011) 10-m wind vectors for DJF (December, January, and February) compared to (b) the DJF climatological (1971-2000) snow-to-liquid ratio (SLR) contours adapted from Baxter et al. (2005). Stronger wind speeds appear over higher elevations due to their approximate position to mid-tropospheric westerlies. SLR values reveal climatological dry (high SLR) snow conditions over the Rockies and wet (low SLR) snow conditions over the Cascade Mountains, the latter suggesting a lower tendency to drift. Figure 2a also portrays six subdomains over which average station bias (Fig. 1d), DJF climatological NARR 10-m winds (Fig. 2a), and SLR (Fig. 2b) values are computed for high- and low-biased regions. These averages are presented in Table 1 with high-biased domains (boxes 1, 2, and 3) showing higher 10-m wind speeds and SLR values when compared to the low-biased domains (boxes 4, 5, and 6).

SNOTEL stations that exhibited higher frequency and magnitude of inconsistent yearly MSWE and AP occur in regions with dry snow and high average wind speeds. Li and Pomeroy (1997) found that on average, wind speed thresholds for dry snow to drift were 7.7 m s^{-1} compared to 9.9 m s^{-1} for wet snow (snow conditions defined by snowpack cohesiveness). Combined with higher average wind speeds, stations with dry snow conditions surpass the threshold wind speed would be more likely to cause higher positively biased SWE observations over those regions, and vice versa for lower average wind speeds and wet snow conditions.

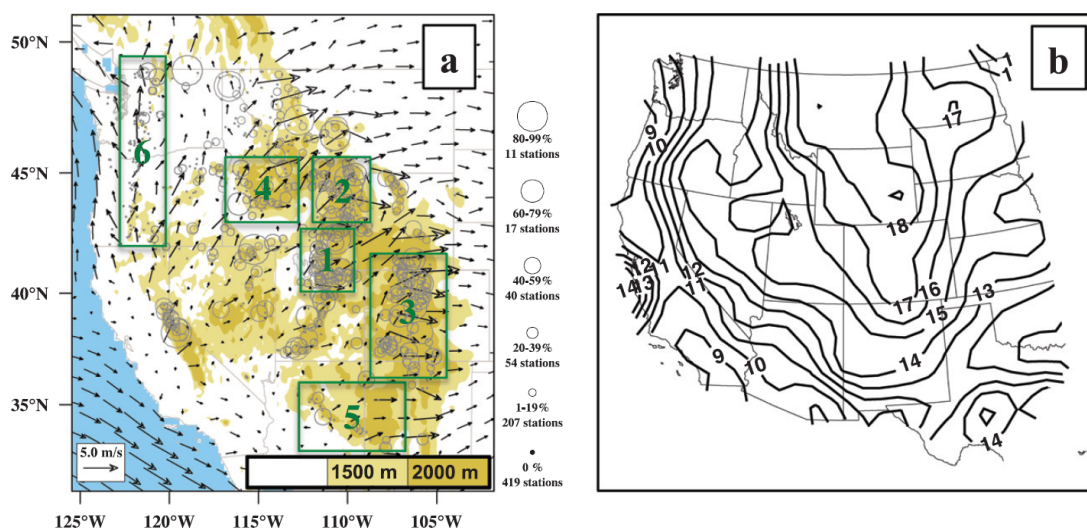


FIG. 2.3. Comparison between climatological wind speed and snow-liquid ratio (SLR). (a) North American Regional Reanalysis (NARR) average December-February 10-m wind vectors from January/February 1979 to December 2011/January and February 2012 overlaid on Fig. 2.1d and (b) a 30-yr climatology of DJF SLR from 1971–2000 adapted from Baxter et al. (2005). High- (boxes 1, 2, and 3) and low-bias SWE regions (boxes 4, 5, and 6) illustrated by the six green boxes.

TABLE 2.1. Comparison of high-bias (boxes 1, 2, and 3) and low-bias SWE regions (boxes 4, 5, and 6) illustrated by the six green boxes in Fig. 2.3a. Domain averages of SNOTEL stations percent number of years on record where MSWE was greater than AP (Fig. 2.1d), December-February climatological North American Regional Reanalysis 10-m winds (m s^{-1}), and snow-to-liquid ratio values are shown as well as the latitude–longitude boundaries of each region.

Region	Domain average			Boundaries
	MSWE > AP (%)	10-m wind (m s^{-1})	Snow-to-liquid ratio	
1. Northern Utah	14.9	1.9	14.4	40.0°–42.5°N 113.0°–110.0°W
2. Northwest Wyoming	15.4	3.8	16.3	43.0°–45.5°N 111.5°–109.0°W
3. Colorado	12.5	2.9	15.1	36.6°–41.5°N 108.7°–104.5°W
4. Southern Idaho	7.7	2.4	14.0	43.2°–45.5°N 116.5°–113.0°W
5. Arizona/New Mexico	4.0	1.2	12.4	32.5°–35.5°N 113.0°–107.0°W
6. Pacific Northwest	1.9	2.3	11.7	41.5°–49.2°N 123.0°–120.5°W

To isolate days when the most likely source of inconsistency leans towards snow drifting as opposed to precipitation under-catchment, we used days when SWE increased and no precipitation was observed (now referred to as drift-days). Fig. 2.4 illustrates (a) spatial drift-day anomaly and (b) NARR 10-m average wind anomaly (vectors) between drift-days and non-drift-days (constant daily SWE with no observed precipitation). For the 672 stations with at least five years of observation, the average number of drift-days per year was 10.75. Additionally, 31% stronger 10-m winds were observed for the drift-days, although wind direction differences were minor. For stations with above average drift-days shown in (a), the wind differences show universal westerly to southwesterly anomalies west of the Rockies, suggesting the influence of incoming Pacific troughs. The wind anomalies change direction to west-northwesterly over the Colorado Rockies and part of Utah mountains indicating drifting associated with the “deep-powder days” of snow normally under the west-northwesterly flow environment (Steenburgh and Alcott 2008). Compared with the patterns of MSWE and AP inconsistency shown in Fig. 2.1, drift-day anomaly correlates well with where more frequent MSWE and AP inconsistencies exist (Rocky Mountains, Sierra Nevada, and Intermountain West regions). Most notably seen over the Cascade Mountain Range, station placement relative to windward or leeward mountain slope illustrates opposing drift-days anomaly. Most likely, this pattern is controlled by the rain shadow effect (Smith, 1979), which could produce a relatively quick transition from wet (windward) to dry (leeward) snow conditions.

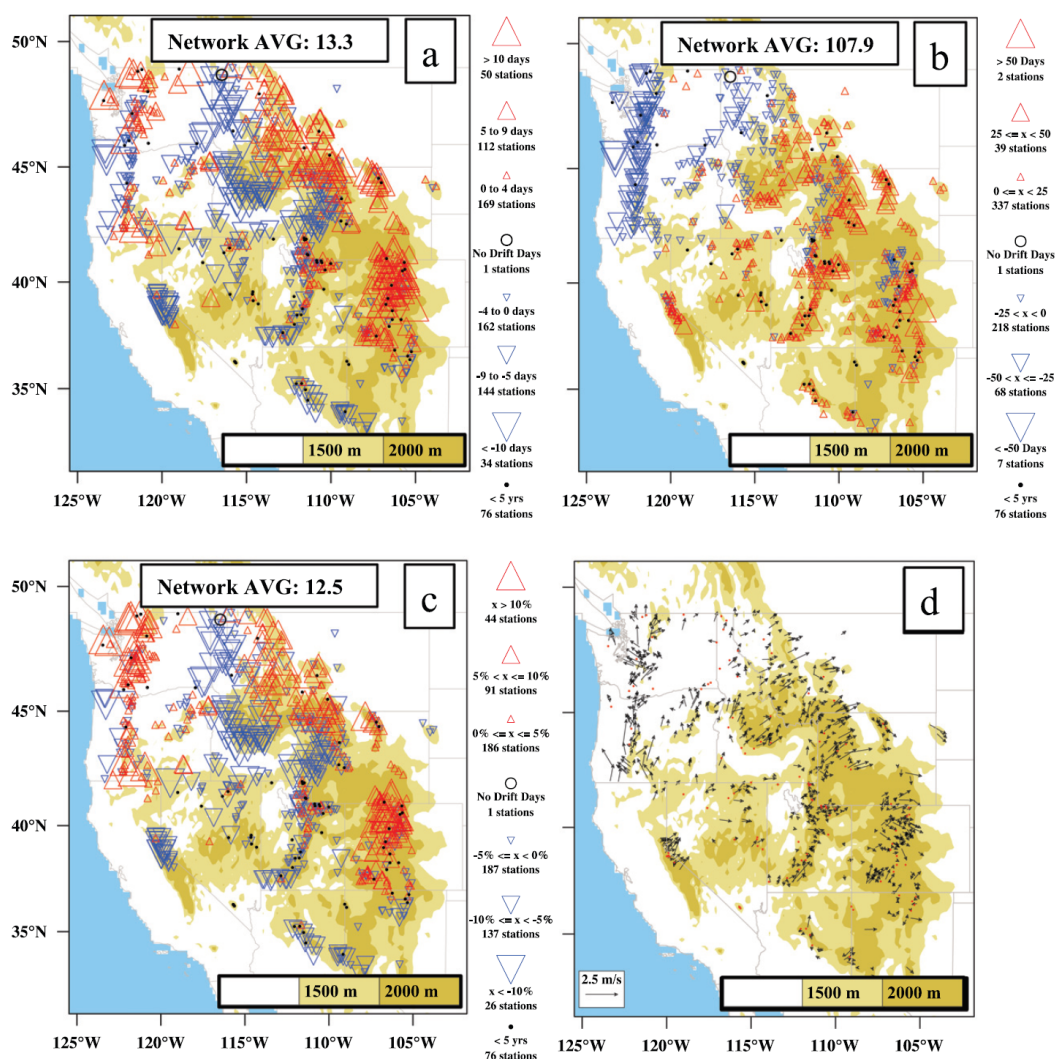


FIG. 2.4. Comparison of SNOwpack TELemetry drifting patterns and wind speed. (a) Anomaly number of drifting days per year ($\text{DriftDay}_{\text{stn}} - \text{DriftDay}_{\text{Networkavg}}$) for each SNOTEL station, where red/blue triangles represent above-/below-average drift days per year with increasing triangle size representing increasing magnitude anomaly. Black circles represent stations that never experienced a “drift day,” while black dots represent stations that had less than 5 years of operation. (b) As in (a), but for the anomaly of average days per year with no precipitation. (c) As in (a), but for the percent relative anomaly of drift days $[(\text{drift days}/\text{no-precipitation days})_{\text{stn average}} - (\text{drift days}/\text{no-precipitation days})_{\text{network average}}]$. (d) Difference vectors from North American Regional Reanalysis (NARR) 10-m winds between drifting and non-drifting scenarios (see text for scenario descriptions). Red dots represent stations with less than 5 years of observation. All panels are shown with elevation contours as in Fig. 2.1.

4. Summary and conclusion

Wintertime snow cover across the western United States is known to influence the timing of NAM onset and is often used as a seasonal predictive tool. Therefore, understanding the systematic biases within the oft-used SNOTEL network is advantageous to regional water resource managers. Agreement between patterns of snow-drift mechanisms (wind and SLR conditions) and drift-day anomalies, as well as the greater wind speeds shown during drift scenarios provides evidence to support the hypothesis that geographical dependence of the MSWE and AP inconsistency (where SWE outpaces AP) is partially a result of drifting snow. Especially across the southern Rocky Mountains, regions exhibiting over-estimation of SWE are relied on to help predict the timing of NAM onset and overall seasonal intensity. It appears that SNOTEL stations at higher elevations (Rocky and Sierra Nevada Mountains, and the Uinta/Wasatch ranges in Utah) and stations within the interior West have an increased potential for yearly MSWE values to grow higher than AP values. These regions commonly exhibit dry snow conditions and high westerly wind speeds – together they increase the potential for drifting snow. This systematic bias potentially allows NAM onset and intensity predictions that are biased towards later onset and less intense rainfall. Conversely, stations throughout the Cascade Mountains as well as lower elevation stations in the interior of the Western U.S. seldom reported any inconsistency, possibly due to the wet snow conditions and/or the lower average wind speeds. Unfortunately, antecedent conditions across these regions have shown little to no correlation to the NAM system, and are therefore less helpful for their predictive value.

While this study focused mainly on positive bias (overestimate) of SWE observations by drifting snow, snow scour (removal of snow from the column) should be considered. It is presumed that station interaction with surrounding topography and land cover will factor into how drifting/scour biases SWE observations (positively or negatively). Scouring of snow could partially explain the various (yet scattered) stations where positive SWE biases are expected but are not observed. Future work should merge surrounding land cover and daily wind data observed by enhanced SNOTEL sites to gain a more comprehensive understanding of the effect snow drift/scour has on the daily SWE and AP relationship.

REFERENCES

- Baxter, A.M., C.E. Graves, and J.T. Moore, 2005: A climatology of snow-to-liquid ratio for the contiguous United States. *Wea. Forecasting*, **20**, 729-744.
- Carson, E.C., 2007: Temporal and seasonal trends in streamflow in the Uinta Mountains, northeastern Utah, and relation to climatic fluctuations. *Arct. Antarct. Alp. Res.*, **39(4)**, 521-528.
- Fassnacht, S.R., K.A. Dressler, and R.C. Bales, 2003: Snow water equivalent interpolation for the Colorado River Basin from snow telemetry (SNOTEL) data. *Water. Resour. Res.*, **39(8)**, 1208-1217.
- Gutzler, D.S., and Coauthors, 2009: Simulations of the 2004 North American Monsoon: NAMAP2. *J. Climate* 22:6716–6740.
doi: <http://dx.doi.org/10.1175/2009jcli3138.1>
- Hamlet, A.F., P.Q. Mote, M.P. Clark, and D.P. Lettenmaier, 2005: Effects of temperature and precipitation variability on snowpack trends in the western United States. *J. of Climate*, **18**, 4545-4561.
- Jin, J., and N. L. Miller, 2011: Improvement of snowpack simulations in a regional climate model, *Hydrol. Processes*, **25**, 2202-2210.

- Johnson, J.B., and D. Marks, 2004: The detection and correction of snow water equivalent pressure sensor errors. *Hydrol. Processes*, **18**, 3513-3525.
- Li, L., and J.W. Pomeroy, 1997: Estimates of threshold wind speeds for snow transport using meteorological data. *J. Appl. Meteor*, **36**, 205-213.
- Mesinger, F., and Coauthors, 2006: North American regional reanalysis. *Bull. Amer. Meteor. Soc.*, **87(3)**, 343-360.
- Mote, P.W., M.P. Clark, and A.F. Hamlet, 2004: Variability and trends in mountain snowpack in western North America, Preprints, *15th Symp. on Global Change and Climate Variations*, Seattle, WA, Amer. Meteor. Soc., 5.1.
[Available online at
https://ams.confex.com/ams/84Annual/techprogram/paper_71019.htm.]
- Neff, E.L., 1977: How much rain does a rain gage gage? *J. Hydrol.*, **35**, 213-220.
- Pederson G.T., S.T. Gray, T. Ault, W. Marsh, D.B. Fagre, A.G. Bunn, C.A. Woodhouse, and L.J. Graumlich, 2011: Climatic controls on the snowmelt hydrology of the northern Rocky Mountains. *J. Climate*, **24**, 1666-1687.
- Schaefer, G.L., and J. Werner, 1996: SNOTEL into the Year 2000. 12th Conference on Biometeorology and Aerobiology, American Meteorological Society, Atlanta, Georgia, United States.
- Serreze, M.C., M.P. Clark, R.L. Armstrong, D.A. McGinnism, and R.S. Pulwarty, 1999: Characteristics of the western United States snowpack from snowpack telemetry (SNOTEL) Data. *Water. Resour. Res.*, **35(7)**, 2145-2160.
- , -----, and A. Frei, 2001: Characteristics of large snowfall events in the montane western United States as examined using Snowpack Telemetry (SNOTEL) data. *Water. Resour. Res.*, **37(3)**, 675-688.
- Smith, R.B., 1979: The influences of mountains on the atmosphere. *Adv. Geophys.*, **21**, 87-230.
- Steenburgh, J.W., and T.I. Alcott, 2008: Secrets of the "Greatest Snow on Earth". *Bull. Amer. Meteor. Soc.*, **89**, 1285-1293.
- WMO, 2008: Guide to meteorological instruments and methods of observation. World Meteorological Organization Publ. WMO-No. 8, 681 pp.
- Zhu, C., D.P. Lettenmaier, and T. Cavazos, 2005: Role of antecedent land surface conditions on North American monsoon rainfall variability. *J. Climate*, **18(16)**, 3104-3121.

CHAPTER III

BIAS CORRECTION FOR IMPROVED REGIONAL CLIMATE MODELING OF THE
NORTH AMERICAN MONSOON**Abstract**

This chapter investigates how a form of climatological (mean) bias correction using linear regression improves the limitations of the Community Climate System Model (CCSM) version 4 when it is dynamically downscaled with the Weather Research and Forecasting (WRF) model for the North American Monsoon (NAM). To determine the mean bias, a 32-year historical climatological (1979-2010) baseline was established using the Climate Forecast System Reanalysis (CFSR). A comparison between the historical CFSR and version 4 of the Community Climate System Model (CCSM4) output revealed dramatic systematic biases in temperature, moisture, wind speed and direction, and geopotential height. CCSM4 biases occurred across the globe and throughout the profile of the atmosphere, but were most egregious across regions of complex terrain—underscoring the limitations of coarse grid resolution GCMs.

To quantitatively identify the effects of CCSM data on the NAM simulations, three 32-year climatologies were generated with WRF driven by (1) CFSR, (2) original CCSM, and (3) bias-corrected CCSM output. The WRF-CFSR simulations serve as a baseline for comparison. While NAM onset dates produced when downscaling original CCSM data occur up to three to four weeks too early over the core of the NAM, bias correction

produced onset dates that were generally within a week of the WRF-CFSR climatology. Additionally, bias-correction led to improvements in the mature phase of the NAM, reducing August root-mean-square-error values by 26% over the core of the NAM and 36% over the northern periphery. Comparison of the CFSR and the bias-corrected CCSM climatologies showed marked consistency in the general evolution of the NAM system. Dry biases in the NAM precipitation existed in each climatology with the original CCSM performing the poorest when compared to observations. The poor performance of the original CCSM simulations stem from biases in the thermodynamic profile supplied to the model through lateral boundary conditions. Bias-correction improved the excessive capping inversions, and mid-level mixing ratio dry biases ($2-3 \text{ g kg}^{-1}$) present in the CCSM simulations. Improvements in the bias-corrected CCSM data resulted in greater convective activity and a more representative seasonal distribution of precipitation.

1 Introduction

Providing a global perspective of the climate system, general circulation models (GCM) offer insight into basic climate variables on the large scale. Due to their coarse resolutions, GCMs are unable to accurately resolve fine-scale forcing such as those found by complex orography, coastlines, or land surfaces with strong heterogeneity (McGregor 1997). An increasing demand by the scientific community, policy makers, and the public to understand and anticipate changes to regional-scale climate systems have existed for several decades (Giorgi and Mearns 1991). At present, either statistical or dynamical methods are used to describe valuable small-scale processes that are not captured by GCM output. Statistical downscaling is the least computationally intensive method and

uses an empirical relationship between GCM output and finer scale or station observations. Dynamical downscaling utilizes a higher resolution limited area model based on physical principles (Dickinson et al. 1989). Commonly referred to as regional climate models (RCM), dynamic downscaling applications are often considered more capable due to their physical-based dynamical cores that capture fine spatial-scale non-linear effects that statistical downscaling does not (Denis et al. 2002; Antic et al. 2004). With higher resolutions and more sophisticated physics, dynamic modeling results are greatly improved, thus resulting in stronger reliability in future climate projections over the coarser resolution GCM output (Xu and Yang 2012). As summarized in Warner et al. (1997), one limitation of RCMs is their dependence on GCM output for initial conditions (IC), lateral boundary conditions (LBC), and sea surface temperatures (SST). Systematic biases inherent to the GCM output are subsequently transmitted, and potentially magnified by internal model feedbacks within the RCM (Warner et al. 1997; Noguer et al. 1998; Misra et al. 2003; Christensen et al. 2008; Bruyère et al. 2013). These transmitted biases add uncertainty within the RCM and in extreme cases can render the RCM inferior to the GCM (Kanamaru and Kanamitsu 2007).

Recently, in an attempt to reduce uncertainties in RCMs, various RCM bias correction techniques have proven effective in improving their performance (Kanamaru and Kanamitsu 2007; Misra 2007; Jin et al. 2011; Colette et al. 2012; Bruyère et al. 2013; White and Toumi 2013). This study focuses on the specific bias correction process where individual LBC variables are subjected to long-term, mean (climatological) bias correction (MBC). MBC is a simple and straightforward procedure that has proven

effective in improving the RCM's performance in climate modeling (Kirtman et al. 2002; Misra and Kanamitsu 2004; Sato et al. 2007; Cook and Vizu 2008; Wu et al. 2009; Patricola and Cook 2009; Xu and Yang 2012; Jin et al. 2011; Bruyère et al. 2013). Referencing the MBC method of correcting each LBC variable individually, Mishra and Kanamitsu (2004) notes "[this method] introduces a dynamical imbalance to the [LBCs] because the nonlinear terms are not necessary additive." While no previous studies have attempted to investigate RCM sensitivity to dynamical imbalances within the LBCs, imbalances potentially degrade the positive impact from bias correction. Furthermore, dynamic imbalances add an additional source of RCM uncertainty, ultimately reducing the reliability of future climate projections.

This study introduces and evaluates a form of bias correction using simple linear regression (SLR) and atmospheric dynamic equations, which minimize the dynamic imbalance problem across the LBC variables. To assess our bias correction procedure, three historical 32-year climatologies of the North American Monsoon (NAM) were simulated with a control simulation based on reanalysis to evaluate both original GCM, and bias-corrected GCM data.

The NAM is characterized by a pronounced increase in precipitation in June and July for northwestern Mexico and the southwestern United States. Dominated by perennially dry conditions, the NAM contributes approximately 40% and 70% of the annual total precipitation for the southwest U.S. and northwest Mexico, respectively (Douglas et al. 1993; Higgins et al. 1997). Although primarily a convective environment, a suite of

diverse processes spanning the mesoscale to the synoptic scale act in concert to produce the NAM (for a summary of these processes, refer to Barlow et al. 1998). For a comprehensive summary of the NAM, refer to Adams and Comrie (1997). With strong surface forcing and numerous feedbacks across the scales, the NAM performance in coarse resolution GCM applications tends to have notable biases (Meehl et al. 2006, Cook et al. 2012, Carvalho and Jones 2013; Bukovsky et al. 2013; Geil et al. 2013). Studies have shown that dynamic downscaling applications produce more realistic simulations of the NAM due to the improved surface representation (Higgins et al. 2006; Gutzler et al. 2009; Castro et al. 2012; Bukovsky et al. 2013). The intent of this study is to evaluate our RCM for the NAM over historical periods as well as to assess the efficacy of our bias correction process.

The data sources, the RCM model and the bias correction process are introduced in Section 2. Section 3 presents a performance evaluation and inter-comparison of the RCM results. Discussion, conclusions, and suggestions for future work are offered in Section 4.

2 Methodology and model configuration

Acting as an RCM, the Weather Research and Forecasting (WRF; Skamarock et al. 2008) model version 3.5.1 was used with initial conditions and LBCs provided by 1) the observation-based Climate Forecast System Reanalysis (CFSR; Saha et al. 2010) and 2) the Community Climate System Model version 4 (CCSM; Gent et al. 2011). The CCSM dataset is a subset of the output of the Community Earth System Model version 1. As

aforementioned, bias correction was performed on the CCSM dataset in an effort to reduce LBC uncertainties, resulting in a third set of forcing conditions provided to the WRF model. A description of the CFSR and CCSM datasets are presented as well the WRF model configuration as follows.

2.1 Data

2.1.1 Climate Forecast System Reanalysis data

Reanalysis data are often considered the best available representation of the historical state of the atmosphere and surface with the combination of modeling results and available observations. Produced by the National Center for Environmental Prediction (NCEP), the CFSR dataset provides global $\frac{1}{2}$ -degree grid spacing for upper-air data at 6-hour intervals on 37 vertical pressure levels. CFSR surface data are provided on a higher resolution 0.31° Gaussian latitude-longitude grid. The relatively higher resolution of the CFSR dataset than that of other reanalysis products such as the NCEP reanalysis better resolves surface forcing and mesoscale feedbacks. Additionally, by assimilating the high-quality Optimum-Interpolation Sea Surface Temperatures (OISST; Reynolds et al. 2007), the CFSR dataset captures the important seasonal cycle of Gulf of California (GoC) SST that are important to the development of the NAM (Mitchell et al. 2002).

2.1.2 Community Climate System Model output

This study used 6-hourly CCSM version 4 data provided on a $0.9^\circ \times 1.25^\circ$ latitude-longitude grid for the years 1979 to 2005 from the climate of the 20th century dataset, and the years 2006-2010 from the Representative Concentration Pathway 6.0 (RCP 6.0)

‘Mother of All Runs’ dataset. The RCP 6.0 member represents a specific pathway for atmospheric radiative forcing in response to climate forcing such as greenhouse gases as well as land use change (Van Vuuren et al. 2011). Falling in the middle of available RCP scenarios available, the RCP 6.0 scenario was chosen due to its middle-of-the-ground approach to future changes in radiative forcing.

To summarize an in-depth investigation on NAM performance across phase 5 of the Coupled Model Inter-comparison Project (CMIP5), Geil et al. (2013) found that when compared to the previous CMIP3 generation, CMIP5 members produced similar overall root-mean-square errors (RMSE) with improvements to onset and decay phases. However, while Geil et al. (2013) found noticeable improvements in onset and decay phases over CMIP3, the specific CCSM4 member was found to have some of the larger onset and retreat biases across the 21 CMIP5 model members. Median onset dates for CCSM4 between 1979 and 2005 were 41 days too early compared to observations, with retreat dates an average of 18 days too late. During the retreat stage, Geil et al. (2013) points to an extended connection to tropical moisture during the fall and winter seasons which hurts the ability to accurately capture the decay of the NAM. When comparing how CMIP5 members captured the 500-hPa height and wind fields, the CCSM4 member ranked in the top five for the development (May-June) and mature (July-August) phase, but not the retreat phase (September-October). Furthermore, when comparing 850-hPa circulation or surface precipitation patterns, the CCSM4 member had spatial correlations that were not among the top five (or bottom five) performing members. The comparisons presented by Geil et al. (2013) show that while the CCSM4 model improves over

previous generation models, the model's inability to accurately capture even the low-level circulation features limit the confidence in future scenarios of NAM influence. These weaknesses point to the necessity of dynamic downscaling coupled with bias-correction techniques in order to improve confidence in future NAM projections.

For CCSM data ingested into WRF, atmospheric data originally spanning 26 vertical sigma-hybrid levels were first interpolated to pressure levels. For consistency, we chose to match the 37 vertical pressure levels used by the CFSR. Following the CFSR convention, below-ground grid points (i.e. where the pressure level falls below the surface pressure) of moisture and wind speed variables were set to the surface values and lowest above-ground model level, respectively. Lastly, below-ground temperature and geopotential heights were subjected to extrapolation following the European Center for Medium range Weather Forecasting techniques described in Trenberth et al. (1993).

2.1.3 Gridded observation data

To evaluate the model, this study used the $\frac{1}{2}$ -degree resolution Climatic Research Unit dataset (CRU; Harris et al. 2014). The CRU dataset was chosen for its spatial coverage of both the southwestern U.S. and Mexico, as well as for its length of record. As a drawback to the spatial and temporal constraints of our NAM evaluation, the lower resolution of the CRU dataset limits the fidelity of the finer spatial variability and extremes of the NAM precipitation.

2.2 Regional climate model configuration

Developed by the National Center for Atmospheric Research (NCAR) with numerous community-contributed model physics, the WRF v3.5.1 model is well suited as an RCM due to its numerical stability for long-term integration. Spanning 1979 – 2010, our WRF simulations are initialized 00:00 UTC 01 April for each individual year and completed 00:00 UTC 01 November (to capture the full seasonal cycle of the NAM system), with the first month of each simulation disregarded to account for model spin-up. In an attempt to limit climate drift within the model, the choice to reinitialize individual years versus a single continuous simulation was based on findings by Pan et al. (1999) and Qian et al. (2003). These studies showed an inverse relationship between simulation length and model performance due to interactions between biased forcing data and internal model feedbacks.

The model domain (Fig. 3.1) uses a 150x180 horizontal grid centered over the southwestern U.S. and northern Mexico with 20-km grid spacing and 33 vertical sigma levels. Indicated by a solid red line, two regions used for our model evaluation are shown. These regions were adapted from eight smaller domains based on principal component analysis by Comrie and Glenn (1998) and explicitly defined in Castro et al. (2012). These two regions roughly delineate the core of the NAM, as well as the northern periphery. Land-use classification and topography for WRF was provided by the 2-minute United States Geologic Survey 24-category dataset, and the 6-hourly sea surface temperatures (SST) provided by the forcing data were assimilated into the model.

Sensitivity tests to determine the optimal suite of WRF physics for our domain were first conducted over the 1999 NAM season. Using spatial statistics of bias, correlation, and RMSE, precipitation and temperature patterns from approximately 100 permutations of the available WRF physics were compared to observations (Figures not shown). The 1999 NAM season was chosen for testing as this year is considered an above average (or wet year) for both the core region in Mexico and the northern periphery in the southwestern U.S. Calibrating model physics over an active monsoon year ensures the presence of the convective environment associated with the NAM. With both model stability and precipitation accuracy in mind, we selected physics options of Lin et al. (Microphysics; Lin et al. 1983), the Rapid Radiative Transfer Model scheme (Longwave; Mlawer et al. 1997), Dudhia (Shortwave; Dudhia 1989), Monin-Obukhov (Surface layer physics; Jimenez 2012), MYNN2.5 (Planetary Boundary Layer; Nakanishi and Niino 2006), and Grell-3 (Cumulus; Grell and Devenyi 2002). Land surface physics were described using the Community Land Model version 4.0 (Lawrence et al. 2011). These model physics were used for the subsequent simulations described throughout the remainder of this paper.

2.3 Simple linear regression bias correction

Throughout this paper, we will highlight some of the more noticeable systematic long-term biases throughout the CCSM atmosphere when compared to the CFSR dataset. Through our comparison of both CFSR and CCSM atmospheric variables (e.g. temperature (T), relative humidity (RH), geopotential height (Z), and zonal (U) and meridional (V) winds), we note that varying degrees of bias can be found throughout the

atmosphere over the NAM region for each of these variables both spatially and temporally. In addition, the coarse CCSM grid results in significant bias for surface variables such as 2-meter T and RH, and surface pressure--most notably over complex orography.

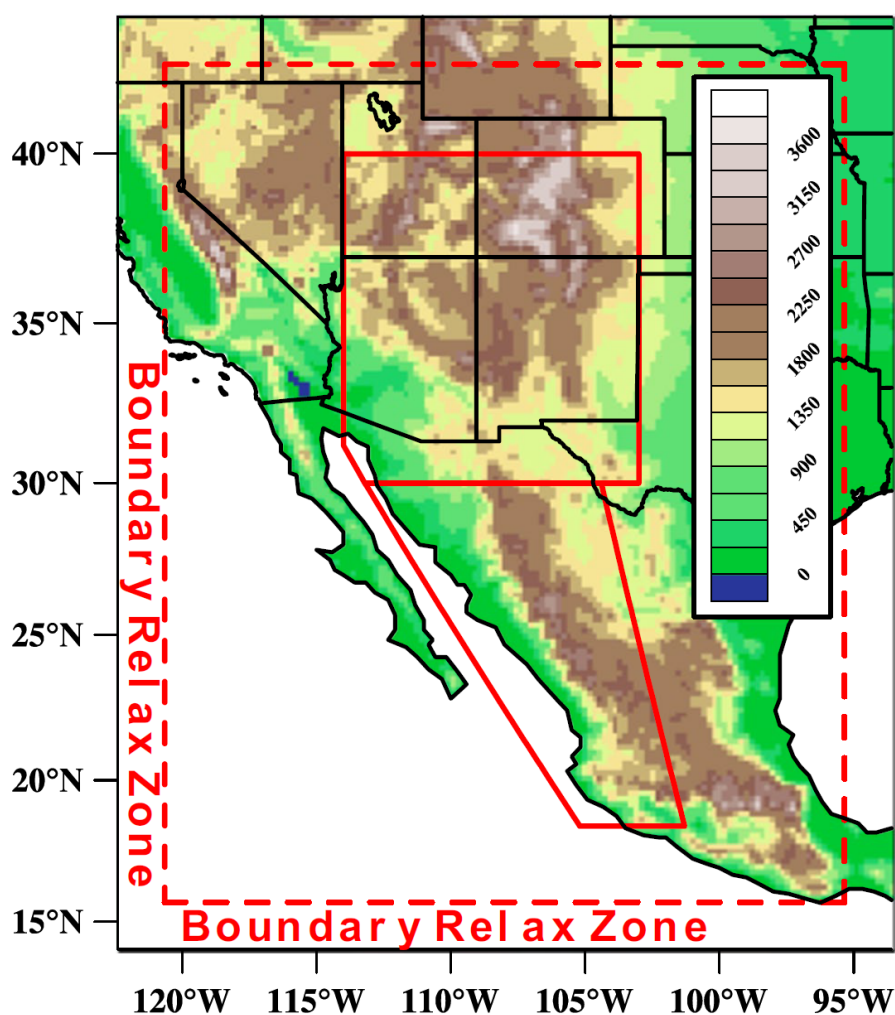


Fig. 3.1 WRF model domain with model-resolved topography (meters). The boundary relax zone where lateral boundary conditions are assimilated is illustrated with a dashed red line. Two regions used for model evaluation (adapted from Castro et al., 2012) are drawn using a solid red line.

In order to improve the quality of our simulations when using the CCSM dataset, long-term biases must first be reduced. The final step before bias correction was performed was horizontal bilinear-interpolation re-gridding of the CCSM output to match the $\frac{1}{2}^\circ$ resolution CFSR domain. This was accomplished using the Earth System Model Framework regridding software included in the National Center for Atmospheric Research Command Language (<https://www.ncl.ucar.edu/Applications/ESMF.shtml>). Although the process of bilinear-interpolation can itself introduce bias (especially for surface variables over complex terrain), the re-gridded CCSM data only serves as an intermediate step before bias correction is performed. Therefore, any biases introduced through the regridding are accounted for by the regression model, and subsequently removed during the bias correction process. Meanwhile, the original CCSM data used in our downscaled simulations remain on the original $1.25^\circ \times 0.9^\circ$ grid. With the CCSM data now sharing the same vertical and horizontal grids as CFSR data, 32 years of historical data for each 6-hour time step in the calendar year were used to build an SLR model at every grid point in the atmosphere and along the surface. Using the SLR model, the original CCSM output undergoes a correction:

$$CCSM_{Corrected} = m \cdot CCSM_{Original} + b \quad (1)$$

where m is the regression coefficient, and b represents the intercept of the best-fit regression line. For the remainder of the paper, the original CCSM data are referred to as $CCSM_O$ while the bias-corrected CCSM data are referred to as $CCSM_{BC}$.

Whereas bias correcting every variable independently introduces physical inconsistencies, we identify T and RH (atmospheric and 2-meter height), surface temperature (T_{SFC} ; including SST) and surface pressure (P_{SFC}) as key variables that can be used to derive the remaining forcing dataset. With several options to quantify atmospheric moisture [i.e. RH or specific humidity (Q)], steps were taken to determine the most appropriate variable. Initial tests correcting Q showed that when combined with the corrected T, unrealistic RH values were produced where saturation vapor pressures are very small (e.g. upper atmosphere and polar regions etc.). These unrealistic scenarios occurred because of the reliance on independently corrected T and Q to compute RH, which is physically bounded between values of 0% and 100%. While the long-term bias for these variables looks improved, certain conditions on individual time frames led to the unrealistic values and greater RH biases than in the original data. For this reason, RH data were bias corrected rather than Q. CCSM_O RH were obtained by computing vapor pressure and saturation vapor pressure:

$$RH = \frac{e(Q)}{e_s(T)} \cdot 100 \quad (2)$$

where e is the vapor pressure (a function of Q), and e_s represents saturation vapor pressure (a function of T). For this step, e and e_s were computed using a higher-order polynomial valid within ± 100 °C according to International Temperature Scale standards (ITS-90) described in Hardy (1998). By correcting RH and calculating Q, we remove the bias in the CCSM_O atmospheric saturation state, while maintaining the consistency between T and Q.

Low- and mid-level atmospheric moisture supply is a critical component of the NAM, and findings by Bukovsky et al. (2013) demonstrated the limitations these dry biases have when dynamically downscaling the NAM. Focusing over the Eastern Tropical Pacific, CCSM_O data contains RH dry-biases on the order of 20-30% in the CCSM_O data, and T warm-biases on the order of 1-2 degrees Celsius. To further illustrate biases in the CCSM_O data, and demonstrate improvements in the CCSM_{BC} data, the May-August mixing ratio (g kg^{-1}) climatology at 850-hPa is compared in Fig. 3.2, with Fig. 3.3 comparing 700-hPa mixing ratio climatologies of (A) CFSR, (B) CCSM_O, and (C) CCSM_{BC}. Panels (D) and (E) show the difference between CCSM_O, CCSM_{BC}, and CFSR, respectively. When computing CCSM_O mixing ratios (a function of T and RH), dry biases exist on the order of 0.5 g kg^{-1} lower than the CFSR at 850-hPa and 2 to 3 g kg^{-1} lower at 700-hPa. We note the consistency between the CCSM_{BC} and the CFSR mixing ratio climatologies, especially over the complex terrain across the Western United States. Despite not directly correcting mixing ratio data, the correction of T and RH and subsequent calculation of mixing ratio produced a climatology consistent with CFSR.

2.4 Deriving the remaining bias corrected variables

2.4.1 Mean sea level pressure

With mean sea level pressure (P_{MSL}), a function of P_{SFC} , we used the bias corrected P_{SFC} data to derive P_{MSL} using the barometric formula:

$$P_{\text{MSL}} = P_{\text{SFC}} \cdot e^{\left(\frac{g \cdot Z_{\text{SFC}}}{R_d \cdot T_v}\right)} \quad (3)$$

where P_{SFC} is the surface pressure, g is the acceleration due to gravity, Z_{SFC} is the surface geopotential height, R_d is the dry air constant, and T_v is virtual temperature.

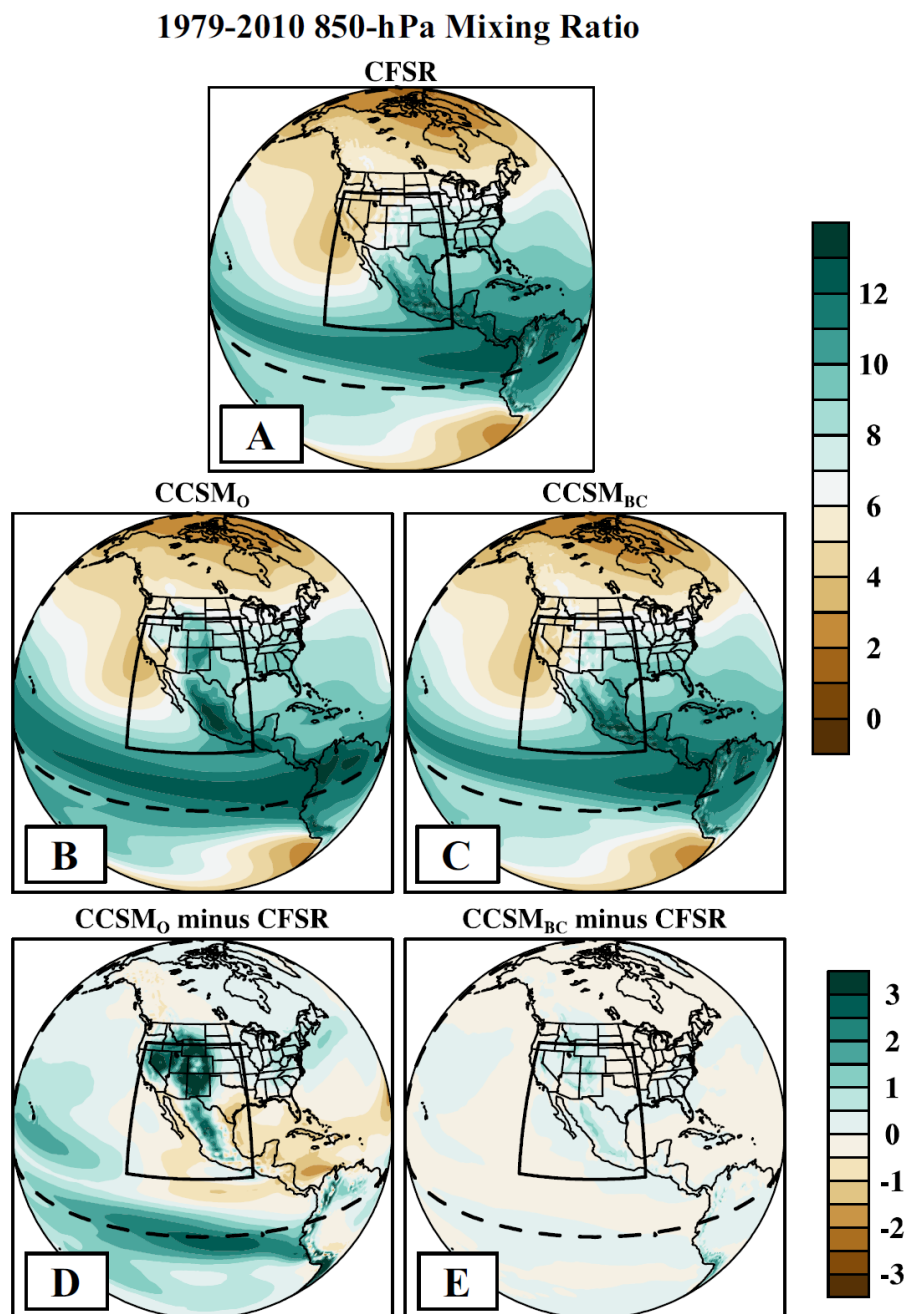


Fig. 3.2 Climatological (1979-2010) May-October 850-hPa Mixing Ratio (g kg^{-1}) for (A) CFSR, (B) original CCSM, and (C) bias-corrected CCSM datasets. Differences between the original CCSM and CFSR (D) and the bias-corrected CCSM and CFSR (E) are shown. The model domain is overlaid to illustrate the differences each set of lateral boundary conditions will supply the model.

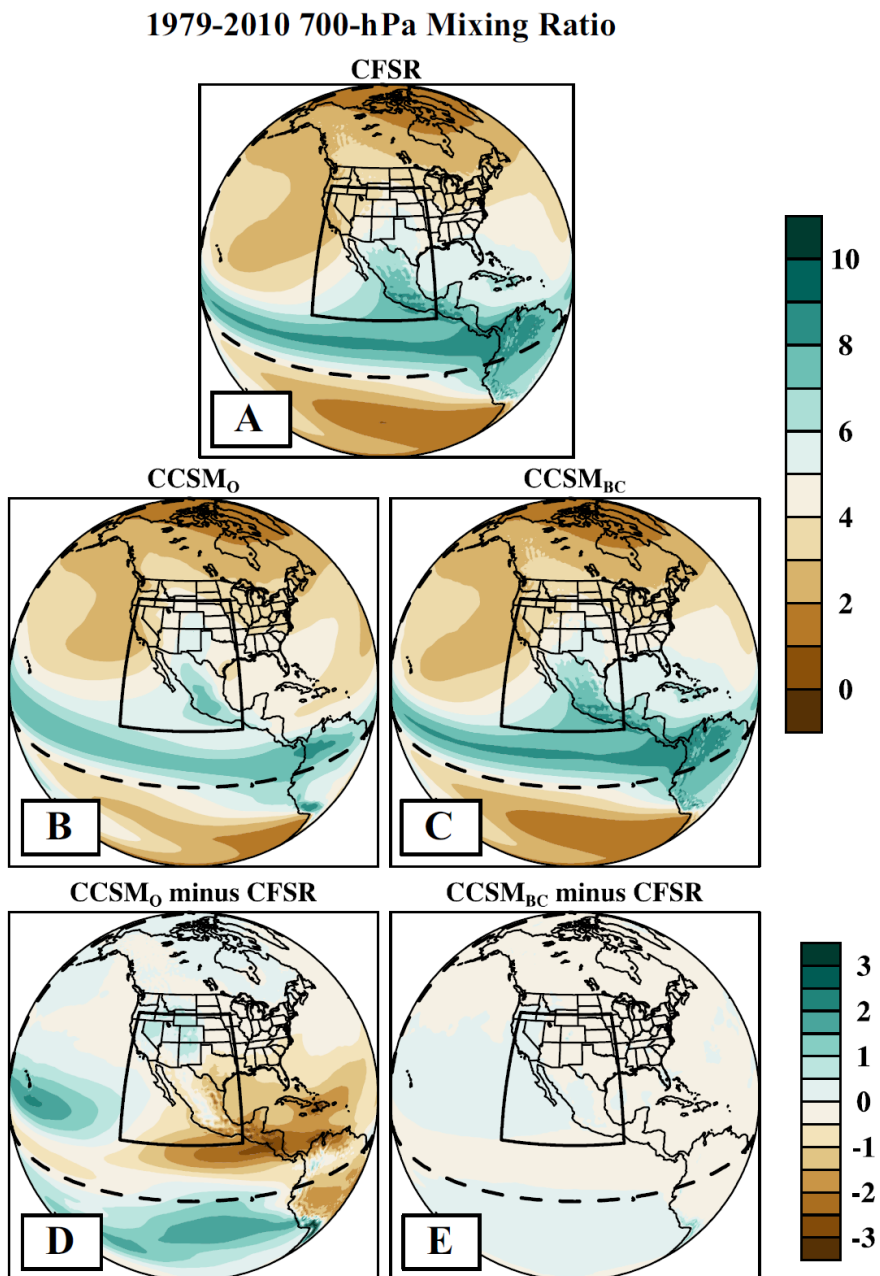


Fig. 3.3 As in Figure 3.2, but for 700-hPa. Note the significant dry bias in the original CCSM data (D) along the Eastern Tropical Pacific.

Due to a lack of Z_{SFC} provided on the $\frac{1}{2}$ -degree grid, we created our own. This process is discussed in detail in Part b of this section. T_v uses mixing ratio data acquired after bias correction of RH and T to adjust the temperature to account for water vapor's effect on air density:

$$T_v = T \frac{w + \varepsilon}{\varepsilon(1+w)} \quad (4)$$

where T is the actual temperature, w is the mixing ratio, and ε represents the ratio of the mass of dry air versus the mass of moist air.

2.4.2 Geopotential height

With the bias-corrected T and RH fields, a corrected Z field is derived by summing the thicknesses produced when solving the hypsometric equation between each pressure level:

$$Z = \frac{R_d \bar{T}_v}{g} \cdot \ln \left(\frac{P_1}{P_2} \right) \quad (5)$$

where R_d represents the gas constant for dry air, \bar{T}_v represents the mean-layer virtual temperature, g represents the acceleration due to gravity, and P_1 and P_2 represent the pressure at the top and bottom of the layer (Holton and Hakim 2013).

2.4.3 Zonal and meridional winds

Using the corrected Z field, the remaining U- and V-winds can be approximated by the geostrophic wind. Geostrophic wind is the wind resulting from a balance between the pressure gradient force and the Coriolis effect.

The geostrophic wind can be expressed by zonal and meridional terms, which are functions of gradients in the corrected Z:

$$U_g = -\frac{g}{f} \cdot \frac{\partial Z}{\partial y}, \quad V_g = \frac{g}{f} \cdot \frac{\partial Z}{\partial x} \quad (6)$$

where f is the latitudinal-dependent Coriolis parameter. The geostrophic component controls the atmospheric circulation patterns, with cyclonic (counter-clockwise) rotation around low- pressure systems and anti-cyclonic rotation (clockwise) around high- pressure systems in the northern hemisphere and vice-versa in the southern hemisphere.

However, actual winds are comprised of both a geostrophic component (\overline{V}_g) and an ageostrophic component (\overline{V}_a).

$$\overline{V} = \overline{V}_g + \overline{V}_a \quad (5)$$

Representing the deviation of the true winds from geostrophy, \overline{V}_a is difficult to quantify. For mid-latitudes, \overline{V}_a is generally an order of magnitude smaller than \overline{V}_g , but where external forces such as friction near the surface and centripetal forces in curved flow exist, large deviations from geostrophy can occur. With pure geostrophy rarely occurring in the atmosphere, \overline{V}_a winds play a critical role in the general dynamics of the atmosphere.

Aside from improvements to the spatial variability near the surface due to the higher grid resolution, alterations to the general storm track were minor. Knowing this, we decided the original \overline{V}_a field was likely a reasonable approximation of the general

dynamics associated with the corrected wind fields. To ensure \overline{V}_a is best represented, we compared two different sets of wind using the CCSM_O \overline{V}_a and a bias corrected \overline{V}_a with the CFSR data following the similar SLR method as previously described. These comparisons showed minimal deviation between either source of \overline{V}_a . WRF simulations driven by the complete set of CCSM_{BC} data and both sets of \overline{V}_a were conducted over a dry and a wet monsoon year. In each case, comparative precipitation patterns were produced. Thus, we chose to use the bias-corrected \overline{V}_a data for the sake of consistency with how the previous variables were corrected.

In the tropics where the Coriolis effect becomes minimal, the local Rossby number shows that the use of geostrophic components (assuming a balance between Coriolis and pressure gradient terms) to approximate winds is inappropriate below approximately 20° latitude. Within this zone, we rely on the CCSM_O winds. In order to retain a smooth transition between the CCSM_O winds in the tropics, and the derived winds above 20° latitude, a region between 15° and 20° was first set to missing values. By using the non-missing neighboring grid cells bounding each line of longitude as boundary conditions, the Poisson's equation was solved via relaxation. To further smooth the transition zone, the region between 17.5° and 20° latitude was averaged with the derived wind field. With the final wind fields computed, only soil temperature and moisture remained.

2.4.4 Soil temperature and moisture

Soil properties are required for the initial conditions provided to the land-surface model (LSM) within WRF. The LSM is responsible for computing the subsequent soil properties based on the modeled land-air interactions. Two WRF scenarios using the CCSM_{BC} were tested for years with above- and below-average NAM precipitation. Each simulation was initialized with either the actual CFSR soil initial conditions for that year or a 32-year climatology of the model start date of the CFSR soil conditions. Due to the LSMs interaction with the atmospheric radiation and precipitation inputs, both sets of upper soil levels converged on a single solution well before the allotted spin-up period. By running the WRF model for individual years and not continuously, the influence of the lower soil properties is minimal. For our application, climatology soil conditions are reasonable to use with the CCSM_{BC}.

2.5 Evaluation of impacts from bias correction

To understand how the bias-correction process impacts characteristics of the CCSM_O data beyond the removal of the long-term bias, we investigated how trends were changed, as well as how the seasonal cycle of individual years were affected. Preserving the original trend produced by the RCP6.0 radiative pathway within the CCSM_{BC} is important when downscaling for long climatologies as well as future projections. Xu and Yang (2012) reported that their form of MBC did not affect original trends. Despite using a different form of bias correction, when focusing on the atmospheric profile of T and RH over the NAM region, we confirmed that our SLR method preserves long-term trends associated with the CCSM_O data (Figures not shown).

Comparing seasonal variability for individual years demonstrated the impact our SLR model has on the day-to-day weather and state of the atmosphere. Assessing the three datasets at specific grid points over individual years showed the day-to-day weather variability remained intact. The overall seasonal cycle remained largely consistent with the original pattern. More will be presented in Section 3 regarding the adjustment of the long-term seasonal variability. With a mostly linear correction of the CCSM_O data (Eq. 1), only the yearly mean showed noticeable correction. With GCM models not representative of historical inter-annual variability, comparison between CFSR and both CCSM datasets is not informative and assessment of whether a specific year is improved is not possible.

3 Historical evaluation

This section demonstrates the differences in the LBCs from each of the three sets of forcing data (Section 3.1) as well as the impact these differences have when forcing the WRF model (Section 3.2). The remainder of this paper focuses on comparisons between the 1979-2010 climatologies.

3.1 Lateral boundary conditions

Compared to the CFSR LBCs, improvements are noticeable at all levels of the bias-corrected LBCs. Fig. 3.4 plots the 1000- to 100-hPa average bias and RMSE of T and mixing ratio of the CCSM_O and the CCSM_{BC} along each of the four boundary relax zones shown in Fig. 3.1. Cold biases on the order of 2-4 °C are most notable in the upper atmosphere of the CCSM_O data, with the northern boundary containing the largest biases.

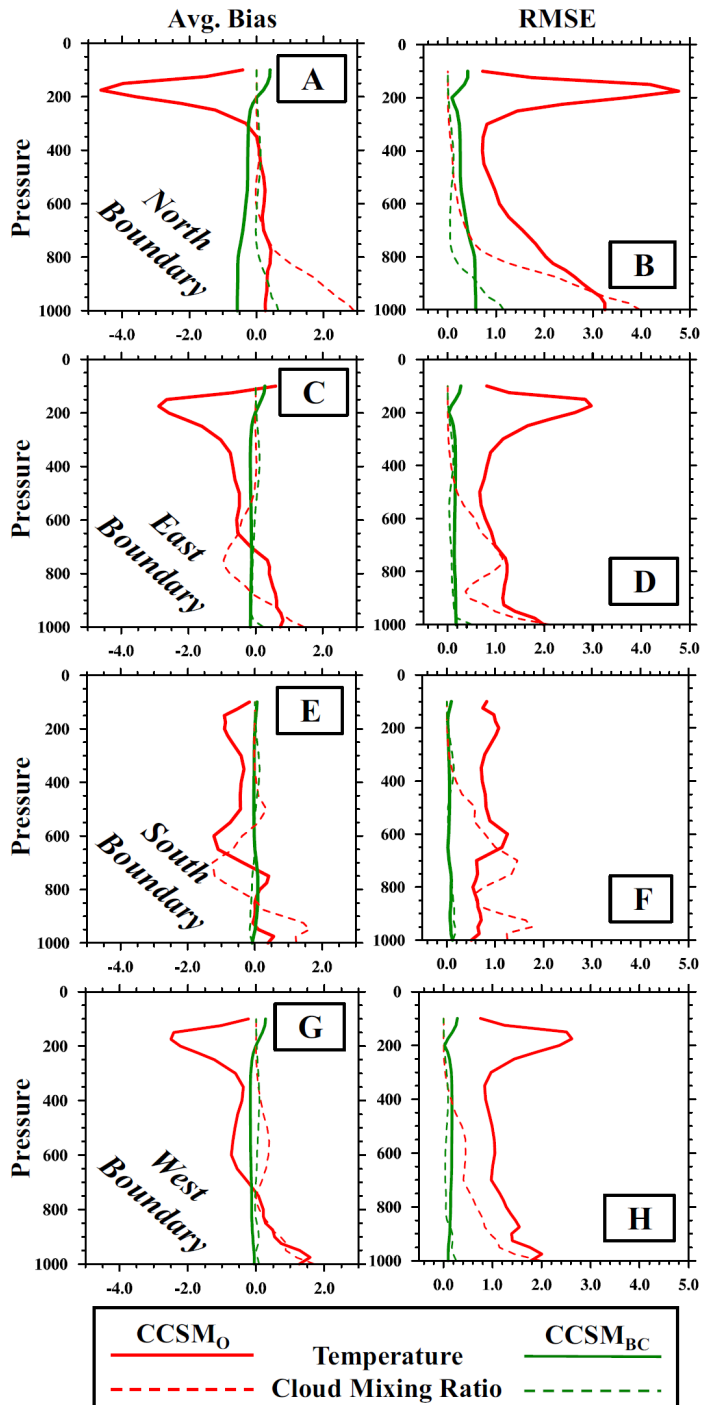


Fig. 3.4 Comparison of the vertical profile of average bias (left) and RMSE (right) along each lateral boundary relax zone for temperature ($^{\circ}\text{C}$; solid lines) and mixing ratio (g kg^{-1} ; dashed lines) forcing data provided by CCSM_O (red) and CCSM_{BC} (green).

Already demonstrated in Fig. 3.2 and Fig. 3.3 are the dry biases in mid-level mixing ratio along the Eastern Tropical Pacific. When interpolated to the LBCs, these dry biases translate to RMSE values on the order of 1 to 1.5 g kg⁻¹ along the southern and eastern boundaries.

To address how the bias-correction process not only improves the spatial pattern but seasonal evolution of the NAM as well, we compare the three forcing datasets 700-hPa temperature and moisture climatologies where dry biases were most evident, especially along the southern boundary (refer to Fig. 3.4). Using a 5-day running average spanning 01 April to 01 November, Fig. 3.5 compares the LBCs of T and mixing ratio. Averaging over the four boundary relax zones, Fig. 3.5 illustrates how our bias correction improved both the seasonal evolution and peak values of the forcing data.

The evolution of the warm-season SSTs over the GoC are important for the land-sea interaction influencing diurnal processes such as the low-level jet and the orographic flows over the Sierra Madre Occidental (Douglas 1995; Douglas et al. 1998; Mitchell et al. 2002). Having a geospatially difficult shape to resolve with coarse resolution grids, the GoC characteristics are poorly resolved by the CCSM_O. Averaging over the area indicated by grey shading, Fig. 3.6 shows how the three forcing datasets (interpolated to the 20-km WRF grid) capture the evolution of GoC SST. With the CFSR relying on the high-fidelity OISST dataset, the bias-corrected SST resolves a more accurate warming during the onset period, and more appropriate timing of the peak SSTs than the CCSM_O SSTs.

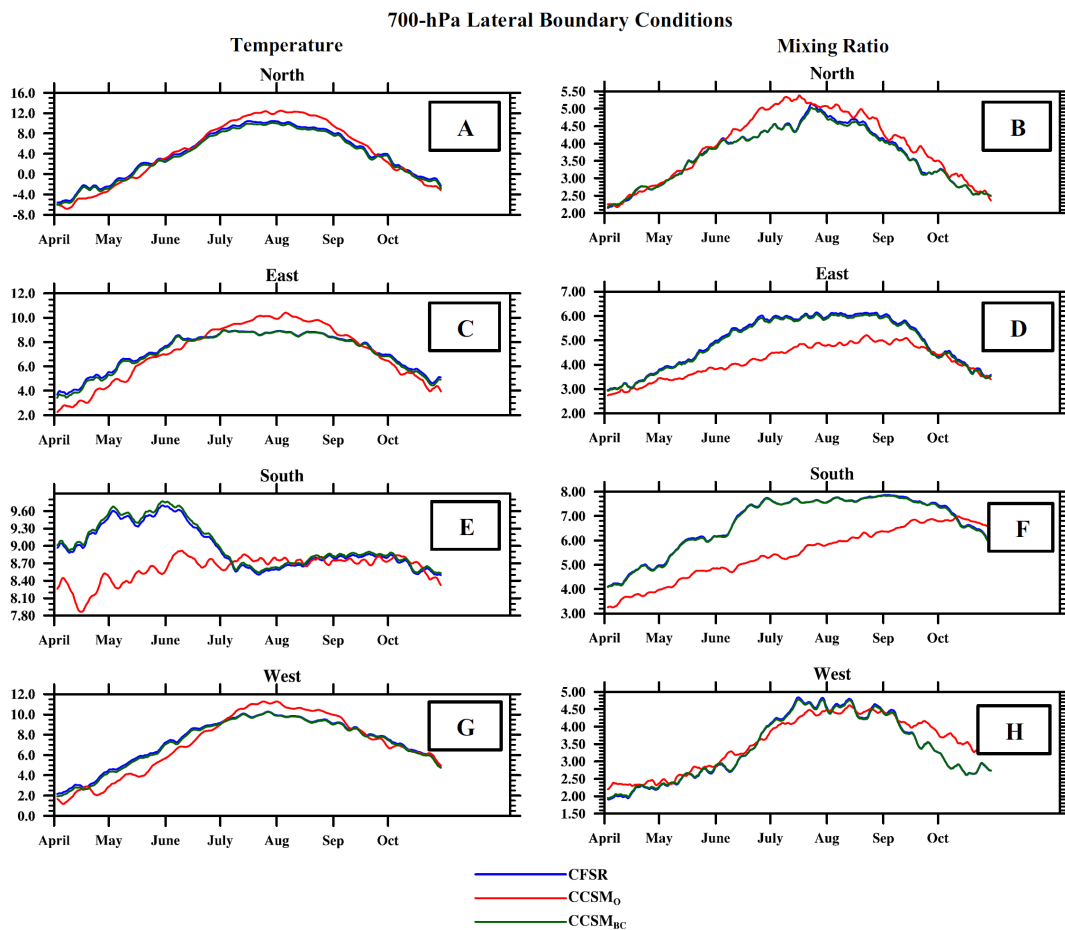


Fig. 3.5 Timeseries showing the climatological (1979-2010) 700-hPa lateral boundary conditions of temperature ($^{\circ}\text{C}$) and mixing ratio (g kg^{-1}) through the 01-Apr to 01-Nov time period. Temperatures are shown in the left column with mixing ratio in the right column. Averages for each panel are taken over the northern (A, B), eastern (C, D), southern (E, F), and the western boundary (G, H) relax zones.

These differences in seasonal timing and peak values between the CCSM_O and the CCSM_{BC} GoC SST data directly affect the contribution of low-level heat and moisture through surface fluxes. With the CCSM_O having warmer GoC SSTs preceding the NAM onset, warming and moistening of the low-levels occurs too early. Furthermore, the

cooler GoC SSTs in the CCSM_O during the mature phase suppress the contribution of surface fluxes. With a less dramatic land-sea temperature contrast during the mature NAM phase in CCSM_O, the low-level jet off the west coast of Mexico is limited (Figure not shown) as is the moisture advection associated with this mechanism.

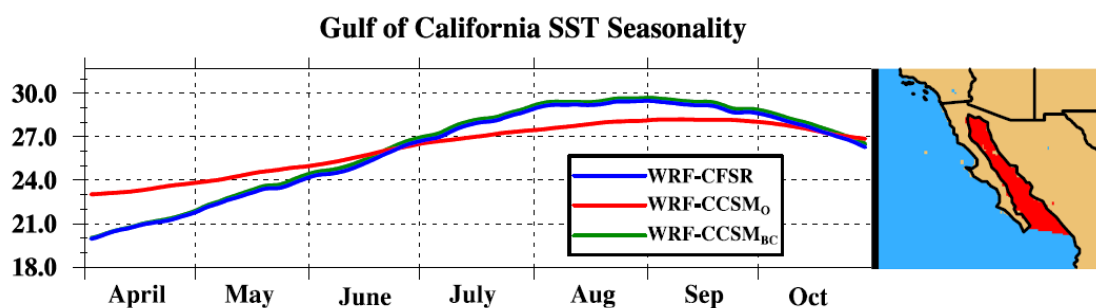


Fig. 3.6 Timeseries of the sea surface temperatures in the Gulf of California for the CFSR (blue line), original CCSM (red line), and the bias-corrected CCSM (green line) after interpolation to the 20-km model grid. The specific grid points included in the average are shaded with red in the spatial map attached to the right of the figure.

3.2 Regional climate model simulations

3.2.1 North American monsoon precipitation

CRU observations of the average 1979-2010 JJAS precipitation climatology are compared to the three WRF climatologies in Fig. 3.7. A systematic dry bias is present in each of the three WRF climatologies with the WRF-CCSM_O having the largest bias, and the WRF-CCSM_{BC} producing biases more consistent with the WRF-CFSR climatology.

1979-2010 J-J-A-S Precipitation [mm day⁻¹]

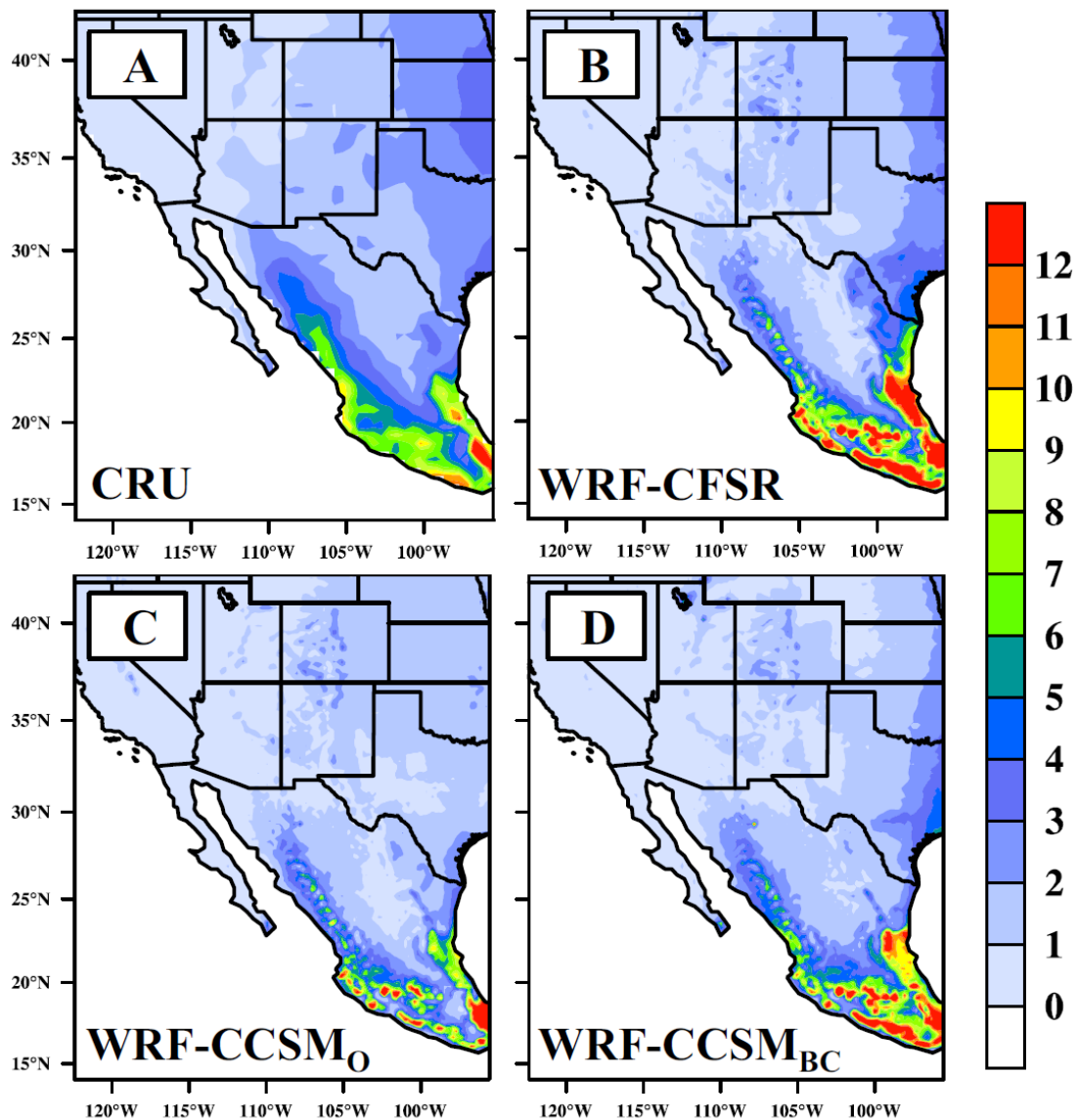


Fig. 3.7 Average 1979-2010 June-July-August-September precipitation (mm day⁻¹) for (A) the CRU gridded-observations, (B) downscaled CFSR, (C) downscaled original CCSM, and (D) the downscaled bias-corrected CCSM.

Comparing against CRU observations, Table 3.1 provides monthly and JJAS average bias and RMSE values (mm month^{-1}) over the northern evaluation region (NER) and southern evaluation region (SER) for each of the three climatologies. Coinciding with the spatial average shown in Fig. 3.7, the WRF-CCSM_{BC} JJAS period saw improvements over the WRF-CCSM_O of 16.5 versus 17.1 and 50.1 versus 55.0 mm month^{-1} in the NER and SER, respectively. For monthly comparisons, most notable are WRF-CCSM_{BC} improvements during the mature phase when the NAM is most active. The month of August showed a 36% improvement in RMSE for the NER (24.0 versus 37.5 mm month^{-1}) and a 26% improvement for the SER (56.5 versus 75.6 mm month^{-1}). Whereas the month of May saw improvements similar to August over both evaluation regions, the month of June featured a 45% greater RMSE for WRF-CCSM_{BC} over the SER (46.7 versus 32.3 mm month^{-1}) and a 9% improvement for the NER (13.7 versus 15.0 mm month^{-1}). For July, RMSE values are comparable in magnitude in both evaluation regions, but while the WRF-CCSM_{BC} NER was better in June, July showed a 7% higher RMSE. Similarly, while the SER was worse in June for the WRF-CCSM_{BC}, a modest 3% improvement was found in July compared to WRF-CCSM_O. The timing of the specific month where the WRF-CCSM_{BC} performs worse than WRF-CCSM_O coincides with the timing of the onset of the NAM where June (July) is typically considered the month of onset in the SER (NER). To investigate this, we look to the differences in NAM onset timing between each forcing dataset.

Table 3.1 Monthly and JJAS average bias and RMSE statistics for the northern and southern evaluation regions (Fig. 3.1) for the three WRF climatologies when compared to the CRU gridded observations. Before computing the statistics, the WRF output was first re-gridded to match the CRU grid.

	May	Jun	Jul	Aug	Sep	Oct	JJAS
<i>Northern evaluation region</i>							
Average bias							
WRF-CFSR	9.5	0.3	-8.8	-15.2	-11.3	0.2	-8.7
WRF-CCSM _O	18.2	7.9	-12.2	-34.8	-12.1	2.4	12.8
WRF-CCSM _{BC}	8.0	-0.5	-15.9	-19.4	-12.7	-2.6	12.1
RMSE							
WRF-CFSR	15.5	8.9	16.4	20.7	16.7	8.7	13.7
WRF-CCSM _O	24.0	15.0	20.1	37.5	16.6	9.9	17.1
WRF-CCSM _{BC}	18.5	13.7	21.6	24.0	18.2	9.7	16.5
<i>Southern evaluation region</i>							
Average bias							
WRF-CFSR	1.9	-20.9	15.9	14.5	29.8	-5.8	-20.3
WRF-CCSM _O	28.5	-6.1	-46.2	-53.3	-43.1	11.4	37.2
WRF-CCSM _{BC}	-0.8	-33.1	-21.2	-7.5	-45.5	-18.2	26.8
RMSE							
WRF-CFSR	6.4	40.3	69.4	70.3	56.5	19.2	55.1
WRF-CCSM _O	37.1	32.3	65.2	75.7	63.1	25.6	55.0
WRF-CCSM _{BC}	6.1	46.7	63.6	56.5	61.0	26.5	50.1

Higgins et al. (1997) defines a monsoon onset date as the first three-day period where the daily precipitation exceeds 0.5 mm day^{-1} . Fig. 3.8 shows the average onset date over the 32-year climatology for each of the three climatologies, as well as the difference between the WRF-CFSR and the WRF-CCSM_O and WRF-CCSM_{BC}. Corresponding to larger May and June precipitation for the WRF-CCSM_O (Table 3.1), earlier onset dates are overwhelmingly found when compared to the WRF-CFSR. Furthermore, the later onset dates shown for the WRF-CCSM_{BC} coincide with the drier month of June over the SER, as well as the drier month of July over the NER. With the model producing overall

dry biases, the WRF-CCSM_O onset months of June in the SER and July in the NER produce better RMSE values due to the earlier onset offsetting the dry biases inherent to the model itself. We have demonstrated the poor seasonal cycle associated with the CCSM_O GoC SST's, which would promote earlier development of associated NAM mechanics. Although the warmer early-season GoC SSTs in the CCSM_O would promote earlier onset in the surrounding areas, the domain-wide consistency of earlier onset dates suggests a linkage to biases in the LBCs. Further discussion on the impact of the LBCs on the evolution of NAM features is given in the following section.

3.2.2 North American monsoon evolution

Biases within the CCSM_O data have been discussed, but how these biases influence the seasonal cycle of the NAM within the model domain is the focus of this section. To begin, Fig. 3.9 focuses on the climatological northward migration of NAM moisture using a time-versus-latitude average of the precipitable water (Pwat). Pwat represents the total integrated atmospheric moisture within the model column (surface to model-top). The spatial region over which the average is taken is attached to the right of each panel with model terrain height as in Fig. 3.1 included. Panels D and E show the Pwat differences between the CFSR and the two CCSM climatologies. While Pwat values do not directly relate to precipitation, higher Pwat allows more intense rainfall rates when convection does occur. Similar to the comparison of GoC SSTs (Fig. 3.6), the seasonal evolution and timing of peak values appear relatively consistent between the WRF-CFSR and WRF-CCSM_{BC}.

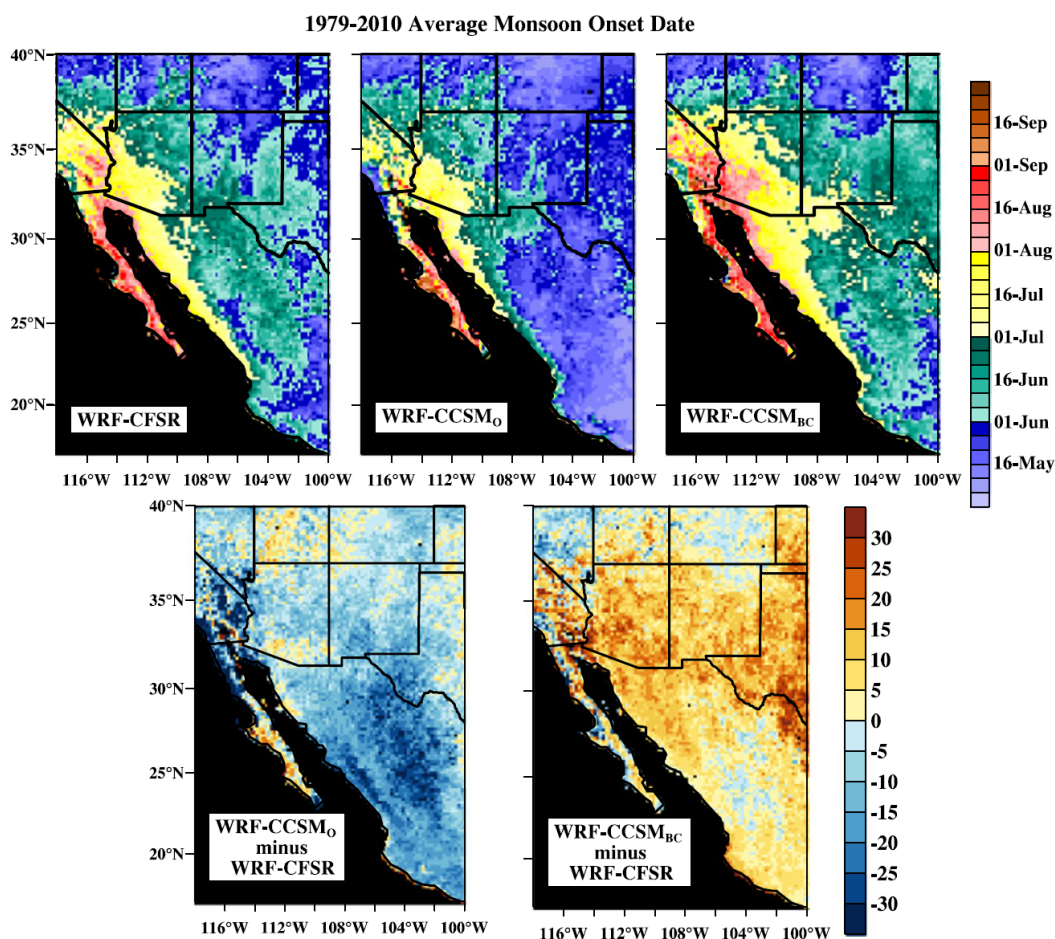


Fig. 3.8 1979-2010 average monsoon onset dates for the three WRF climatologies (top row) with differences between the two WRF CCSM climatologies and WRF-CFSR (Bottom row). Onset dates are defined as the first three-day period where greater than 0.5 mm day⁻¹ occurred each day.

In agreement with earlier onset dates of the WRF-CCSM_O, the April-May-(early) June Pwat within the WRF-CCSM_O is characterized by positive (wet) biases at all latitudes on the order of 2 to 10 mm with the largest biases occurring in the tropics between 20°N and 30°N. By late June, each climatology successfully captures the

northward progression of higher Pwat values. However, between 30°N and 40°N, both CCSM climatologies contain Pwat values that are generally 2 to 6 mm lower than the WRF-CFSR, although the WRF-CCSM_{BC} was slightly less biased overall. Positive biases in the WRF-CCSM_O return during the decay period (late September and October), with 4 to 10 mm higher Pwat, while the WRF-CCSM_{BC} is more comparable to WRF-CFSR with biases between -2 and +2 mm.

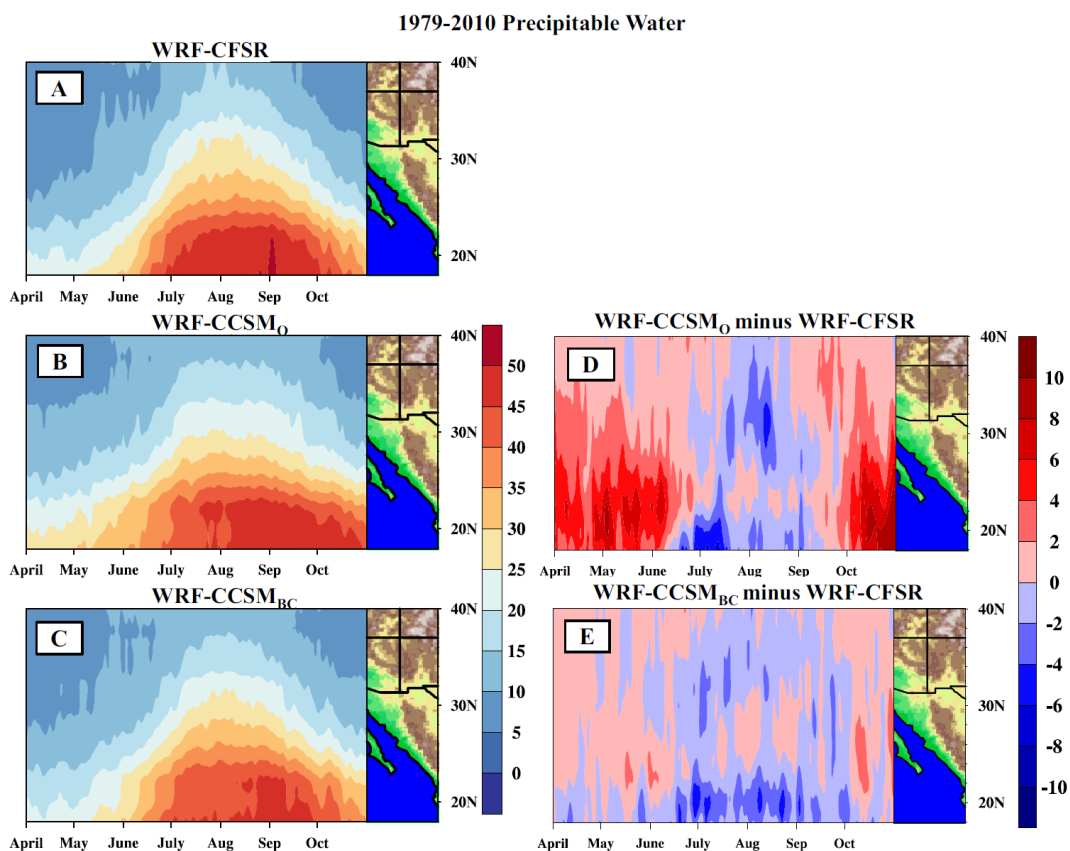


Fig. 3.9 Time-versus-latitude plot for climatological precipitable water (mm) spanning 01 April to 01 November for WRF-CFSR (A), WRF-CCSM_O (B), and WRF-CCSM_{BC} (C). Difference plots are shown for WRF-CCSM_O (D) and WRF-CCSM_{BC} (E). The area used to compute the time average is attached to the right of each panel with color fill representing terrain height as in Fig. 3.1.

With the primary driver of NAM precipitation coming from thermodynamic forcing as opposed to synoptic forcing, we look to understand how LBC biases influence the thermodynamic profile within the model. Above the planetary boundary layer, where surface forcing becomes negligible, the thermodynamic profile is primarily controlled by the LBCs. A useful indicator of the seasonal cycle of convective potential, a time-versus-latitude plot showing convective available potential energy (CAPE; color contours) is presented in Fig. 3.10, with contour lines of convective inhibition (CIN) overlaid. CAPE represents the positive buoyancy of the atmosphere and is an indicator of atmospheric instability, while CIN represents the amount of energy that acts to prevent rising air from attaining the level of free convection (LFC). We point out that although all three climatologies have comparable CAPE values north of $\sim 30^\circ\text{N}$, below this latitude, the WRF-CCSM_O contains significantly more CAPE than the other climatologies with the majority of biases above 500 J kg^{-1} and the largest biases in excess of 1000 J kg^{-1} . CIN contours shown in Fig. 3.10 indicate the presence and strength of low-level temperature ‘capping’ inversions. Large CIN values indicate strong capping inversions, which act to suppress deep convection. Small CIN values indicate an environment more favorable for convection. Both the WRF-CFSR and the WRF-CCSM_{BC} climatologies exhibit large CIN values below 30°N preceding the onset phase compared to the WRF-CCSM_O. While these climatologies depict a weakening of CIN during the mature phase, the WRF-CCSM_O show increasing CIN, expanding northward.

The presence of persistent and strengthening CIN throughout the NAM environment in the WRF-CCSM_O lends evidence to why despite similar P_{wat} to the WRF-CCSM_{BC},

the mature NAM phase produces noticeably less precipitation. Furthermore, the lower CIN, higher CAPE, and larger Pwat during the months leading up to the NAM helps explain the earlier onset dates produced by the WRF-CCSM_O.

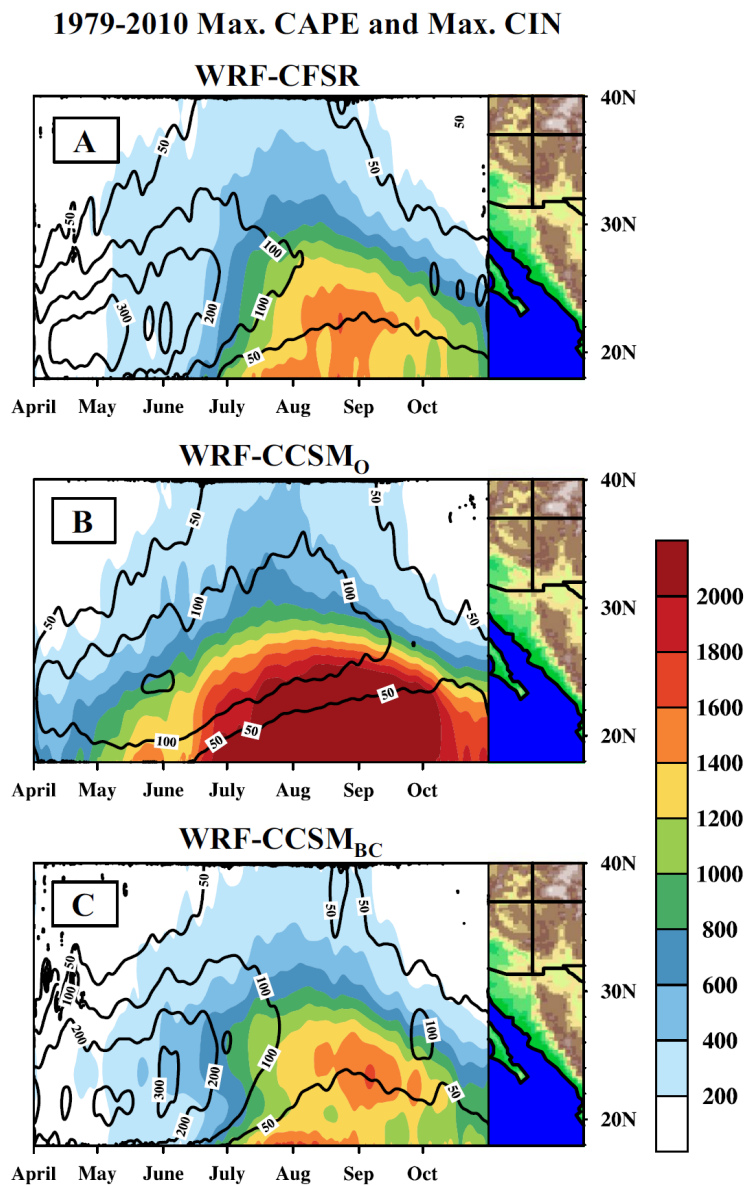


Fig. 3.10 As in figure 3.9, but for convective available potential energy (CAPE; color fill contours) and convective inhibition (CIN; contour lines). CIN contours are drawn at 50, 100, 200, and 300 J kg^{-1} .

Continuing to focus on why the WRF-CCSM_{BC} produced better precipitation, we examined the lifting condensation level (LCL) and the LFC. A function of surface temperature and air moisture, the LCL is a useful indicator of convective probability and intensity as well as moisture supply. The LFC indicates at what height the positive CAPE region becomes available and is dependent on several characteristics of the overall atmospheric thermodynamic profile. Evaluating the evolution of LCL (meters; color contours) and LCF (meters; contour lines) height in Fig. 3.11 continues to help explain the source of precipitation biases in the WRF-CCSM_O and subsequent improvements for the WRF-CCSM_{BC}. Coinciding with earlier onset dates, the WRF-CCSM_O is characterized by lower LCLs and LFCs above $\sim 25^{\circ}\text{N}$ on the order of 500 to 1,000 meters. Furthermore, while the WRF-CFSR and WRF-CCSM_{BC} depict lowering in LCL and LFCs during the mature phase, the WRF-CCSM_O fails to capture the magnitude of this lowering resulting in LCLs that are generally 500 meters higher, and LFCs that are generally 1000 meters higher. The higher LCLs and LFCs during the mature phase provide evidence for why the WRF-CCSM_O has lower overall precipitation despite the earlier onset dates. The later onset dates shown in Fig. 3.8 for the WRF-CCSM_{BC} are likely a result of a slightly more suppressive convective environment. During the late June/early July period, the WRF-CCSM_{BC} features slightly lower average CAPE values ($\sim 100\text{-}200 \text{ J kg}^{-1} \text{ K}^{-1}$), slightly lower Pwat ($\sim 2 \text{ mm}$), and higher average LCL and LFC (100-200 meters and 500-1500 meters respectively).

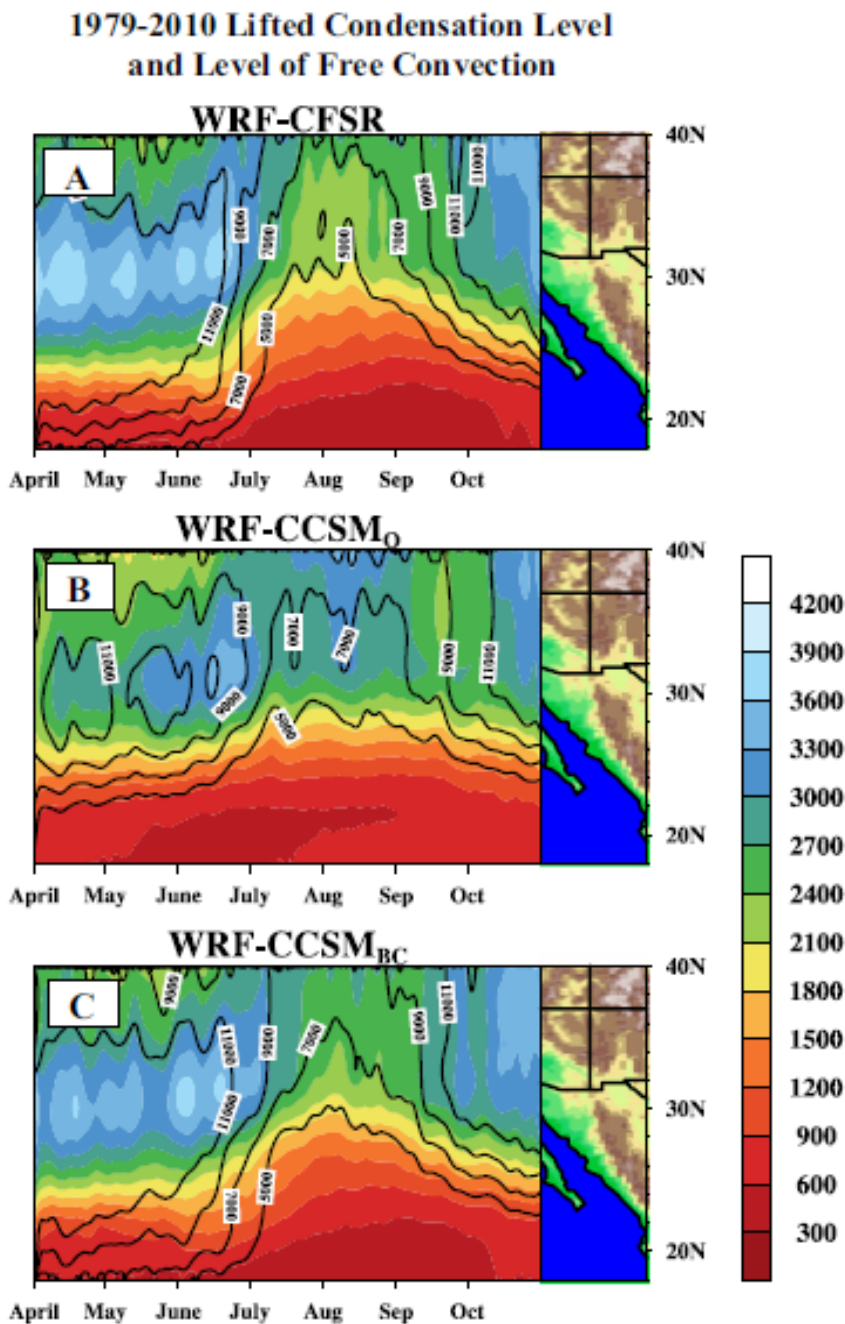


Fig. 3.11 As in figure 3.9, but for Lifted Condensation Level (meters; color fill contours) and Level of Free Convection (meters; contour lines). LFC contours are drawn at 5000, 7000, 9000, and 11,000 m.

While feedbacks within the model can play a role in the enhancement of CCSM_O biases in the thermodynamic profile, the root-source stems from the LBCs. Consistent with CAPE and CIN patterns illustrated in Fig. 3.10, biases in the CCSM_O LBC thermodynamic profile showed stronger low-level capping inversions (larger CIN; generally along the southern and eastern boundaries) and larger middle- and upper-level temperature lapse rates (larger CAPE). Additionally, while LCLs will have a strong dependence on surface feedbacks, the WRF-CCSM_O seasonal pattern of convection favoring LCL and LFC heights during the onset-phase, transitioning to convection suppressing heights during the mature phase parallel patterns shown in the LBCs. Reflecting the improved LBCs, the WRF-CCSM_{BC} contains an atmospheric profile and thus a convective environment that is more comparable to the WRF-CFSR climatology.

4 Summary and conclusions

The WRF model was used at 20-km resolution to assess the limitations when dynamically downscaling CCSM version 4 data for the NAM. For this study, the RCP6.0 scenario was used. Three sets of forcing data were used to produce historical 32-year climatologies of the NAM with the CCSM climatology compared to a control climatology driven by the CFSR data. A third forcing dataset was created using SLR and the CFSR data to remove the long-term biases in the CCSM data. In an attempt to preserve the physical relationships across the forcing variables, we limited our bias correction to only temperature (surface, 2-m height, and atmospheric), relative humidity (2-m height and atmospheric), and surface pressure. In doing so, we were able to subsequently derive the remaining necessary forcing variables (geopotential height, zonal

and meridional winds, and sea-level pressure) using physical equations. With the impact of dynamically inconsistent LBCs unknown on internal model feedbacks, our process produces a set of LBCs that are more consistent than would be produced by simply removing the bias of each variable independently. Comparison between the three forcing datasets revealed the SLR bias correction successfully removed long-term biases and improved both the timing and magnitude of seasonal patterns. Furthermore, long-term trends were not affected, preserving the connection with the specific RCP6.0 scenario.

Compared to CFSR over the NAM domain, the CCSM_O thermodynamic profile contains varying degree of bias at all levels. Headlining these biases are upper atmospheric cold-biases of two to four degrees Celsius, along with mid-level mixing ratio dry-biases on the order of 2 to 3 g kg⁻¹ over the Eastern Tropical Pacific. Additionally, the dramatic warming present throughout the GoC, which plays a role in the development and maturing of the NAM is not appropriately resolved by CCSM_O SST. Compared to the high-fidelity CFSR SST, the CCSM_O GoC SST warms too early in the month preceding the NAM, and fails to capture the strength of the warming during the mature phase.

When compared to CFSR data, biases throughout the CCSM_O atmosphere yielded less accurate NAM onset and intensity. While all climatologies produced too little NAM precipitation, when compared to the CFSR and bias-corrected climatologies, CCSM_O simulations produced the weakest NAM precipitation, despite having the earliest onset dates, which in some cases were three to four weeks earlier than CFSR. Due to biases in

the CCSM_O LBCs, the May-June atmosphere preceding the expected onset of the NAM contained greater atmospheric P_{wat} compared to the CFSR simulations. Furthermore, during these months, the CCSM_O simulations featured a more convectively favorable environment characterized by lower LCLs and higher CAPE values, as well as lower CIN.

While downscaled CCSM_O data produced a more favorable convective environment earlier than CFSR, biases in the LBCs during the NAM mature phase (July and August) suppressed convection and therefore precipitation intensity. Despite P_{wat} values comparable with CFSR, large CIN caused by a stronger mid-level temperature inversion coupled with higher LCLs and LFCs to suppress NAM convection. Also, the magnitude of warming in the GoC SSTs during the peak summer months is not captured in the CCSM_O data. When compared to the high-fidelity CFSR SST, cooler SSTs provided by CCSM_O limit the contribution of surface heat and moisture fluxes to the lower atmosphere as well as lessen the important land-sea temperature contrast. In all cases, the biases in the CCSM_O driven simulations reflect those found in the LBCs, a finding consistent with the multi-model analysis of Bukovsky et al. (2013).

With better atmospheric temperature and moisture fields, the CCSM_{BC} LBCs produced a more accurate development and strengthening of the NAM. Downscaling the bias-corrected data produced a convective environment comparable to the CFSR simulations, resulting in a precipitation climatology that was closer to CRU observations for both monthly and seasonal patterns than the CCSM_O. While the CCSM_O produced far

too early onset dates, the bias correction resulted in onset dates that were later than CFSR, but generally much closer to CFSR than the CCSM_O was. Overall, the bias-correction process yielded a more representative NAM seasonal cycle providing confidence when using the bias-corrected data for future climate projections of the NAM.

One limitation of our bias-correction process is that in order to preserve the physical relationships, the geopotential height and wind fields were not directly corrected. It is unclear whether the limiting factor when downscaling the CCSM data for the NAM is the thermodynamic properties of the atmosphere (temperature and moisture), or errors associated with the development of circulation features. With the NAM being primarily a convective environment, we opted to directly correct temperature and moisture and have shown this process improved NAM precipitation. While some of the circulation biases are reduced (mostly in the magnitude and strength of systems), the bias-corrected dataset is still very much dependent on the original wind field. This dependence likely limits the overall effectiveness of the bias correction as the evolution of the CCSM_O synoptic pattern does contain biases.

At the time of this paper, the authors are not aware of any study that directly addresses the uncertainties associated with internal model feedbacks from physically inconsistent LBCs. However, the governing equations and dynamics within a numerical model such as WRF do have some capacity to adjust inconsistencies across atmospheric fields as they are advected into the model domain. Just how sensitive the model is to inconsistent forcing variables is yet to be determined. Further work testing the impact of

varying degrees of inconsistent LBCs is needed before the uncertainties associated with these inconsistencies can be ignored.

References

- Adams D, Comrie A (1997) The North American Monsoon. *Bull Am Meteorol Soc* 78:2197–2213.
doi:[http://dx.doi.org/10.1175/1520-0477\(1997\)078<2197:TNAM>2.0.CO;2](http://dx.doi.org/10.1175/1520-0477(1997)078<2197:TNAM>2.0.CO;2)
- Antic S, Laprise R, Denis B, de Elia R (2004) Testing the downscaling ability of a one-way nested regional climate model in regions of complex topography. *Clim Dyn* 23:473–493. doi:<http://dx.doi.org/10.1007/s00382-004-0438-5>
- Barlow M, Nigam S, Berbery EH (1998) Evolution of the North American monsoon system. *J Clim* 11:2238–2257.
doi:[http://dx.doi.org/10.1175/1520-0442\(1998\)011<2238:EOTNAM>2.0.CO;2](http://dx.doi.org/10.1175/1520-0442(1998)011<2238:EOTNAM>2.0.CO;2)
- Bruyère CL, Done JM, Holland GJ, Fredrick S (2013) Bias corrections of global models for regional climate simulations of high-impact weather. *Clim Dyn*
doi:<http://dx.doi.org/10.1007/s00382-013-2011-6>
- Bukovsky MS, Gochis DJ, Mearns LO (2013) Towards Assessing NARCCAP Regional Climate Model Credibility for the North American Monsoon: Current Climate Simulations. *J Clim* 26:8802–8826.
doi:<http://dx.doi.org/10.1175/JCLI-D-12-00538.1>
- Carvalho LMV, Jones C (2013) CMIP5 Simulations of Low-Level Tropospheric Temperature and Moisture over the Tropical Americas. *J Clim* 26:6257–6286.
doi:<http://dx.doi.org/10.1175/JCLI-D-12-00532.1>
- Castro CL, Chang H-I, Dominguez F, Carrillo C, Schemm J-K, Juang H-M (2012) Can a Regional Climate Model Improve the Ability to Forecast the North American Monsoon? *J Clim* 25:8212–8237.
doi:<http://dx.doi.org/10.1175/JCLI-D-11-00441.1>
- Christensen JH, Boberg F, Christensen OB, Lucas-Picher P (2008) On the need for bias correction of regional climate change projections of temperature and precipitation. *Geophys Res Lett* 35:L20709.
doi:<http://dx.doi.org/10.1029/2008gl035694> .

- Colette A, Vautard R, Vrac M (2012) Regional climate downscaling with prior statistical correction of the global climate forcing. *Geophys Res Lett* 39:L13707. doi:<http://dx.doi.org/10.1029/2012gl052258>
- Comrie AC, Glenn EC (1998) Principal components-based regionalization of precipitation regimes across the southwest United States and northern Mexico, with an application to monsoon precipitation variability. *Clim Res* 10:201–215. doi:<http://dx.doi.org/10.3354/cr010201>
- Cook KH, Vizzy EK (2008) Effects of Twenty-First-Century Climate Change on the Amazon Rain Forest. *J Clim* 21:542–560. doi:<http://dx.doi.org/10.1175/2007JCLI1838.1>
- Cook KH, Meehl GA, Arblaster JM (2012) Monsoon Regimes and Processes in CCSM4. Part II: African and American Monsoon Systems. *J Clim* 25:2609–2621. doi:<http://dx.doi.org/10.1175/JCLI-D-11-00185.1>
- Denis B, Laprise R, Caya D, Cote J (2002) Downscaling ability of one-way nested Regional climate models: the Big-Brother Experiment. *Clim Dyn* 18:627–646. doi:<http://dx.doi.org/10.1007/s00382-001-0201-0>
- Dickinson RE, Errico RM, Giorgi F, Bates GT (1989) A regional climate model for the western United States. *Clim Change*, 15(3):383-422. doi:<http://dx.doi.org/10.1007/bf00240465>
- Douglas MW, Maddox RA, Howard K, Reyes S (1993) The Mexican Monsoon. *J Clim* 6:1665–1677. doi:[http://dx.doi.org/10.1175/1520-0442\(1993\)006<1665:tmm>2.0.co;2](http://dx.doi.org/10.1175/1520-0442(1993)006<1665:tmm>2.0.co;2)
- Douglas MW, (1995) The Summertime Low Level Jet Over The Gulf of California. *Mon Wea Rev* 123:2334–2347. doi:[http://dx.doi.org/10.1175/1520-0493\(1995\)123<2334:tssljo>2.0.co;2](http://dx.doi.org/10.1175/1520-0493(1995)123<2334:tssljo>2.0.co;2)
- Douglas MW, Valdez-Manzanilla A, Garcia Cueto R (1998) Diurnal variation and horizontal extent of the low-level jet over the northern Gulf of California. *Mon Wea Rev* 126:2017–2025. doi:[http://dx.doi.org/10.1175/1520-0493\(1998\)126<2017:dvaheo>2.0.co;2](http://dx.doi.org/10.1175/1520-0493(1998)126<2017:dvaheo>2.0.co;2)
- Dudhia J (1989) Numerical Study Of Convection Observed During The Winter Monsoon Experiment Using A Mesoscale Two Dimensional Model. *J Atmos Sci* 46:3077–3107. doi:[http://dx.doi.org/10.1175/1520-0469\(1989\)046<3077:nsocod>2.0.co;2](http://dx.doi.org/10.1175/1520-0469(1989)046<3077:nsocod>2.0.co;2)

- Geil KL, Serra YL, Zeng X (2013) Assessment of CMIP5 Model Simulations of the North American Monsoon System. *J Clim* 26:8787–8801. doi: <http://dx.doi.org/10.1175/jcli-d-13-00044.1>
- Gent PR, et al (2011) The Community Climate System Model Version 4. *J Clim* 24:4973–4991. doi: <http://dx.doi.org/10.1175/2011jcli4083.1>
- Giorgi F, Mearns LO (1991) Approaches To The Simulation Of Regional Climate Change. *Rev Geophys* 29:191–216. doi: <http://dx.doi.org/10.1029/90rg02636>
- Grell GA Dévényi D (2002) A generalized approach to parameterizing convection combining ensemble and data assimilation techniques. *Geophys Res Lett* 29(14). doi: <http://dx.doi.org/10.1029/2002gl015311>
- Gutzler DS, Coauthors (2009) Simulations of the 2004 North American Monsoon: NAMAP2. *J Clim* 22:6716–6740. doi: <http://dx.doi.org/10.1175/2009jcli3138.1>
- Hardy B (1998) ITS-90 Formulations for Vapor Pressure, Frostpoint Temperature, Dewpoint Temperature, and Enhancement Factors in the Range –100 to +100 C. In *Proceedings of the Third International Symposium on Humidity and Moisture*, Teddington, London, England.
- Harris I, Jones PD, Osborn TJ, Lister DH (2014) Updated high-resolution grids of monthly climatic observations - the CRU TS3.10 Dataset. *Int J Clim* 34:623–642. doi: <http://dx.doi.org/10.1002/joc.3711>
- Higgins RW, Yao Y, Wang XL (1997) Influence of the North American monsoon system on the US summer precipitation regime. *J Clim* 10:2600–2622. doi: [http://dx.doi.org/10.1175/1520-0442\(1997\)010<2600:iotnam>2.0.co;2](http://dx.doi.org/10.1175/1520-0442(1997)010<2600:iotnam>2.0.co;2)
- Higgins RW, et al (2006) The NAME 2004 Field Campaign and Modeling Strategy. *Bull Am Meteor Soc* 87:79–94. doi: <http://dx.doi.org/10.1175/bams-87-1-79>
- Holton JR, Hakim GJ (2013) *An introduction to dynamic meteorology*. Academic Press, London
- Jiménez PA, Dudhia J, González-Rouco JF, Navarro J, Montávez JP, García-Bustamante E (2012) A revised scheme for the WRF surface layer formulation. *Mon Wea Rev* 140:898–918. doi: <http://dx.doi.org/10.1175/mwr-d-11-00056.1>
- Jin J, Wang S-Y, Gillies R (2011) An improved dynamical downscaling for the western United States. *Clim Change Res Technol Adapt Mitig*. doi: <http://dx.doi.org/10.5772/22991>

- Kanamaru H, Kanamitsu M (2007) Scale-Selective Bias Correction in a Downscaling of Global Analysis Using a Regional Model. *Mon Wea Rev* 135:334–350. doi:<http://dx.doi.org/10.1175/mwr3294.1>
- Kirtman BP, Fan Y, Schneider EK (2002) The COLA global coupled and anomaly coupled ocean-atmosphere GCM. *J Clim* 15:2301–2320. doi:[http://dx.doi.org/10.1175/1520-0442\(2002\)015<2301:tcgcaa>2.0.co;2](http://dx.doi.org/10.1175/1520-0442(2002)015<2301:tcgcaa>2.0.co;2)
- Lawrence DM, et al (2011) Parameterization Improvements and Functional and Structural Advances in Version 4 of the Community Land Model. *J Adv Model Earth Syst* 3:M03001. doi:<http://dx.doi.org/10.1029/2011ms000045>
- Lin Y-L, Farley R, Orville H (1983) Bulk Parameterization of the Snow Field in a Cloud Model. *J Clim Appl Meteorol* 22:1065–1092. doi:[http://dx.doi.org/10.1175/1520-0450\(1983\)022<1065:bpotsf>2.0.co;2](http://dx.doi.org/10.1175/1520-0450(1983)022<1065:bpotsf>2.0.co;2)
- McGregor JL (1997) Regional climate modelling. *Meteorol Atmos Phys* 63:105–117. doi:<http://dx.doi.org/10.1007/bf01025367>
- Meehl GA, Arblaster JM, Lawrence DM, Seth A, Schneider EK, Kirtman BP, Min D (2006) Monsoon regimes in the CCSM3. *J Clim* 19:2482–2495. doi:<http://dx.doi.org/10.1175/jcli3745.1>
- Mitchell DL, Ivanova D, Rabin R, Brown TJ, Redmond K (2002) Gulf of California sea surface temperatures and the North American monsoon: Mechanistic implications from observations. *J Clim* 15:2261–2281. doi:[http://dx.doi.org/10.1175/1520-0442\(2002\)015<2261:gocsst>2.0.co;2](http://dx.doi.org/10.1175/1520-0442(2002)015<2261:gocsst>2.0.co;2)
- Misra V, Dirmeyer PA, Kirtman BP (2003) Dynamic downscaling of seasonal simulations over South America. *J Clim* 16:103–117. doi:[http://dx.doi.org/10.1175/1520-0442\(2003\)016<0103:ddosso>2.0.co;2](http://dx.doi.org/10.1175/1520-0442(2003)016<0103:ddosso>2.0.co;2)
- Misra V, Kanamitsu, M (2004) Anomaly nesting: A methodology to downscale seasonal climate simulations from AGCMs. *J Clim* 17:3249–3262. doi:[http://dx.doi.org/10.1175/1520-0442\(2004\)017<3249:anamtd>2.0.co;2](http://dx.doi.org/10.1175/1520-0442(2004)017<3249:anamtd>2.0.co;2)
- Misra V, (2007) Addressing the Issue of Systematic Errors in a Regional Climate Model. *J Clim* 20:801–818. doi:<http://dx.doi.org/10.1175/jcli4037.1>
- Mlawer EJ, Taubman SJ, Brown PD, Iacono MJ, Lough SA (1997) Radiative Transfer For Inhomogeneous Atmospheres: RRTM, a validated correlated-k model for the longwave. *J Geophys Res* 102:16663–16682. doi:<http://dx.doi.org/10.1029/97jd00237>

- Nakanishi M, Niino H (2006) An Improved Mellor–Yamada Level-3 Model: Its Numerical Stability and Application to a Regional Prediction of Advection Fog. *Bound Layer Meteor* 119:397–407.
doi:<http://dx.doi.org/10.1007/s10546-005-9030-8>
- Noguer M, Jones R, Murphy J (1998) Sources of systematic errors in the climatology of a regional climate model over Europe. *Clim Dyn* 14:691–712.
doi:<http://dx.doi.org/10.1007/s003820050249>
- Pan Z, Takle E, Gutowski W, Turner R (1999) Long simulation of regional climate as a sequence of short segments. *Mon Wea Rev* 127:38–321.
doi:[http://dx.doi.org/10.1175/1520-0493\(1999\)127<0308:lsorca>2.0.co;2](http://dx.doi.org/10.1175/1520-0493(1999)127<0308:lsorca>2.0.co;2)
- Patricola CM, Cook KH (2009) Northern African climate at the end of the twenty-first century: an integrated application of regional and global climate models. *Clim Dyn* 35:193–212. doi:<http://dx.doi.org/10.1007/s00382-009-0623-7>
- Qian J-H, Seth A, Zebiak S (2003) Reinitialized versus continuous simulations for regional climate downscaling. *Mon Wea Rev* 131:2857–2874.
doi:[http://dx.doi.org/10.1175/1520-0493\(2003\)131<2857:rvcsfr>2.0.co;2](http://dx.doi.org/10.1175/1520-0493(2003)131<2857:rvcsfr>2.0.co;2)
- Reynolds RW, Smith TM, Liu C, Chelton DB, Casey KS, Schlax MG (2007) Daily High-Resolution-Blended Analyses for Sea Surface Temperature. *J Clim* 20:5473–5496. doi:<http://dx.doi.org/10.1175/2007jcli1824.1>
- Saha S, et al (2010) The NCEP Climate Forecast System Reanalysis. *Bull Amer Meteorol Soc* 91:1015–1057. doi:<http://dx.doi.org/10.1175/2010bams3001.1>
- Sato T, Kimura F, Kitoh A (2007) Projection of global warming onto regional precipitation over Mongolia using a regional climate model. *J Hydrol* 333:144–154. doi:<http://dx.doi.org/10.1016/j.jhydrol.2006.07.023>
- Skamarock WC, Klemp JB, Dudhia J, Gill DO, Barker D, Duda MG, Huang X-Y, Wang W (2008) A description of the Advanced Research WRF version 3. NCAR Technical Note NCAR/TN-475+STR. doi:10.5065/D68S4MVH
- Trenberth KE, Berry JC, Buja LE (1993) Vertical interpolation and truncation of model-coordinate data. NCAR Technical Note NCAR/TN-396+STR
- Van Vuuren DP et al (2011) The representative concentration pathways: an overview. *Clim Change* 109:5–31.
doi:<http://dx.doi.org/10.1007/s10584-011-0148-z>

- Warner TT, Peterson RA, Treadon RE (1997) A Tutorial On Lateral Boundary Conditions As A Basic And Potentially Serious Limitation To Regional Numerical Weather Prediction. *Bull Am Meteorol Soc* 78:2599–2617. doi:[http://dx.doi.org/10.1175/1520-0477\(1997\)078<2599:atolbc>2.0.co;2](http://dx.doi.org/10.1175/1520-0477(1997)078<2599:atolbc>2.0.co;2)
- White RH, Toumi R (2013) The limitations of bias correcting regional climate model inputs: BIAS CORRECTION LIMITATIONS. *Geophys Res Lett* 40:2907–2912. doi:<http://dx.doi.org/10.1002/grl.50612>
- Wu P-L, Lin P-L, Juang H-MH (2009) Local Mean Bias Correction in a Regional Model Downscaling: A Case Study of the South China Sea Summer Monsoon of 1998. *Mon Wea Rev* 137:2869–2892. doi:<http://dx.doi.org/10.1175/2009mwr2784.1>
- Xu Z, Yang Z-L (2012) An Improved Dynamical Downscaling Method with GCM Bias Corrections and Its Validation with 30 Years of Climate Simulations. *J Clim* 25:6271–6286. doi:<http://dx.doi.org/10.1175/jcli-d-12-00005.1>

CHAPTER 4

THE RESPONSE OF FUTURE PROJECTIONS OF THE NORTH AMERICAN
MONSOON WHEN COMBINING DYNAMICAL DOWNSCALING AND BIAS
CORRECTION OF CCSM4 OUTPUT**Abstract**

A 20-km regional climate model (RCM) dynamically downscaled the Community Climate System Model version 4 (CCSM4) to compare 32-year historical and future “end-of-the-century” climatologies of the North American Monsoon (NAM). CCSM4 and other phase 5 Coupled Model Intercomparison Project (CMIP5) models have indicated a delayed NAM and overall general drying trend. Here, we test the suggested mechanism for this drier NAM where increasing atmospheric static stability and reduced early-season evapotranspiration under global warming will limit early-season convection and compress the mature-season of the NAM.

Through our higher resolution RCM, we found the role of accelerated evaporation under a warmer climate is likely understated in coarse resolution models such as CCSM4. Improving the representation of mesoscale interactions associated with the Gulf of California and surrounding topography produced additional surface evaporation, which overwhelmed the convection-suppressing effects of a warmer troposphere. Furthermore, the improved land-sea temperature gradient helped drive stronger southerly winds and greater moisture transport.

Finally, we addressed limitations from inherent CCSM4 biases through a form of mean bias correction, which resulted in a more accurate seasonality of the atmospheric thermodynamic profile. After bias correction, greater surface evaporation from average peak GoC SSTs of 32 °C compared to 29 °C from the original CCSM4 led to roughly 50 percent larger changes to low-level moist static energy compared to that produced by the downscaled original CCSM4.

The increasing destabilization of the NAM environment produced onset dates that were one to two weeks earlier in the core of the NAM and northern extent, respectively. Furthermore, a significantly more vigorous NAM signal was produced after bias correction, with greater than 50 mm month⁻¹ increases to the June-September precipitation found along east and west coasts of Mexico and into parts of Texas. A shift towards more extreme daily precipitation was found in both downscaled climatologies, with the bias-corrected climatology containing a much more apparent and extreme shift.

1 Introduction

Occurring over a drought susceptible region, the North American Monsoon (NAM) plays a critical role in the hydrologic cycle throughout Mexico and the southwestern United States. Regional ecology, agriculture, and socioeconomic systems are all highly dependent on NAM rainfall while experiencing threats from severe weather, flash flooding, and lightning-triggered wildfires (Ray et al. 2007).

Similar to other global monsoons, the NAM bisects a period of extremely dry climate both preceding and following the pronounced seasonal shift in atmospheric circulation and moisture transport. Upper-air observations indicate the NAM system typically begins to organize in early June, with rainfall onset first occurring along the southernmost extent of the Sierra Madre Occidental (SMO) mountain range. This elevated topographical feature gives way to lowlands which receive up to 80% or 90% of the maximum possible solar insolation leading to summer surface air temperatures which often exceed 40 °C (Adams and Comrie, 1997). Bounded by the warm water bodies of the Gulf of California (GoC) to the west and the Gulf of Mexico (GoM) to the east, the most persistent storm activity occurs along the SMO, where upwards of 70% of the annual precipitation can fall over the four-month monsoon season (Douglas et al. 1993; Higgins et al. 1997). As the warm season progresses, the NAM system intensifies and expands northward bringing convective rain throughout the southwest United States before it reaches maturity around mid-July. The annual precipitation decreases from northwest Mexico to the southwest United States during each monsoon season, where in the latter a less influential 40% of the annual total can fall. A clear definition of the terminal date for the NAM season is muddled by ambiguity between synoptic- and NAM-driven rainfall, but lingering remnants of the NAM often last into late September.

With a historical perspective on the sensitivity of the region's population to drought, the call for a more comprehensive understanding of the NAM system has existed for several decades (Giorgi and Mearns, 1991). Further exacerbating the region's vulnerability to prolonged drought is the expected doubling of population by the middle

of the 21st century and the subsequent increased water demand throughout the United States (Liverman and Merideth 2002) and northern Mexico (Magaña and Conde 2000). Reasonably so, regional planners are highly motivated to gain insight into the impacts a warmer climate might have on future NAM rainfall.

Due to the obvious societal implications, much effort has been given to investigating the impact of global warming on the NAM system. Future projections of the NAM have been simulated using both global general circulation models (GCMs) and regional climate models (RCMs). The Climate Model Intercomparison Project (CMIP) is an international assembly of GCM models independently developed by various nations including U.S. agencies. At the global scale, investigation into monsoon projections in each of the phases 2, 3 and 5 of CMIP GCM simulations has shown an ensemble consensus for a shift in seasonality (delayed onset and retreat phases) with greater late-season rainfall for the global monsoon system (Seager et al. 2007, CMIP2; Seth et al. 2011, CMIP3; Cook and Seager, 2013, Seth et al. 2013, CMIP5). Pertaining to all monsoon systems in general, these GCM global warming scenarios produce a pre-onset stage of the monsoon season (May and June) that features greater tropospheric stability from a warmer climate and lesser low-level atmospheric moisture from decreased evapotranspiration. These mechanisms reinforce each other to create what is commonly referred to as the springtime “convective barrier.” As the warm season progresses, increasing moisture convergence eventually overcomes this convective barrier resulting in a period of moderately enhanced precipitation activity relative to historical normals (Seth et al. 2010). Focusing on the NAM, Bukovsky et al. (2013) reported that a

combination of poorly resolved land-atmosphere interactions and biased atmospheric circulation led to CMIP simulations that contained sufficient uncertainty and spread between individual ensemble members. Their findings highlight the limitation of GCM projections of the NAM, which depends on processes these models struggle to resolve.

One deficiency of CMIP models stems from horizontal grid spacing that is too coarse to appropriately describe finer-scale processes linked to complex terrain, coastlines or large surface heterogeneities (McGregor, 1997); all of which play a measureable role in the NAM system. In fact, mountain/no mountain GCM experiments performed by Broccoli and Manabe (1992) highlighted the importance of regional topography when developing a vigorous monsoon circulation. Furthermore, studies by Lee et al. (2007) and Collier and Zhang (2007) describe the positive impact from increased horizontal resolution on the diurnal cycle of precipitation and the role of mesoscale processes such as those dependent on the Gulf of California (GoC). Through higher horizontal resolution, RCMs have already proven to add value over GCM applications and produce a more realistic historical NAM (Higgins et al. 2006; Gutzler et al. 2009; Castro et al. 2012; Bukovsky et al. 2013; Bukovsky et al. 2015; Meyer and Jin 2015). By including more of the interactions across spatial scales, future projections simulated using an RCM can be considered more reliable when compared to a GCM where certain climate mechanisms are diminished or even neglected.

Great effort has been spent on improving North American climate projections by dynamically downscaling CMIP models through a RCM. Notably, the North American

Regional Climate Change Assessment Program (NARCCAP; Mearns et al. 2009) downscaled phase 3 of the CMIP models. With respect to the NAM, historical evaluation of NARCCAP simulations showed general improvements to the representation of the overall NAM system relative to parent GCMs (Bukovsky et al. 2013). A future evaluation of historically top-performing NARCCAP models suggested a small but significant drying trend across the southwest U.S (Bukovsky et al. (2015).

While RCM models help to improve the representation of NAM processes, Bukovsky et al. (2013, 2015) highlights a limiting factor when using an RCM. Their findings showed the negative impacts from a biased parent GCM when transmitted through the lateral boundary conditions (LBC). For this reason, Bukovsky et al. (2015) concludes “the ensemble-mean precipitation projections lack credibility” and “...it would be ideal to complete simulations where they are forced with a less biased set of GCMs.” By merging GCM bias correction before dynamically downscaled with an RCM, our study takes a step towards a more credible future projection of the NAM.

Here, we compare a 32-year historical climatology and a future “end-of-the-century” climatology of the NAM produced by downscaling both original and bias-corrected GCM output. Our study expands on previous work described in Meyer and Jin (2015); (hereafter referred to as MJ15) where a historical evaluation of the downscaled original GCM and bias-corrected GCM climatologies was presented. This historical evaluation highlighted the strong dependence the maturation of the NAM convective environment has on LBCs. Before bias correction, inherent deficiencies in the seasonality and peak

magnitudes of the profiles of temperature and moisture from the parent GCM favored early- and late-season convection while suppressing peak-season rainfall. Additionally, when downscaling the coarse-resolution GCM—which fails to accurately resolve the GoC landmask—interpolation of GoC SSTs from the surrounding Pacific Ocean was required. Whereas the Pacific Ocean SSTs can often be upwards of 5° C cooler than the GoC during the mature phase of the NAM (Adams and Comrie 1997), the reduced surface convective forcing acts to further limit storm activity. After bias correction, historically consistent seasonality and peak magnitudes of the NAM environment led to improved rainfall simulations. Using these historical climatologies as a reference period, this study compares the impact global warming has on the future state of the NAM.

The objective of this study is to (1) assess the limitations of current GCM projections of the NAM due to insufficient model resolution and (2) assess how the inherent systematic biases associated with a GCM can hinder dynamical downscaling of the NAM. To accomplish this objective, we used a higher-resolution RCM to compare dynamically downscaled climatologies driven by both the original GCM and bias-corrected GCM LBCs. We explored the sensitivity of NAM mechanisms to a warming climate while examining the simulated effects a changing NAM system could have on the spatiotemporal distributions of rainfall by the end of the 21st century. In doing so, we aim to improve the current perspective on the future state of interannual variability, seasonality, and spatial distribution of NAM rainfall. A description of our methodology and the datasets used for this study is provided in Section 2. Section 3 presents our results and future comparison while Section 4 offers a summary and discussion of our findings.

2 Data and methodology

2.1 General circulation model output

GCM forcing data was provided by the Community Climate System Model version 4 (CCSM4; Gent et al. 2011). Termed a representative concentration pathway (RCP), future projections by CMIP5 models contain one of several specific trajectories for greenhouse gas concentration forcing and land-use change (Van Vuuren et al. 2011). RCP 6.0 was chosen for this study as its trajectory falls between the optimistic RCP 2.5 and the more aggressive 8.5 scenario. CCSM4 is one of the higher resolution CMIP5 models at 0.93° latitude by 1.25° longitude (CMIP5 models range from 0.57° to 3.76° in a latitude-longitude resolution). Although Geil et al. (2013) found no correlation between CMIP5 model resolution and NAM performance, CCSM4 produced a relatively minor wet bias in precipitation relative to other CMIP5 models. Furthermore, a comparison of 500-hPa circulation patterns in CMIP5 models showed CCSM4 was a top-5 performer across the warm season period (May-October) and the best performer for the mature season (July-August). Thus, with upper-air atmospheric circulation strongly associated with the evolution of the NAM system, CCSM4 is a credible GCM to downscale. With that said, Geil et al. (2013) did highlight some deficiencies in CCSM4, which produced an extended monsoon season that started too early (-41 day lag; ensemble average of -22) and lasted too long (+18 day lag; ensemble average of +8).

2.2 Regional climate model configuration

With a wide-ranging set of available model physics, the Weather Research and Forecasting (WRF) model version 3.5.1 (Skamarock 2008) was chosen for our RCM. A

detailed description of the calibration phase of the WRF model physics employed for these simulations can be found in MJ15. This historical evaluation showed that a 20 km resolution WRF can realistically reproduce the NAM. Thus, along with convective model parameterization, we think 20-km grid spacing is a reasonable resolution to capture the main physical features of the NAM.

The regional topography as resolved by the CCSM4 and WRF domains is provided in Fig. 4.1 and illustrates the distinct differences between key surface features such as the SMO, the GoC, and the Mogollon Rim in Arizona. Masking out ocean grid cells (white color fill) exposes perhaps the largest limitation of the coarse resolution CCSM4 domain, which fails to resolve well over half of the GoC. However, we do note that the CCSM4 ocean and land surface models operate at a slightly higher grid resolution than the atmosphere model grid shown in Fig. 4.1a. Subsequent coupling between the atmosphere model requires upscaling, which introduces the possibility that the fidelity of GoC processes can be lost. Also included in Fig. 4.1b are two evaluation zones and the boundary relax zones (where 6-hourly LBC data is integrated into the WRF domain). These areas are used in several comparisons discussed in the results section. The southern evaluation zone is placed over the SMO and represents the core of the NAM where orographic effects and greater moisture convergence produce a strongly diurnal cycle of more intense persistent convection. The northern zone depends on moisture advection and convergence to initiate convection and is characterized by more localized but less frequent and intense convection.

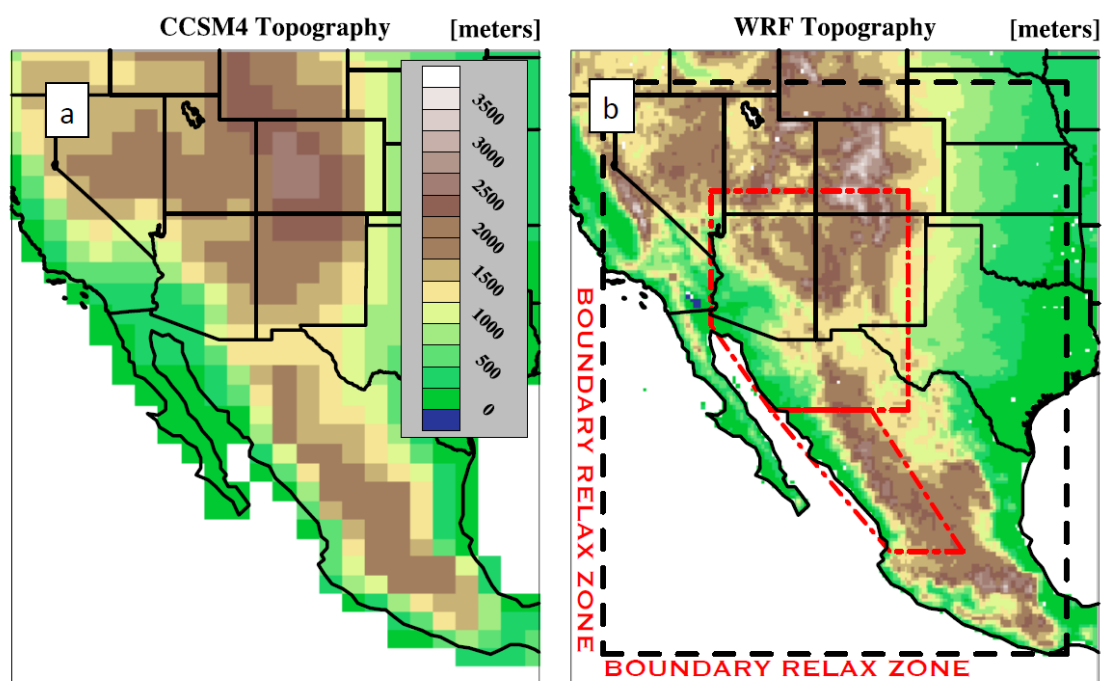


Fig. 4.1 Model resolved terrain for Community Climate System Model version 4 (CCSM4) (a) and the 20-km WRF domain (b). Respective landmasks are used to show only the land surface to demonstrate the difference in coastlines and the Gulf of California. Also included in (b) are the boundary relax zones for the WRF domain (black dashed lines) and two evaluation regions (red dashed lines).

Expanding on the 32-year (1979-2010) historical climatologies described in MJ15, we produced two sets of 32-year (2068-2099) “end-of-the-century” climatologies driven with both the original and bias-corrected CCSM4 LBCs. To better facilitate a seamless future downscaling projection, we note that this version of the WRF model allowed the internal radiative forcing to exactly match the RCP scenario of radiative forcing employed in the CCSM4 output used for LBCs.

2.3 Bias correction of GCM output

To reduce potential uncertainty in future climate projections, an RCM approach is often paired with a form of GCM bias correction. Although discussed in MJ15, our process of bias correction used the observation-based Climate Forecast System Reanalysis (CFSR; Saha et al. 2010) with linear regression to reduce the systematic bias in the CCSM4 data. We addressed the potential for dynamic imbalances between interdependent atmospheric and surface variables (Misra and Kanamitsu 2004) by correcting select atmospheric state variables, which are subsequently used to derive the necessary remaining LBC variables. Bias correction of the future data relies on the historical linear regression equation at each grid point and follows the same process to preserve the physical dependencies among the corrected variables.

3 Evaluation of future projections

Our comparisons presented in this section will concentrate on two main areas. First, we explore the benefits of better-resolved terrain and surface forcing included in the WRF domain compared to the original CCSM4 output. This comparison shows the added value simply from improved terrain and mesoscale interactions, while highlighting the limitations from biased LBCs. Second, by comparing the downscaled original and bias-corrected simulations we aim to better understand the role GCM biases have on simulated NAM mechanisms.

3.1 North American monsoon forcing

We begin by first comparing changes to a few key CCSM4 LBCs driving the WRF model. Hereafter, we use the term CCSM4_O for original model output and CCSM4_{BC} for bias-corrected model output when describing the forcing datasets. A common frame of reference to understand changes in a convective environment is through the atmosphere's moist static energy profile (MSE):

$$MSE = C_p T + gz + L_v r \quad (1)$$

where C_p is the specific heat of air, T is air temperature, g is the gravitational acceleration, z is geopotential height, L_v is the latent heat of vaporization, and r is the water vapor mixing ratio. MSE is analogous to equivalent potential temperature when geopotential height rather than pressure is used as a vertical coordinate. MSE is therefore a more appropriate variable to understand the combined convective changes from three of the fundamental LBC variables. Greater low-level MSE indicates a more convectively favorable atmosphere, while greater upper-level MSE indicates a more convectively suppressive atmosphere.

Averaged over the boundary relax zones, Fig. 4.2 compares the future minus historical changes to the vertical profile of temperature, mixing ratio, and MSE for the early (May-June), mature (July-August), and late (September-October) monsoon season. Fig. 4.2 reinforces the interactions between the aforementioned tropospheric warming and increased evapotranspiration mechanisms. The profiles for both original and bias-

corrected LBCs are quite similar with the bias-corrected LBCs containing slightly larger MSE changes in the future, but with a similar profile curve as the original. Warming tropospheric temperatures between 2 °C and 3 °C were reported at all levels with local maxima found at approximately 850- and 250-hPa. In each time frame, the bias-corrected LBCs have slightly greater temperature change. The most apparent deviation from the original LBC temperature changes is found below 500-hPa in the May/June period and above ~600-hPa for the July/August period. Whereas upper-level maxima in MSE change ($\sim 4 \text{ MJ kg}^{-1}$) correspond to warming temperatures, greatest MSE changes (~ 5 to 7 MJ kg^{-1}) are found in the lower levels as you approach the surface. Here, increasing atmospheric mixing ratio ($\sim 1.5 \text{ g kg}^{-1}$) drives the larger near-surface changes to MSE, and indicates LBCs from each original and bias-corrected models drive an overall destabilization of the future NAM domain. Close to the surface, the bias-corrected LBCs indicate a slightly larger increase to mixing ratio, helping to create the greater near-surface MSE changes.

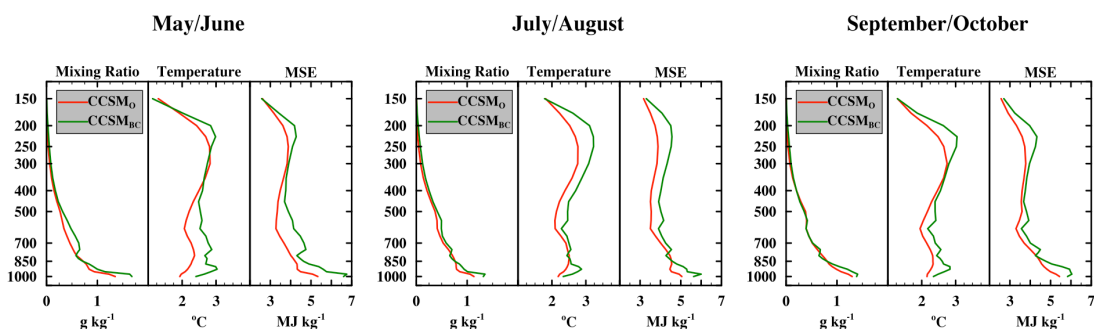


Fig. 4.2 Future change (future minus historical) for lateral boundary conditions vertical profile of mixing ratio (g kg^{-1}), temperature ($^{\circ}\text{C}$), and moist static energy (MSE; MJ kg^{-1}) for the original Community Climate System Model (CCSM₀; red lines) and bias-corrected Community Climate System Model (CCSM_{BC}; green lines).

Moisture and its effects on stability mean that dynamically downscaled GCMs—and their known dry biases during the NAM season (Bukovsky et al. 2013)—will struggle to accurately capture the atmospheric static stability profile (MJ15). The majority of NAM moisture is now well understood to originate from either the distant Eastern Tropical Pacific or the GoC (Adams and Comrie 1997). The seasonal evolution of the comparatively warm GoC SSTs has shown a correlation with both the seasonal timing and the interannual variability of the NAM. Using high spatial and temporal resolution GoC SST observations and satellite measurements of rainfall, Mitchell et al. (2002) found that (1) onset of rainfall generally did not occur prior to SSTs exceeding 26 °C with the northward progression of this 26 °C threshold also coinciding with the northward progression of rainfall, (2) 75% of rainfall across the northern periphery (e.g. Arizona and New Mexico) fell after the northern GoC SSTs exceeded 29 °C and (3) to some degree, GoC SSTs influence interannual variability of the northern periphery rainfall where wet years often occur during a warm phase of northern GoC SST early in the season.

Clearly, GoC SSTs are important to the NAM system, and one of the most glaring issues when downscaling a coarse resolution GCM like CCSM4 for the NAM is the missing GoC (Fig. 4.1a). Described in MJ15, the historical seasonality of interpolated CCSM_O GoC SSTs feature early-season warm biases (2-3 °C) and mature-season cold biases (~2 °C) as the model must rely on interpolated surrounding Pacific SSTs over the GoC. To visualize the net result of GCM SST interpolation on the GoC, refer to Fig. 18 in Bukovsky et al. (2013). The poor seasonality and colder mature-season SSTs limit the modeled evolution of the NAM system. Fig. 4.3 provides some perspective on future

changes to the downscaled GoC SSTs (solid lines). Peak GoC SSTs warmed from 27.75 °C to 29.0 °C (1.25 °C warming) by the end of the century in CCSM_O and from 30 °C to 32 °C (2.0 °C warming) in CCSM_{BC}. Also shown in Fig. 4.3 is the corresponding change to saturation vapor pressure (e_s ; dashed lines). With a 60 percent larger rate of warming (2.0 °C vs. 1.25 °C) and higher peak SSTs (32.0 °C vs. 29.0 °C) in the future CCSM_{BC}, the net result of the non-linearity of the Clausius-Clayperon relationship is an 82% larger (500 Pa vs. 275 Pa) peak increase to e_s . The resulting impact on NAM mechanisms turns out to be a key difference between the two downscaled simulations.

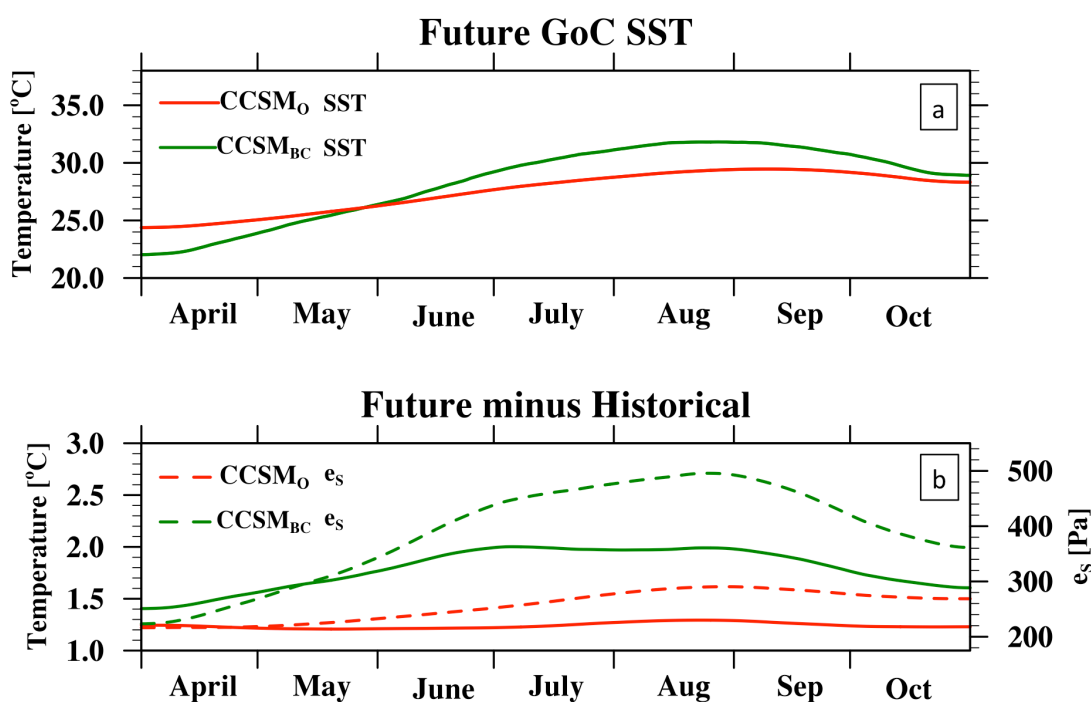


Fig. 4.3 Future changes to Gulf of California (GoC) sea surface temperature (SST) and saturation vapor pressure. (a) Future 32-year (2068-2099) climatology of GoC SSTs for original Community Climate System Model (CCSM_O; red) and bias-corrected Community Climate System Model (CCSM_{BC}; green) forcing datasets. (b) Future change (future minus historical) over the historical 32-year (1979-2010) climatology for SST (solid lines; left y-axis) and saturation vapor pressure (dashed lines; right y-axis)

3.2 North American monsoon mechanisms

In previous sections, we described how limited the fidelity of NAM mechanisms are when dynamically downscaling original GCM forcing data. We also compared the future changes between the original and bias-corrected forcing conditions. Here, we examine the impact original CCSM4 versus bias-corrected CCSM4 LBCs have on NAM mechanisms when downscaled to a higher resolution. Hereafter, when referring to a comparison between the WRF climatologies, we use the terms WRF-CCSM_O and WRF-CCSM_{BC} to describe the original and bias-corrected simulations.

Continuing to show the influence of GoC SSTs on the NAM system, we first look to the seasonality of moisture flux from the surface. Evaporation from a water surface is dependent on both the water surface's available energy (a function of SST) and the overriding atmospheric humidity and wind speed conditions. As a function of SSTs, the saturation vapor pressure combines with atmospheric conditions to determine the vapor gradient between the air and the water surface, which affects the rate of evaporation. Fig. 4.4 shows the historical and future 32-year climatology of modeled moisture flux from the GoC. Historically, while the WRF-CCSM_{BC} moisture flux closely follows the climatology of the reanalysis-driven simulations (WRF-CFSR), the WRF-CCSM_O once again is characterized by poor seasonality with excessive early-season and insufficient mature-season evaporation. Historical mature-season evaporation rates produced by WRF-CFSR show approximately 3 to 5 mm day⁻¹ with peak evaporation of ~7 mm day⁻¹ occurring after mid-October. Comparing the future changes to GoC evaporation, WRF-CCSM_O remains relatively unchanged for either the seasonality, or peak evaporation. On

the other hand, while early-season evaporation remains comparable for WRF-CCSM_{BC}, the timing of peak evaporation by the end of the century advances earlier in the season and now coincides with the timing of the mature phase of the NAM. We note that the actual peak evaporation remains consistent with the historical peak rates ($\sim 7 \text{ mm day}^{-1}$) with the timing of these values shifting from mid-October to mid-August in the future climatology.

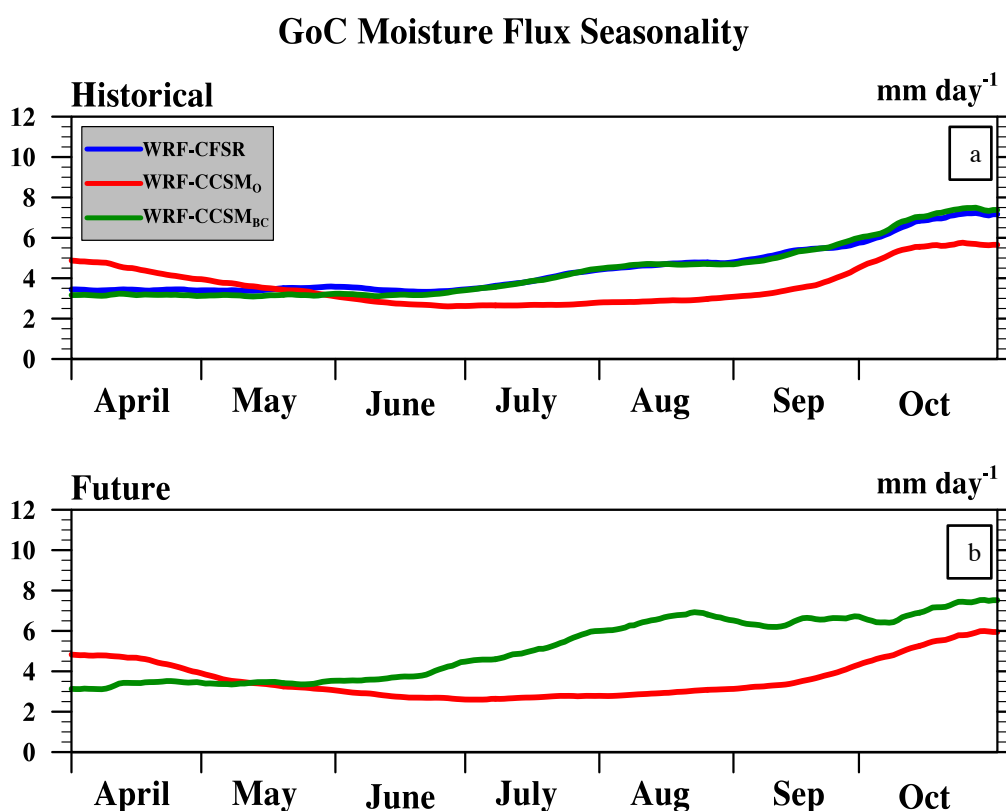


Fig. 4.4 Historical vs. future Gulf of California (GoC) moisture flux comparison. (a) 32-year historical (1979-2010) and (b) future (2068-2099) GoC moisture flux (mm day^{-1}) for WRF driven by observation-based Climate Forecast System Reanalysis (WRF-CFSR; blue), original Community Climate System Model (WRF-CCSM_O; red) and bias-corrected Community Climate System Model (WRF-CCSM_{BC}; green).

To frame the modeled evaporation rates with observations, we point to satellite estimates of evaporation from the Tropical Rainfall Measuring Mission reported by Prakash et al. (2011). While the GoC is not fully resolved by their study and satellite estimates of evaporation operate with a large margin of error, estimates for the mouth of the GoC shows July evaporation rates of roughly 4 to 5 mm day⁻¹ with surrounding Pacific evaporation rates between 1 and 3 mm day⁻¹. The modeled evaporation rates appear to fall within the historical margins, leading us to conclude that the future changes to simulated evaporation are within reason.

We showed the dramatic differences in the seasonality and peak values of GoC SST's and simulated evaporation. Moving next to the impacts these differences have on the NAM system, we look to the changes in the modeled MSE profile. Averaging over the NAM core and northern periphery regions outlined in Fig. 4.1b, Fig. 4.5 compares future changes to the MSE profile (solid line), temperature (long dash), and mixing ratio (short dash) for the CCSM4 model and each of the downscaled WRF climatologies. Upper air changes to MSE continue to reflect the effect from increasing tropospheric temperatures working to suppress convection. Whereas Fig. 4.2 indicated both original and bias-corrected simulations should contain similar near-surface changes, after downscaling, a substantial difference between the WRF-CCSM_O and WRF-CCSM_{BC} is evident, especially along the NAM core and during the mature season. Near-surface MSE changes produced in the WRF-CCSM_{BC} suggest a much greater destabilization of the atmosphere when compared to the CCSM4 or WRF-CCSM_O. Much of the change to near-surface MSE profile appears to come from changes to mixing ratio, with an increase of 1 to 2 g

kg^{-1} during the mature phase of the NAM for the WRF-CCSM_{BC} compared to 0.5 to 1.0 g kg^{-1} for the WRF-CCSM_O. We suggest the differences between the two downscaled simulations (where both showed similar future changes in the LBC forcing data; Fig. 4.2) stems from the greater GoC SSTs and larger subsequent surface evaporation.

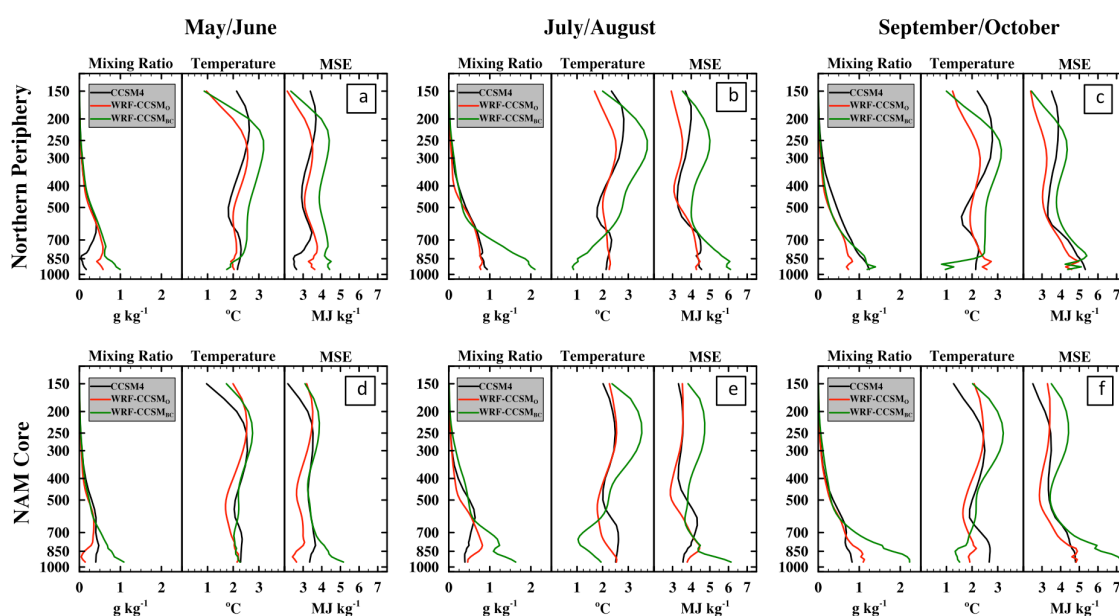


Fig. 4.5 Same as Fig. 4.2, but for the northern periphery (a,b,c) and North American monsoon core (d,e,f) evaluation regions shown in Fig. 4.1b. Model comparison shows Community Climate System Model version 4 (CCSM4; black line), WRF driven by original CCSM4 (WRF-CCSM_O; red line), and bias-corrected Community Climate System Model (WRF-CCSM_{BC}; green line).

Despite being a major contributor to NAM moisture, evaporation is not the only reason that the GoC is important. Both observational (Douglas 1995; Berbery 2001) and numerical studies (Stensrud et al. 1997; Anderson et al. 2000; Gao et al. 2008) have

confirmed the role of the regional terrain on the transport of moisture onshore. Land-sea temperature contrasts between the GoC and the SMO highlands drive an onshore, diurnal sea-breeze circulation during the day, shifting to a nighttime and predawn low-level jet (Douglas 1995). Enhanced afternoon moisture convergence occurs over the SMO highlands resulting in persistent rainfall over the core of the NAM throughout the season (Berbery 2001). Scenarios where the mesoscale mechanisms and the synoptic circulation align result in the strongest moisture surge events, bringing NAM rainfall deep into the interior southwest U.S (Stensrud et al. 1997).

With such large discrepancy between the $CCSM_O$ and $CCSM_{BC}$ LBCs and GoC SSTs, it is not surprising that downscaling resulted in quite dissimilar southerly flow patterns. Fig. 4.6 shows a cross section of the historical climatology of July-August V-winds for the CFSR (a) reanalysis and CCSM4 (b) and their respective downscaled climatologies (d,e,f). The coarse resolution CCSM4 clearly does not resolve the mesoscale interactions appropriately, with much of the low- and mid-level flow showing a northerly component between 2 and 3 $m s^{-1}$. The region that does have a southerly component is greatly limited in extent with slightly lower magnitude values (0-2 $m s^{-1}$ versus 1-3 $m s^{-1}$). With identical grids, downscaling produces similar low-level flows between 1 and 3 $m s^{-1}$ for each forcing datasets. The upper-level anticyclone is consistent in each of the historical climatologies, although WRF- $CCSM_{BC}$ over predicts the strength by approximately 1.0 $m s^{-1}$.

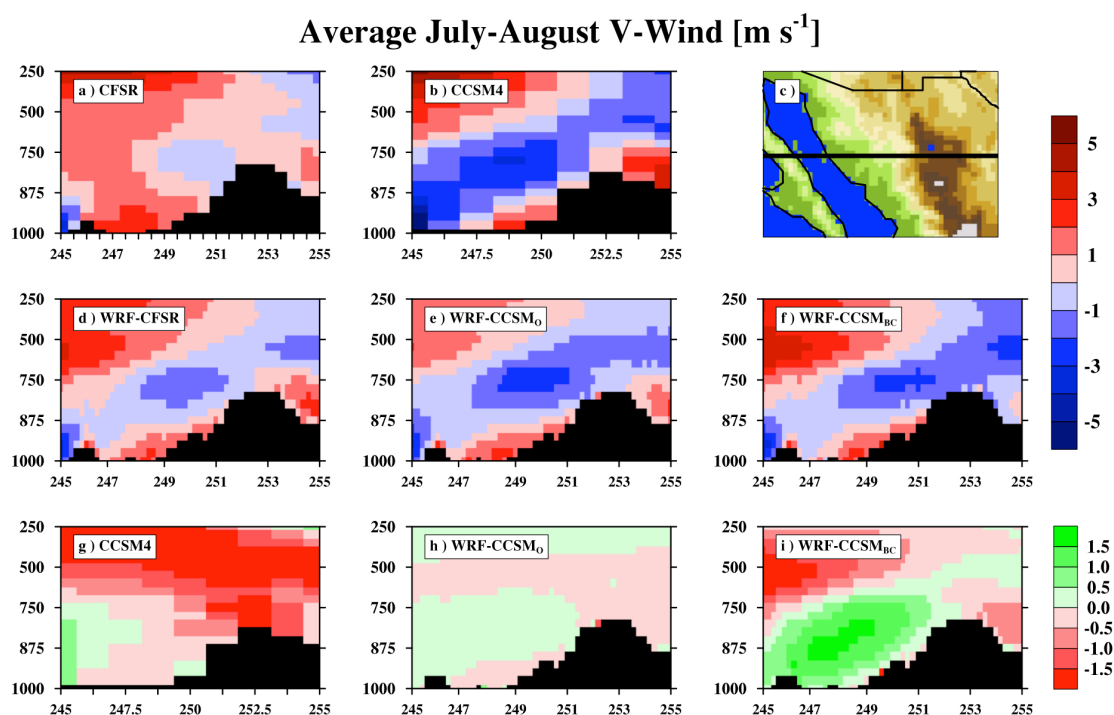


Fig. 4.6 Vertical cross section of historical climatological July-August meridional component V-wind (m s^{-1}) for observation based Climate Forecast System Reanalysis (CFSR; a), and Community Climate System Model version 4 (CCSM4; b). Historical downscaled WRF climatologies for CFSR (d), original CCSM4 (e) and bias-corrected CCMS4 (f) are used to compare future differences (g,h,i) where green/red represents stronger/weaker V-winds in the future climatology. The area covered by the cross section is indicated with the black line in (c).

Also included in Fig. 4.6 is the future change to the July-August V-wind (g,h,i), with green indicating a strengthening southerly wind and red denoting a reduction of southerly winds. Without an accurate zonal temperature gradient, CCSM4 projects southerly winds to decrease in strength during the mature season across most of the cross-section. After downscaling, little change is produced in the future WRF-CCSM₀ with slightly decreasing southerly winds near the surface, and slightly increasing southerly winds in the mid-levels. After bias correction—with a more appropriate prescription of GoC

SSTs—the future period of WRF-CCSM_{BC} indicates a discernable strengthening of the southerly winds above 1.5 m s^{-1} throughout the lowest 2.5 km over the GoC and SMO foothills.

When factoring in the additional water vapor stored in the atmosphere under a global warming scenario, the strengthening of southerly winds becomes even more impactful to the NAM. Not only does extra moisture convergence occur over the highlands of the SMO but the additional moisture transport in the future period produces stronger, more frequent moisture surges that can penetrate deeper into the northern periphery of the NAM domain.

3.3 North American monsoon precipitation

Our results up to this point demonstrate that simply by dynamically downscaling CCSM4, the improvements to surface processes related to the GoC and SMO terrain interactions yield more realistic NAM features such as the LLJ and surface evaporation. Although not shown, we can infer that improvements to wind patterns and atmospheric moisture lead to improvements in the overall moisture transportation associated with the NAM. These improvements are in spite of the limitations imposed on the WRF model by biased boundary conditions. With bias correction of the CCSM4 data, these limitations are greatly reduced and yield quite different changes to the atmospheric profile through both land-surface interactions included in the model, and different boundary condition seasonality and peak values. This sub-section focuses on the differences to precipitation fields each model version prescribes in the future.

Starting with the most basic analysis, Fig. 4.7 shows the climatological changes to June-September precipitation for CCSM4 and the two downscaled projections. Reaffirming CMIP trends, a modest overall drying signal is produced by CCSM4. A few locations around northwestern Mexico and the states of New Mexico and Texas show minor increases to NAM precipitation on the order of 0-10 mm month⁻¹. Simply downscaling CCSM4 output and including GoC processes and improving the land surface representation, the southwestern U.S.—and especially Texas—reverses trends towards a wetter NAM. One consistency with CCSM4 is the drying trend produced along the GoC coastline at lower elevations. Interestingly, the entirety of the WRF-CCSM_O SMO ridgeline exhibits a wetter signal whereas the CCSM4 output only hints at a few higher elevation locations becoming wetter. This suggests that even by improving the GoC evaporation and surrounding topography description, the WRF-CCSM_O atmosphere itself is not becoming more thermodynamically unstable. Here, cooler WRF-CCSM_O GoC SST's (Fig. 4.3) and lesser moisture flux (Fig. 4.4) limits the near-surface MSE increases relative to the mid- and upper-level increases (Fig. 4.5). This helps explain why WRF-CCSM_O appears to need the onshore, upslope flow fueling enhanced moisture convergence over the SMO highlands to initiate increased convective activity. After bias correction, a substantially wetter future NAM is produced throughout the core areas and across the eastern half of Mexico and into Texas. The southwest U.S. exhibits a mixed signal with a drying trend across the farthest northern areas in Utah and Colorado. The largest increasing pattern above 50 mm month⁻¹ exists along the GoC and GoM coastlines as well as into Texas.

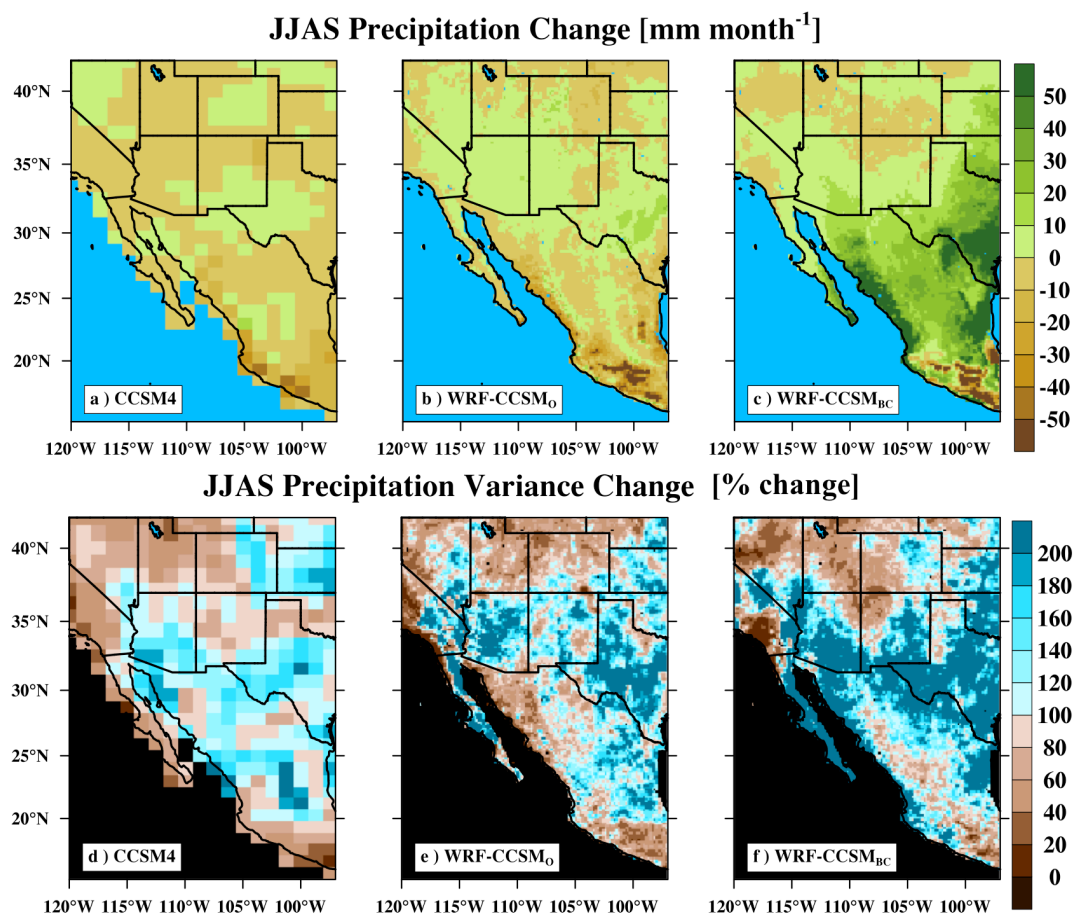


Fig. 4.7 Future June-September (JJAS) precipitation change (mm month^{-1}) comparison. Top row shows future difference relative to the historical climatology from the same model/forcing dataset (a,b,c). Bottom row (d,e,f) represents the percent change of the future variability relative to the historical normal with blue (increasing interannual variability) or brown (decreasing interannual variability) colors.

Also shown in Fig. 4.7 is the change to the interannual June-September precipitation variability. In such arid conditions, the interannual variability across the NAM domain can often exceed the seasonal mean and is strongly connected to the synoptic variability of the NAM anticyclone (Higgins et al. 1997). By taking the difference between the historical and future variance of yearly June-September precipitation, this set of figures

shows where the interannual variability is decreasing (brown colors) or increasing (blue colors). The general idea that interannual variability will increase under a global warming scenario is displayed in the CCSM4 panel with increasing variability across much of the NAM core and into Arizona and Texas. WRF-CCSM_O suggests that while northwest Mexico has less variable rainfall in the future, the rest of the NAM domain exhibits increasingly variable monsoon rainfall, especially in Texas and along the eastern half of Mexico. After bias correction, we see that with the exception of the SMO highlands, the bulk of the NAM domain contains greater rainfall variability.

NAM onset is a profoundly important consideration for the regional hydrology. Earlier onset dates allow a naturally prolonged period of NAM rainfall to occur, and thus typically relate to a wetter season while the opposite is true for later onset dates (Higgins et al. 1998). Following the historical evaluation presented in MJ15, we define NAM onset as the first three-day period with consecutive daily rainfall greater than 0.5 mm day^{-1} . Comparing average onset dates, Fig. 4.8 reiterates the aforementioned delayed onset date due to the ‘spring convective barrier’ produced in the CCSM4 model where brown and blue colors indicate later or earlier onset, respectively. Across the NAM core, WRF-CCSM_O produced a similar yet less aggressive delay to the NAM, while across the entire southwest U.S. the trend reverses towards earlier NAM onset. Historical analysis in MJ15 showed the WRF-CCSM_O triggered NAM onset up to three weeks earlier than the reanalysis driven simulations so it is perhaps surprising to see the southwest NAM onset occurring even earlier than the historical period. However, with poor seasonality and LBCs that favor early-season convection, this pattern is not considered out of the

question. After bias correction, WRF-CCSM_{BC} indicates a general advance of NAM onset dates across the region, with only parts of central and eastern Mexico characterized by delayed onset dates. The variability of onset is also an important factor in the regional hydrology and although not shown, we note that the CCSM4 shows increasingly variable onset dates in the future, while both downscaled climatologies generally produced a less variable onset date. With both synoptic and surface forcing (i.e. warming of GoC SSTs past a certain threshold; Mitchell et al. 2002) controlling the NAM onset, a transition to a less variable onset seems to suggest a growing influence from surface forcings which inherently contain much less interannual variability themselves.

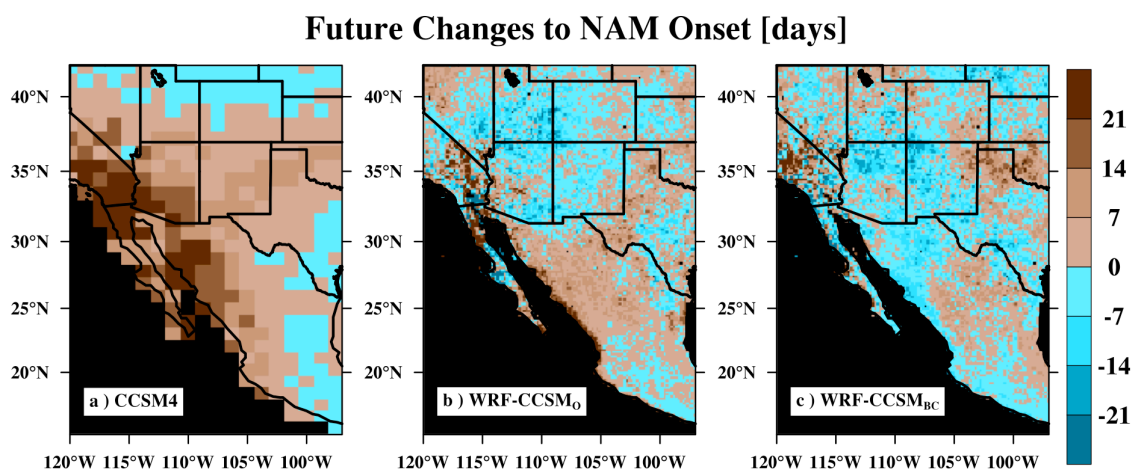


Fig. 4.8 Changes to future average North American Monsoon (NAM) onset with earlier onset (blue colors) or later onset (brown colors). Onset day is defined as the first occurrence after 01 May with three consecutive days with at least 0.5 mm day⁻¹.

Regarding precipitation trends and onset dates, our results highlight the extreme sensitivity to model resolution and even to the parent model biases. We next show how each model type captures daily precipitation intensity, and how the distribution of rainfall intensity changes by the end of the 21st century. A histogram of the historical and future JJAS daily precipitation distribution for the NAM core and the northern periphery zones is plotted in Fig. 4.9. For all years, the daily precipitation was calculated spanning a 24-hour cycle beginning 12:00 UTC (early morning local time) to capture the full diurnal cycle of thunderstorm activity. Days with rainfall below the measureable trace rainfall threshold of 0.254 mm (0.01 inches) were considered non-events, and are not factored into this histogram. Two y-axis scales are used to better visualize the frequency of extreme events on the same plot. Over each evaluation domain and both historical and future climatology, the two WRF forcing datasets are more heavily skewed towards light rainfall events between trace and 5 mm day⁻¹. The mean daily rainfall for CCSM4 is shifted towards larger events greater than 5 mm day⁻¹. Relative to CCSM4 and WRF-CCSM_{BC} distributions in each domain and time period, WRF-CCSM_O produces fewer large daily rainfall events.

Shown in the bottom row of Fig. 4.9 are the changes to the distribution by the end of the century. In both regions, CCSM4 indicates daily rainfall with increasing light rainfall and more frequent large events at the expense of events between 1 to 15 mm day⁻¹. With modest increases to atmospheric moisture and instability, future WRF-CCSM_O shifts the daily events away from light rainfall and more towards the 1 to 5 mm day⁻¹, but with no apparent change to more extreme events. With much larger increases to atmospheric

moisture, and near-surface MSE, the future WRF-CCSM_{BC} simulations in both regions

indicate a considerable shift away from lighter rainfall towards larger rainfall events.

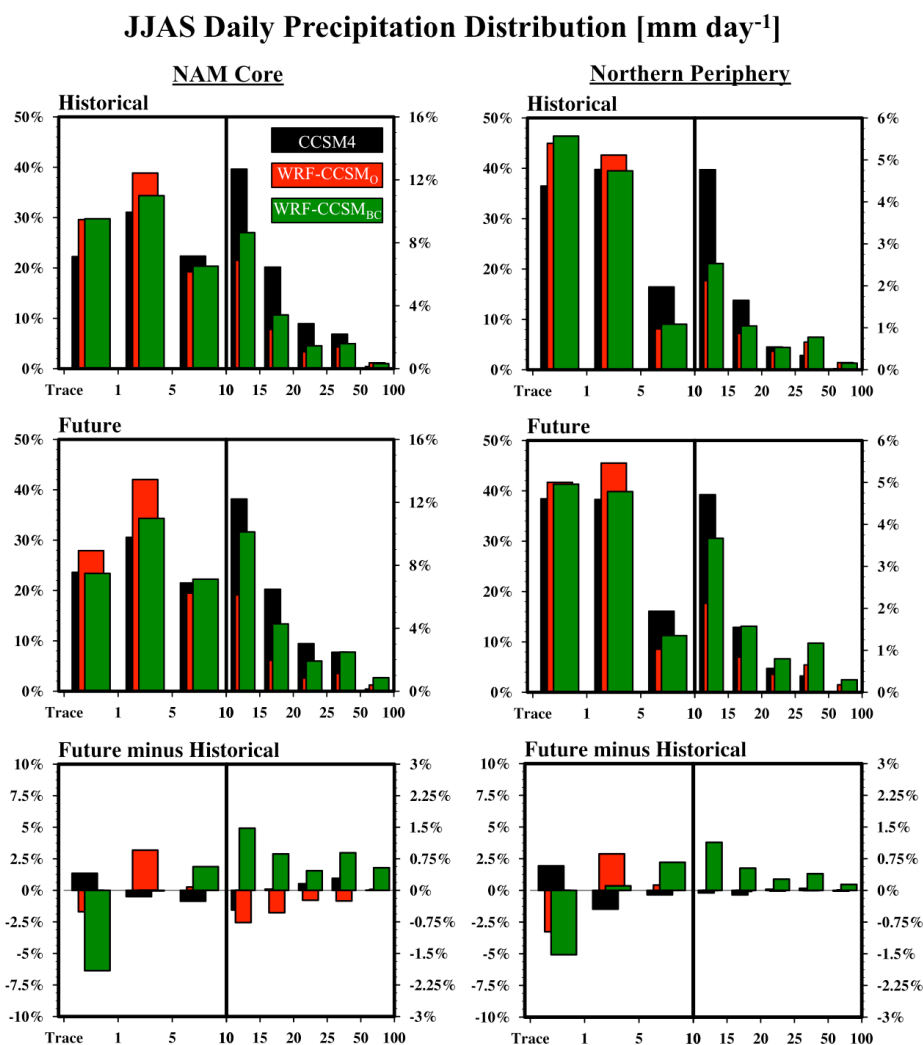


Fig. 4.9 Histogram distribution of June-September (JJAS) daily precipitation over the NAM core (left column) and the northern periphery (right column). Community Climate System Model version 4 (CCSM4; black bars), WRF driven with original CCSM4 (WRF-CCSM_O; red bars), and bias-corrected CCSM4 (WRF-CCSM_{BC}; green bars) are included. Distributions are split into two y-axis scales to better display the extreme event bins. Bottom row represents the future change in the daily precipitation distribution. Days with none, or less than trace amounts of rainfall ($< 0.254 \text{ mm day}^{-1}$) were not included in the frequency count.

Lastly, to better understand changes to daily event-scale precipitation, we look at the changes to the number of JJAS days without precipitation. Referred to as ‘dry days’, the number of days without precipitation in a year is important when understanding the changes to the regional hydrology. Conceptually, the daily frequency and amount of precipitation delivered to the soil column throughout the NAM season can lead to very different hydrology. Less frequent, more intense rainfall leads to greater surface runoff and less useable water infiltrating into the soil column whereas more frequent, less intense rainfall tends to not penetrate deep into the soil column and is quickly removed through evapotranspiration pathways. Furthermore, near-surface soil moisture not only impacts the surface energy budget, but also how moisture recycling can enhance downstream rainfall (Dominquez et al. 2008).

Fig. 4.10 shows the future difference in average yearly dry days as well as the change to the interannual variability. While CCSM4 points to an increasing number of JJAS dry days by the end of the century, both WRF simulations indicate the NAM domain generally experiences less days without precipitation with the exception found along the GoC coast in the WRF-CCSM_O simulations and New Mexico in the WRF-CCSM_{BC} simulations. Regarding changes to the variability of the number of June-September dry days, a mixed signal is shown for CCSM4 with the most dramatic changes coming to the east of the SMO where a significant reduction to the variability is found. WRF-CCSM_O shows a marked delineation from the eastern and western relief of the SMO with the eastern edge exhibiting less variability in the number of dry days similar to CCSM4, but the western slope shows increasing variability. For the WRF-CCSM_{BC}, a general pattern

4 Summary and conclusion

Simply put, the motivation behind this work was to improve the current perspective on the future state of the spatial distribution, seasonality, and interannual variability of NAM rainfall. Here, using a high-resolution RCM we tested (1) the effect of improved surface interactions, and (2) the influence biased LBCs have when downscaling the NAM region. In this study, we established that spanning daily to climatological timescales, dramatic differences in precipitation patterns are produced depending on whether a coarse resolution GCM or dynamical downscaling with an RCM is used as well as whether bias correction is employed to LBCs driving an RCM.

In complex climate systems such as the NAM, we add to the growing body of evidence that GCMs such as CCSM4 are not accurately capturing all of the interactions across spatial scales—especially on the mesoscale. Ultimately, the interplay between increasing tropospheric stability (acting to suppress convection and delay NAM onset) and increasing evaporation from an accelerated hydrologic cycle (acting to enhance convective activity) dictates how the NAM will change under a global warming scenario. Working in opposite directions, the interaction between these two mechanisms must be more accurately resolved beyond what a GCM can provide before future projections to onset, duration, and intensity of the NAM season can be trusted.

Compared to the general drying trend indicated by CCSM4 and other CMIP5 models, increasing model resolution with a RCM produced a more cohesive pattern of a wetter NAM across the SMO highlands, and the southwest U.S. We argue that while GCMs

suggest large-scale tropospheric warming leads to an overall drying trend and a delayed NAM, these models at best suppress the effects from the local enhancement to surface evaporation, and at worst even neglect this effect in some areas (i.e. immediately downstream of the unresolved GoC). When downscaling, the improved surface representation increased regional evaporation and better described low-level moisture transport driven by the land-sea temperature gradient. However, original CCSM4 LBCs provided the RCM with a poorly evolving thermodynamic profile and too cold GoC SSTs. The resulting NAM mature season atmosphere contained convectively inhibiting conditions (reinforcing the suppression of convection due to warmer troposphere) and too little surface evaporation from the GoC (diminishing the destabilization of the atmosphere through reduced near-surface atmospheric moisture content). The end result of downscaling original CCSM4 output was an NAM with earlier onsets across the southwest U.S. with greater interannual variability while the core region indicated a delayed onset along the core region in Mexico with lesser interannual variability. Generally, the entire NAM showed less intense rainfall, and a reduction in the average number of dry days in the NAM season. We conclude that although a higher resolution RCM projection offers a better overall picture of NAM mechanisms, due to poor LBCs (e.g. inaccurate seasonal evolution of atmospheric static stability, and too cold GoC SSTs) simply downscaling a GCM such as CCSM4 shares similar uncertainty as the parent GCM projection.

With bias corrected CCSM4 LBCs, our end-of-the-century simulations suggest a climatological shift towards earlier onset dates, more intense daily rainfall rates and

fewer average dry days per year, resulting in a much stronger monsoon. Evidence points that this dramatic shift from both the parent and downscaled original CCSM4 projections occurred because of (1) an improved seasonal cycle of atmospheric static stability in the LBCs, allowing a more convectively favorable atmosphere, and (2) greater regional evaporation from the surrounding water bodies (e.g. GoC and GoM). These two processes created an NAM environment that was much more convectively active and shows the influential role enhanced evaporation has on future atmospheric stability.

While this work provides a scenario that increases the regional climatological water resources, evidence for more extreme year-to-year precipitation variability is a cause for concern for a fast-growing drought-susceptible population across a region that might need to endure more frequent and intense prolonged periods of drought. After seeing such stark variations between future projection of the NAM depending on modeling approach, we caution the use of GCMs to draw conclusions about how a climate system controlled by many mesoscale mechanisms such as the NAM might be affected by a warming climate. Furthermore, our findings echo comments in Bukovsky et al. (2015) that without some form of bias correction, even a dynamical downscaling approach contains large uncertainty. With that being said, bias correction techniques rely on an empirical relationship to a historical climatology. There is no guarantee that a historical climatology is representative of the future state of the climate system. However, our findings—and many previous studies—have justified the use of bias correction methods to improve confidence in future projections.

While our modeling approach certainly improves confidence in simulating the future of the NAM through a more comprehensive depiction of the interaction of mechanisms across scales, our approach was limited by computation resources to a single realization from the vast CMIP5 suite. Future work on this subject should consider the benefits of an ensemble approach to further quantify the sensitivity of the aforementioned competing mechanisms of atmospheric stability to specific model type and RCP scenario. With that said, we are confident that the role of surface evaporation and the subsequent atmospheric destabilizing effects produced when coupling bias correction and dynamic downscaling is a feature neglected by any coarse resolution GCMs independent of model type or RCP scenario.

References

- Adams D, Comrie A (1997) The North American monsoon. *Bull Am Meteorol Soc* 78:2197–2213.
doi:[http://dx.doi.org/10.1175/1520-77\(1997\)078<2197:TNAM>2.0.CO;2](http://dx.doi.org/10.1175/1520-77(1997)078<2197:TNAM>2.0.CO;2)
- Anderson BT, Roads JO, Chen SC (2000) Large-scale forcing of summertime monsoon surges over the Gulf of California and the southwestern United States. *J Geophys Res Atmos*, 105(D19):24455–24467. doi:<http://dx.doi.org/10.1029/2000jd900337>
- Berbergy EH (2001) Mesoscale moisture analysis of the North American monsoon. *J Clim* 14(2):121–137.
doi:[http://dx.doi.org/10.1175/1520-442\(2001\)013%3C0121:mmaotn%3E2.0.co;2](http://dx.doi.org/10.1175/1520-442(2001)013%3C0121:mmaotn%3E2.0.co;2)
- Broccoli AJ, Manabe S (1992) The effects of orography on midlatitude Northern Hemisphere dry climates. *J Clim* 5(11):1181–1201.
doi:[http://dx.doi.org/10.1175/1520-442\(1992\)005%3C1181:teoom%3E2.0.co;2](http://dx.doi.org/10.1175/1520-442(1992)005%3C1181:teoom%3E2.0.co;2)
- Bukovsky MS, Gochis DJ, Mearns LO (2013) Towards assessing NARCCAP regional climate model credibility for the North American monsoon: current climate simulations. *J Clim* 26:8802–8826.
doi:<http://dx.doi.org/10.1175/jcli-d-12-00538.1>

- Bukovsky MS, Carrillo CM, Gochis DJ, Hammerling DM, McCrary RR, Mearns LO (2015) Toward assessing NARCCAP regional climate model credibility for the North American monsoon: Future climate simulations. *J Clim* 28(17):6707-6728. doi:<http://dx.doi.org/10.1175/jcli-d-14-00695.1>
- Castro CL, Chang H-I, Dominguez F, Carrillo C, Schemm J-K, Henry Juang H-M (2012) Can a regional climate model improve the ability to forecast the North American monsoon? *J Clim* 25:8212–8237. doi:<http://dx.doi.org/10.1175/jcli-d-11-00441.1>
- Collier JC, Zhang GJ (2007) Effects of increased horizontal resolution on simulation of the North American monsoon in the NCAR CAM3: An evaluation based on surface, satellite, and reanalysis data. *J Clim*, 20(9):1843-1861. doi:<http://dx.doi.org/10.1175/jcli4099.1>
- Cook BI, Seager R (2013) The response of the North American monsoon to increased greenhouse gas forcing. *J Geophys Res Atmos* 118(4):1690-1699. doi:<http://dx.doi.org/10.1002/jgrd.50111>
- Dominguez F, Kumar P, Vivoni ER (2008) Precipitation recycling variability and ecoclimatological stability-A study using NARR data. Part II: North American monsoon region. *J Clim* 21(20):5187-5203. doi:<http://dx.doi.org/10.1175/2008jcli1760.1>
- Douglas MW, Maddox R, Howard K, Reyes S (1993) The Mexican Monsoon. *J Clim* 6:1665–1677. doi:[http://dx.doi.org/10.1175/1520-0442\(1993\)006%3C1665:tmm%3E2.0.co;2](http://dx.doi.org/10.1175/1520-0442(1993)006%3C1665:tmm%3E2.0.co;2)
- Douglas MW, (1995) The summertime low level jet over the Gulf of California. *Mon Wea Rev* 123:2334–2347. doi:[http://dx.doi.org/10.1175/1520-0493\(1995\)123%3C2334:tslljo%3E2.0.co;2](http://dx.doi.org/10.1175/1520-0493(1995)123%3C2334:tslljo%3E2.0.co;2)
- Gao X, Shi Y, Song R, Giorgi F, Wang Y, Zhang D (2008) Reduction of future monsoon precipitation over China: Comparison between a high resolution RCM simulation and the driving GCM. *Meteorol Atmos Phys* 100(1-4):73-86. doi:<http://dx.doi.org/10.1007/s00703-008-0296-5>
- Geil KL, Serra YL, Zeng X (2013) Assessment of CMIP5 model simulations of the North American monsoon system. *J Clim* 26:8787–8801. doi:<http://dx.doi.org/10.1175/jcli-d-13-00044.1>
- Gent PR, Danabasoglu G, Donner LJ, Holland MM, Hunke EC, Jayne SR, Lawrence DM, Neale RB, Rasch PJ, Vertenstein M et al (2011) The Community Climate System Model Version 4. *J Clim* 24:4973–4991. doi:<http://dx.doi.org/10.1175/2011jcli4083.1>

- Giorgi F, Mearns LO (1991) Approaches to the simulation of regional climate change. *Rev Geophys* 29:191–216. doi:<http://dx.doi.org/10.1029/90rg02636>
- Gutzler DS, Long LN, Schemm J, Roy SB, Bosilovich M, Collier JC, Kanamitsu M, Kelly P, Lawrence D, Lee M-I, et al (2009) Simulations of the 2004 North American monsoon: NAMAP2. *J Clim* 22:6716–6740. doi:<http://dx.doi.org/10.1175/2009jcli3138.1>
- Higgins RW, Yao Y, Wang XL (1997) Influence of the North American monsoon system on the US summer precipitation regime. *J Clim* 10:2600–2622. doi:[http://dx.doi.org/10.1175/1520-0442\(1997\)010%3C2600:iotnam%3E2.0.co;2](http://dx.doi.org/10.1175/1520-0442(1997)010%3C2600:iotnam%3E2.0.co;2)
- Higgins RW, Mo KC, Yao Y (1998) Interannual variability of the U.S. Summer Precipitation regime with emphasis on the Southwestern Monsoon. *J Clim* 11:2582-2606. doi:[http://dx.doi.org/10.1175/1520-0442\(1998\)011%3C2582:ivotus%3E2.0.co;2](http://dx.doi.org/10.1175/1520-0442(1998)011%3C2582:ivotus%3E2.0.co;2)
- Higgins RW, Ahijevych D, Amador J, Barros A, Berbery EH, Caetano E, Carbone R, Ciesielski P, Cifelli R, Cortez-Vazquez M, et al (2006) The NAME 2004 field campaign and modeling strategy. *Bull Am Meteorol Soc* 87:79–94. doi:<http://dx.doi.org/10.1175/bams-87-1-79>
- Lee MI, Schubert SD, Suarez MJ, Held IM, Kumar A, Bell TL, et al (2007) Sensitivity to horizontal resolution in the AGCM simulations of warm season diurnal cycle of precipitation over the United States and northern Mexico. *J Clim* 20(9):1862-1881. doi:<http://dx.doi.org/10.1175/jcli4090.1>
- Liverman DM, Merideth R (2002) Climate and society in the US Southwest: The context for a regional assessment. *Clim Res* 21(3):199-218. doi:<http://dx.doi.org/10.3354/cr021199>
- Magaña VO, Conde C (2000) Climate and freshwater resources in northern Mexico: Sonora, a case study. *Environ Monit Assess* 61(1):167-185. doi:<http://dx.doi.org/10.1023/a:1006399025537>
- McGregor JL (1997) Regional climate modelling. *Meteorol Atmos Phys* 63(1):105-117. doi:<http://dx.doi.org/10.1007/bf01025367>
- Mearns LO, Gutowski WJ, Jones R, Leung L-Y, McGinnis S, Nunes AMB, Qian Y (2009) A regional climate change assessment program for North America. *Eos Trans Am Geo-phys Union* 90:311–312. doi:<http://dx.doi.org/10.1029/2009eo360002>
- Meyer JDD, Jin J (2015) Bias correction of the CCSM4 for improved regional climate modeling of the North American monsoon. *Clim Dyn* doi:<http://dx.doi.org/10.1007/s00382-015-2744-5>

- Misra V, Kanamitsu M (2004) Anomaly nesting: A methodology to downscale seasonal climate simulations from AGCMs. *J Clim* 17:3249–3262.
doi:[http://dx.doi.org/10.1175/1520-0442\(2004\)017%3C3249:anamtd%3E2.0.co;2](http://dx.doi.org/10.1175/1520-0442(2004)017%3C3249:anamtd%3E2.0.co;2)
- Mitchell DL, Ivanova D, Rabin R, Brown TJ, Redmond K (2002) Gulf of California sea surface temperatures and the North American monsoon: Mechanistic implications from observations. *J Clim* 15(17):2261-2281.
doi:[http://dx.doi.org/10.1175/1520-0442\(2002\)015%3C2261:gocsst%3E2.0.co;2](http://dx.doi.org/10.1175/1520-0442(2002)015%3C2261:gocsst%3E2.0.co;2)
- Prakash S, Mahesh C, Gairola RM, Pokhrel S (2011). Surface freshwater flux estimation using TRMM measurements over the tropical oceans. *Atmos Clim Sci* 1(04):225.
doi:<http://dx.doi.org/10.4236/acs.2011.14025>
- Ray AJ, Garfin GM, Wilder M, Vásquez-León M, Lenart M, Comrie AC (2007) Applications of monsoon research: Opportunities to inform decision making and reduce regional vulnerability. *J Clim* 20:1608–1627.
doi:<http://dx.doi.org/10.1175/JCLI4098.1>
- Saha S, Moorthi S, Pan H-L, Wu X, Wang J, Nadiga S, Tripp P, Kistler R, Woollen J, Behringer D, et al (2010) The NCEP Climate Forecast System Reanalysis. *Bull Am Meteorol Soc* 91:1015–1057. doi:<http://dx.doi.org/10.1175/2010bams3001.1>
- Seager R, Ting M, Held I, Kushnir Y, Lu J, Vecchi G, et al (2007) Model projections of an imminent transition to a more arid climate in southwestern North America. *Science* 316(5828):1181-1184. doi:<http://dx.doi.org/10.1126/science.1139601>
- Seth A, Rauscher SA, Biasutti M, Giannini A, Camargo SJ, Rojas M (2013) CMIP5 projected changes in the annual cycle of precipitation in monsoon regions. *J Clim* 26(19):7328-7351. doi:<http://dx.doi.org/10.1175/jcli-d-12-00726.1>
- Seth A, Rauscher SA, Rojas M, Giannini A, Camargo SJ (2011) Enhanced spring convective barrier for monsoons in a warmer world? *Clim Change* 104(2):403-414. doi:<http://dx.doi.org/10.1007/s10584-010-9973-8>
- Skamarock WC, Klemp JB, Dudhia J, Gill DO, Barker DM, Wang W, Powers JG (2005) A description of the advanced research WRF version 2 (No. NCAR/TN-468+STR). National Center For Atmospheric Research Boulder CO Mesoscale and Microscale Meteorology Div
- Stensrud DJ, Gall RL, Nordquist MK (1997) Surges over the Gulf of California during the Mexican monsoon. *Mon Wea Rev* 125(4):417-437.
doi:[http://dx.doi.org/10.1175/1520-0493\(1997\)125%3C0417:sotgoc%3E2.0.co;2](http://dx.doi.org/10.1175/1520-0493(1997)125%3C0417:sotgoc%3E2.0.co;2)

Van Vuuren DP, Edmonds J, Kainuma M, Riahi K, Thomson A, Hibbard K, Hurtt GC, Kram T, Krey V, Lamarque J-F, et al (2011) The representative concentration pathways: an overview. *Clim Change* 109:5–31.
doi:<http://dx.doi.org/10.1007/s10584-011-0148-z>

CHAPTER V

CONCLUSION

The NAM supplies a large percentage of the annual precipitation across the drought-prone southwest United States and Mexico. Therefore, the region's hydrology, ecology, and socioeconomics are all highly sensitive to future changes to the spatiotemporal pattern of rainfall. Exacerbating the already water-resource-limited region are the impressive regional population growth projections, which suggest a doubling of population by the middle of the 21st century. Accordingly, regional planners and resource managers have recently advocated for advances towards more accurate seasonal predictions of NAM rainfall, as well as more reliable future regional climate projections.

Seasonal predictions for NAM rainfall are partially relying on the various correlations between climate teleconnections such as ENSO and PDO. By influencing antecedent wintertime snowpack across the western United States, the variability in these ocean SST patterns have been shown to both directly and indirectly influence the timing of onset and seasonal intensity of the NAM by modulating how energy is partitioned through the surface energy budget. Through this connection, observations from the SNOWpack TELEmetry (SNOTEL) network of the springtime peak SWE represents a unique tool to aid in the seasonal prediction of the NAM. However, our analysis of 748 sites within the SNOTEL network uncovered the propensity for a regionally systematic (and physically unrealistic) scenario where SWE outpaces measurements of AP, which we attribute to a site's tendency for snowpack drifting/scouring. Network wide, we found forty-four

percent of all stations had at least one year with this unrealistic scenario, and sixteen percent of the network exhibited the problem at least twenty percent of their observed years. Unfortunately, several of the same regions exhibiting the highest correlation for seasonal NAM prediction also contained the greatest frequency and discrepancy between SWE and AP; mainly across the Colorado Rockies, which had the third greatest rate of occurrence out of all domains sampled. While the magnitude of the SWE uncertainty is likely not significant enough to dramatically offset the reliability of seasonal predictions on its own, our results underscore the need to account for these systematic wet-biases in SWE.

Regarding future projections of the NAM, historical evaluation for the NAM shows GCMs typically perform poorly. Despite recent advances in computing power permitting global-scale fully-coupled climate models, GCM grid scales are still too coarse to accurately describe complex terrain features and coastlines. Because of this issue and others inherent to GCM model design, the seasonality and magnitude of the NAM convective environment, and thus the regional precipitation distribution, is poorly resolved. The poor historical performance of GCMs calls into question their ability to credibly provide a future projection of the NAM. To improve confidence in future NAM projection beyond current GCMs we tested the idea that increasing model grid resolution will improve the historical performance of the NAM. Using a higher-resolution RCM run at 20-km we found a modest improvement in the modeled historical NAM environment and precipitation fields. However, nesting forcing conditions at the boundary of the RCM, biases associated with the parent GCM produced similarly poor seasonality and

intensity of the NAM. Even with higher grid resolution, NAM onset dates were, on average, 3-4 weeks too early over the core of the NAM—a result of the biased seasonality of the convective environment transmitted through the boundaries of the RCM. Likewise, biased boundary conditions suppressed the mature phase of the NAM, resulting in dry biases in July-August rainfall when compared to observations. The role of biased GCMs to limiting the advantages of higher grid resolution underscores the limiting factor when dynamically downscaling with a RCM. For this reason, we performed a second set of RCM simulations, where bias corrected boundary conditions were used to drive the model. These simulations showed marked improvements in the historical NAM convective environment and precipitation fields, with a reduction of root-mean-square-errors of August over the core of the NAM by 26% and 36% over the southwest United States when compared to the original downscaled simulations. With higher grid resolution and less biased forcing conditions, confidence in future projections increases.

As a result of increasing tropospheric stability under a warming climate, GCM's project the future NAM to feature a delayed onset, minor increase to mature season intensity, and delayed retreat phase. On the other hand, while GCMs are limited to include more large-scale effects from global warming, using a high-resolution dynamical downscaling approach to including more of the controlling dynamics suggests the role of land surface processes on the future state of the NAM are likely understated in GCMs. In fact, comparing both original and bias-corrected downscaled simulations with the parent GCM exposes the potential for land surface and mesoscale mechanisms to overpower the large-scale warming tropospheric mechanism responsible for suppressing convection in

GCMs. These higher-resolution simulations showed a reversal of NAM trends towards earlier onset dates and more intense seasonal- and daily-scale precipitation was produced. Plagued by biased boundary conditions, the reversal in trends produced by the original downscaled simulations was limited to primarily the southwest United States and the highlands of the SMO, with much of the core of the NAM remaining consistent with the parent GCM trends. After bias-correction, a much more apparent and spatially cohesive reversal of NAM trends across the entire NAM domain was produced.

Analysis into the cause for such dramatic reversal in trends highlighted the role low-level atmospheric moisture plays regarding atmospheric stability and convection. While GCMs show greater tropospheric stability from a warming atmosphere, these models struggle to capture the spatial extent of the Gulf of California (GoC)—the primary moisture source for the NAM. When including the effects from warmer SSTs increasing surface evaporation, the RCM improves the interaction between the competing mechanisms of a warmer troposphere (suppressing convection) and increased low-level moisture (enhancing convection). When including the destabilizing effects of increasing low-level moisture, the result of the improved interaction between these competing mechanisms is the reversal from the original GCM drying trend. Additionally, with a better representation of the land-sea temperature gradient, mesoscale circulation features and the resulting onshore moisture transport is more accurate; a mechanism that strengthens in the future simulations.

This study highlights the deficiencies when using a GCM for future projections of climate systems driven by processes beyond the resolvable scales. Furthermore, this study underscores the need for bias correction on GCM data before dynamically downscaling, as biases in the seasonality and intensity of phenomena such as the NAM can greatly limit any advantages through higher resolution RCMs. The result when combining a higher resolution RCM with bias-corrected boundary conditions is a more historically accurate season cycle for the NAM with improved land surface interactions and mesoscale mechanisms.

The improved modeling techniques used for this study indicates the potential for a future NAM that climatologically, brings additional water resources over the historical normal. However, the increase in overall seasonal precipitation totals—while good news compared to current GCM projections of a dryer NAM—is overshadowed by the inter-model consistency for increasing interannual variability across a region already susceptible to extreme and persistent drought. Additionally, increases to extreme rainfall events suggests the region will become more susceptible to flooding and economically challenging conditions during the NAM season.

Future studies aiming to further improve upon these results should consider the following. First, being limited to only evaluating a single set of GCM output constrains the ability of this study to quantify the uncertainty that a larger ensemble modeling approach is better suited for. Second, while the 20-km model resolution in the RCM is substantially greater than the parent GCM, a convective environment such as the NAM

can always benefit from increased resolution. Future studies would ideally begin to approach the explicit convective resolving scales. Third, while this study simulated a sufficiently long period of time to compare the climatological characteristics of changes to the NAM, the disconnect between historical and future periods leaves some ambiguity on when projected changes occur, and whether those changes occur quickly, or are more relaxed.

CURRICULUM VITAE

Jonathan D.D. Meyer
jon.meyer@usu.edu

EDUCATION:

Utah State University , Dept. of Plants, Soils and Climate Ph.D. in Climate Science	Logan, UT Spring 2017
South Dakota School of Mines & Tech. , Dept. of Atmo. Science M.S. in Atmospheric Science	Rapid City, SD 2010
University of Northern Colorado , Dept. of Earth Science B.S. in Meteorology & Minor in Mathematics	Greeley, CO 2008

PUBLICATIONS:

- **Meyer, Jonathan D.D.** and Jiming Jin, 2016: A more realistic future projection of the North American Monsoon using bias correction and a dynamical downscaling approach. *Climate Dynamics*, 46:2961, doi:10.1007/s00382-015-2744-5
- **Meyer, Jonathan D.D.** and Jiming Jin, 2015: Bias Correction of the CCSM4 for improved regional climate modeling of the North American monsoon. *Climate Dynamics*, 46(9), 2961-2976. doi:10.1007/s00382-015-2744-5.
- **Meyer, Jonathan D. D.**, Jiming Jin, Shih-Yu Wang, 2012: Systematic Patterns of the Inconsistency between Snow Water Equivalent and Accumulated Precipitation as Reported by the Snowpack Telemetry Network. *J. Hydrometeorol*, **13**, 1970–1976. doi: <http://dx.doi.org/10.1175/JHM-D-12-066.1>

UTAH STATE UNIVERSITY AWARDS AND ACHIEVEMENTS:

- | | |
|--|------|
| ▪ Graduate Student Senate Graduate Enhancement Award | 2016 |
| ▪ School of Graduate Studies Dissertation Writing Fellowship | 2016 |
| ▪ Spring Runoff Conference Outstanding Student Poster Award | 2016 |
| ▪ Spring Runoff Conference Outstanding Student Poster Award | 2014 |
| ▪ College of Natural Resources Graduate Teaching Assistant of the Year | 2013 |
| ▪ Climate Data and Prediction Workshop Student Travel Award | 2013 |

TEACHING EXPERIENCE:

- | | |
|--|-----------------------------|
| ▪ PSC-4810/6810 Climate and Climate Change | Lecturer |
| Fall 2016; 3 students | Spring 2017; 22 students |
| ▪ PSC-2000 The Atmosphere and Weather | Graduate Teaching Assistant |
| Fall 2014; 119 students | Fall 2013; 131 students |
| Fall 2012; 167 students | Fall 2011; 149 students |

- PSC-3820 Climate and Climate Change w/ lab
Spring 2011; 54 students

Graduate Teaching Assistant